

**Low melting point and amphiphilic polymer microspheres for  
therapeutic protein delivery**

by

Dimitra Louka

**A thesis submitted to the Department of Chemical Engineering In conformity with the  
requirements for the degree of Master of Applied Science**

**Queen's University**

**Kingston, Ontario, Canada**

**November 2015**

**Copyright © Dimitra Louka, 2015**

## **Abstract**

Biodegradable microspheres have been extensively studied for controlled and minimally invasive in situ protein delivery. Their small size and thus ready injectability makes this device extremely popular for localized administration, which is particularly advantageous for protein delivery applications. In this study, amphiphilic low melting biodegradable tri-block copolymers of PEG,  $\epsilon$ -caprolactone and glycolide monomers were synthesized using bulk ring-opening polymerization (ROP). The design and characterization of this biodegradable copolymer was focused on the formation of microspheres for localized, controlled delivery of the therapeutic chemokine protein SDF-1 $\alpha$ . Molecular weight and compositional changes were used to tailor the thermal properties of the copolymers so that the produced materials were solid at room temperature but had minimum crystallinity after hydration at 37 °C. A complete degradation was achieved for the copolymers studied within eight weeks with minor acidic degradation effect on the external and internal microenvironment pH of the microspheres. The copolymers exhibited great ability for microsphere formation with high protein encapsulation efficiency ( $\geq 75\%$ ) using an electrospraying technique. Prolonged release of SDF-1 $\alpha$  was observed with its bioactivity well retained after encapsulation and release, as analysed using cell-based assays.

## **Acknowledgements**

I would like to express my deepest gratitude to my supervisor, Dr. Brian Amsden, for giving me the opportunity to work on a fascinating project. His guidance, support and understanding have been invaluable during my studies.

I am deeply grateful to our laboratory manager, Dale Marecak, for all of his assistance and encouragement towards a safe and organized working routine.

I would also like to thank Roshni Rainbow for taking the time to train me in cell-culture procedures. To the members of the Amsden lab: Fei Chen, Julian Chesterman, Moira Vyner, Shadi Taghavi, Stuart Young, Sara Mohajeri, Bowen Yang, Ming Gong, Fiona Serack and Amanda Brissenden, it has been a great and memorable experience working with such a group of scientists.

Finally, I would like to thank Alexandros Vasileiou for his mentoring, help and honest advice. I'm grateful to have you in my life.

To my family and friends for their unconditional support, thank you.

## Table of Contents

<b>Abstract .....</b>	<b>i</b>
<b>Acknowledgements .....</b>	<b>ii</b>
<b>Table of Contents .....</b>	<b>iii</b>
<b>List of figures.....</b>	<b>vi</b>
<b>List of schemes .....</b>	<b>viii</b>
<b>List of tables .....</b>	<b>viii</b>
<b>List of abbreviations .....</b>	<b>ix</b>
<b>Chapter 1. Introduction .....</b>	<b>1</b>
1. 1 Background.....	1
1. 2 Scope .....	2
<b>Chapter 2. Literature review .....</b>	<b>4</b>
2. 1 Therapeutic protein delivery .....	4
2. 1. 1 Protein structure-activity .....	4
2. 1. 2 Issues in protein delivery .....	5
2. 2 Protein controlled release .....	7
2. 2. 1 Protein encapsulation .....	8
2. 2. 2 Biodegradable polymers in protein delivery .....	9
2. 2. 3 Microsphere delivery systems .....	11
2. 3 Effect of copolymerization on polymer properties .....	15
2. 4 SDF-1 $\alpha$ protein.....	18
<b>Chapter 3. Proposed approach .....</b>	<b>20</b>
<b>Chapter 4. Objectives.....</b>	<b>24</b>
<b>Chapter 5. Tri-block copolymer synthesis .....</b>	<b>25</b>
5. 1 Introduction.....	25
5. 2 Materials.....	26
5. 3 Methods .....	26
5. 3. 1 Bulk ring-opening polymerization.....	26
5. 3. 2 Copolymer composition variables.....	27
5. 3. 3 Purification .....	28
5. 3. 4 Molecular weight fractionation .....	29
5. 3. 5 Optimization of bulk polymerization .....	29
5. 3. 6 Other polymerization methods explored.....	29
5. 3. 7 Polymer characterization .....	31
5. 4 Results and discussion .....	36
5. 4. 1 Polymer characterization .....	36

5. 4. 2 Effect of temperature on ring opening polymerization .....	38
5. 4. 3 Structural analysis using ATR-FTIR .....	40
5. 4. 4 Thermal analysis .....	41
5. 4. 5 Polymer composition parameters.....	44
5. 4. 6 Other polymerizations explored .....	47
5. 5 Conclusion .....	49
<b>Chapter 6. Microspheres: Preparation and degradation .....</b>	<b>50</b>
6. 1 Introduction.....	50
6. 2 Materials.....	50
6. 3 Methods .....	51
6. 3. 1 Electrospraying of microspheres.....	51
6. 3. 2 Microspheres size separation .....	52
6. 3. 3 Mean microsphere diameter determination .....	52
6. 3. 4 Water uptake .....	53
6. 3. 5 Hydrolytic degradation of microspheres.....	53
6. 3. 6 Microenvironmental pH of degrading microspheres .....	54
6. 4 Results and discussion .....	55
6. 4. 1 Microspheres preparation .....	55
6. 4. 2 Microsphere average diameter and morphology .....	57
6. 4. 3 Water uptake .....	57
6. 4. 4 Hydrolytic degradation rate .....	58
6. 4. 5 Microenvironmental and external pH of microspheres degrading in PBS pH 7.4 .....	62
6. 5 Conclusion .....	65
<b>Chapter 7. Protein release and bioactivity .....</b>	<b>66</b>
7. 1 Introduction.....	66
7. 2 Materials.....	66
7. 3 Methods .....	67
7. 3. 1 Protein particles preparation and size reduction.....	67
7. 3. 2 Protein encapsulation in polymer microspheres .....	68
7. 3. 3 Protein encapsulation efficiency.....	68
7. 3. 4 Lysozyme release .....	69
7. 3. 5 SDF-1 $\alpha$ protein particles preparation .....	70
7. 3. 6 SDF-1 $\alpha$ encapsulation .....	71
7. 3. 7 SDF-1 $\alpha$ release .....	71
7. 3. 8 SDF-1 $\alpha$ bioactivity .....	72
7. 3. 9 Cell expansion .....	73

7. 3. 10 Cell counting .....	73
7. 3. 11 Cell viability assays.....	73
7. 4 Results and discussion .....	74
7. 4. 1 Protein particles.....	74
7. 4. 2 Encapsulation efficiency .....	75
7. 4. 3 Lysozyme release.....	76
7. 4. 4 SDF-1 $\alpha$ release .....	81
7. 4. 5 SDF-1 $\alpha$ bioactivity .....	84
7. 5 Conclusion .....	87
<b>Chapter 8. Summary and Conclusion .....</b>	<b>89</b>
<b>Bibliography.....</b>	<b>91</b>

## List of figures

<b>Figure 2. 1</b> Illustration of the drug concentration curve after dosage and therapeutic window margins (MTC: minimum toxic concentration; MEC: minimum effective concentration). .....	7
<b>Figure 2. 2</b> Representative triphasic release profile from PLGA microspheres. Phase I shows high burst release, phase II shows the diffusion-controlled release and phase III shows the fast release rate due to the polymer matrix erosion. <sup>47</sup> .....	14
<b>Figure 3. 1</b> Electrospraying apparatus for fabrication of microspheres.....	23
<b>Figure 5. 1</b> Representative <sup>1</sup> H NMR spectra and microstructure analysis of copolymer C15 (3:1 - PEG1500 - 7.5 kDa). .....	33
<b>Figure 5. 2</b> <sup>1</sup> H NMR peak assignments on a spectrum obtained from copolymer C15 (3:1- PEG1500-7.5 kDa). .....	36
<b>Figure 5. 3</b> Section of <sup>1</sup> H NMR spectra of PEG 4000 initiated copolymers with 3:1 CL:G molar ratio and total molecular weight 10 kDa (3:1 - PEG4000 – 10 kDa) , produced at different temperatures, 150 °C (C3) and 110 °C (C19). Glycolide peaks can be seen at 4.8-4.5 ppm. ....	40
<b>Figure 5. 4</b> FTIR-ATR spectra of two polymer fractions: insoluble (red) and soluble (black) recorded using 1:1 PEG 4000 polymer polymerized at 110 °C (sample C17, Table 5. 2). The characteristic peaks of PG homopolymer (dotted spectrum) that are enhanced in the insoluble fraction are indicated with arrows. ...	41
<b>Figure 5. 5</b> DSC thermogram (1 <sup>st</sup> heating cycle) of dry sample C1 (Table 5. 3). T <sub>m</sub> ,PG at 198 °C was attributed to the melting of PG blocks formed at high G content copolymers.....	42
<b>Figure 5. 6</b> DSC thermogram (2 <sup>nd</sup> heating cycle) of sample C5 (Table 5. 3) exhibiting a cold crystallization (T <sub>cc</sub> ) at -38 °C. ....	44
<b>Figure 5. 7</b> DSC thermograms (1 <sup>st</sup> heating cycle) of PEG4000 initiated copolymers with 3:1 CL:G molar ratio in various Mn from 10 to 25 kDa. [C3: 10 kDa, C11: 15 kDa, C12: 20 kDa and C13:25 kDa at Table 5. 2].....	47
<b>Figure 5. 8</b> DSC thermograms (1 <sup>st</sup> heating cycle) of C27 copolymer (3:1 - 10 kDa - PEG4000) synthesized using DBU catalyst. The characteristic endothermic attributed to the PG blocks melting can be seen at 220 °C.....	48
<b>Figure 6. 1</b> <sup>1</sup> H NMR spectra (A) and DSC thermograms (1 <sup>st</sup> heating cycle) (B) of dry polymer sample C4 before electrospraying (a) and after microsphere formation (b). ....	56
<b>Figure 6. 2</b> Scanning electron microscope (SEM) image obtained from 6:1 PEG4000 (C6) copolymer. ....	57
<b>Figure 6. 3</b> Cumulative mass loss obtained from in vitro hydrolytic degradation kinetics analysis on copolymer microspheres in distilled water with pH adjusted to pH 7.4. Samples C6 (6:1 – PEG4000 - 10 kDa), C5 (5:1 – PEG4000 - 10 kDa), C4 (4:1 – PEG4000 - 10 kDa), and C16 (6:1 – PEG1500 – 7.5 kDa) compared to copolymerized PEG4000 with pure PCL blocks to total 10 kDa molecular weight. n=4 per time point. Straight lines connecting the data points of each sample were used to guide the eye. ....	58
<b>Figure 6. 4</b> Cumulative Mn loss obtained from in vitro hydrolytic degradation kinetics analysis on copolymer microspheres in distilled water with pH adjusted to pH 7.4. Samples C6 (6:1 – PEG4000 - 10 kDa), C5 (5:1 – PEG4000 - 10 kDa), C4 (4:1 – PEG4000 - 10 kDa) were analyzed. n=4 per time point. Straight lines connecting the data points of each sample were used to guide the eye. ....	59
<b>Figure 6. 5</b> pH values of the external incubation medium during degradation of microspheres prepared with copolymers C6 (6:1-PEG4000-10 kDa), C5 (5:1-PEG4000-10 kDa) and C4 (4:1-PEG4000-10 kDa). The	

degradation took place in water with pH adjusted at pH7.4. The incubation medium (water, pH7.4) was refreshed daily. n=4 per time point.....	61
<b>Figure 6. 6</b> DSC thermographs (1 <sup>st</sup> heating cycle) of copolymer C5 (5:1- PEG 4000-10 kDa) during hydrolytic degradation in water at pH 7.4. Graphs obtained from dry samples at day 0, 14 and 21 of the study.....	61
<b>Figure 6. 7</b> Fluorescence images collected at 450nm from lysosensor dextran encapsulated into 6:1-PEG4000-10 kDa (C6) microspheres at pH ~5.4, day 3 (A) and pH ~5.8, day 2 (B).....	62
<b>Figure 6. 8</b> Standard curve of fluorescence ratio versus pH using Lysosensor (A) and SNARF-1 (B) dextrans in pH-adjusted PBS buffer. The excitation of lysosensor was performed at 405nm and the emission was recorded at 450 and 520 nm, while for SNARF-1 dextran the excitation was at 488 nm and emission was recorded at 580 and 640 nm.....	63
<b>Figure 6. 9</b> Microclimate pH change of degrading microspheres into PBS buffer solution (pH 7.4). Mn 10 kDa, 5:1-PEG400 (C5) and 6:1-PEG4000 (C6) polymer microspheres with encapsulated fluorescence dextrans Lysosensor and SNARF-1 were analyzed using confocal microscope.....	64
<b>Figure 6. 10</b> pH change of the incubation medium (PBS pH 7.4) during degradation of microspheres prepared using C5 (5:1 – PEG4000 – 10kDa) and C6 (6:1 – PEG4000 – 10kDa) copolymers. ....	65
<b>Figure 7. 1</b> Lysozyme protein particles with 40% trehalose. Image taken using scanning electron microscopy (SEM).....	75
<b>Figure 7. 2</b> Release profiles of lysozyme from C5 (5:1-PEG4000-10 kDa) polymer microspheres prepared with the same protein particle loading rates (3%) as a function of trehalose content of 10 and 60%. Curve fitting of a theoretical model of diffusion controlled release was applied on each data set and is illustrated with dotted lines. Curve fit data, C5, 60% trehalose: $R^2=0.91$ , $D = 1.81(\pm 0.26) \cdot 10^{-12} \text{ cm}^2/\text{sec}$ – C5, 10% trehalose: $R^2=0.91$ , $D = 1.82(\pm 0.26) \cdot 10^{-12} \text{ cm}^2/\text{sec}$ . ....	77
<b>Figure 7. 3</b> Release profiles of lysozyme from C5 (5:1 - PEG4000 - 10 kDa) copolymer microspheres as a function of loading rate 1.5 and 3%. Trehalose content in the protein particles was 10% for both of the samples. Curve fitting of a theoretical model of diffusion controlled release was applied on each data set and is illustrated with dotted lines. Curve fit data, C5, 1.5% loading: $R^2=0.87$ , $D = 1.98(\pm 0.23) \cdot 10^{-12} \text{ cm}^2/\text{sec}$ – C5, 3% loading: $R^2=0.91$ , $D = 1.82(\pm 0.26) \cdot 10^{-12} \text{ cm}^2/\text{sec}$ .....	79
<b>Figure 7. 4</b> Release profiles of lysozyme from C5 (5:1-PEG4000-10 kDa) and C6 (5:1-PEG4000-10 kDa) microspheres prepared with the same loading rate (1.5%) and same trehalose content (10%) as a function of polymer composition and crystallinity. Curve fitting of a theoretical model of diffusion controlled release was applied on each data set and is illustrated with dotted lines. Curve fit data, C5: $R^2=0.87$ , $D = 1.98(\pm 0.23) \cdot 10^{-12} \text{ cm}^2/\text{sec}$ – C6: $R^2=0.90$ , $D = 1.89(\pm 0.20) \cdot 10^{-12} \text{ cm}^2/\text{sec}$ . ....	80
<b>Figure 7. 5</b> Release profiles of SDF-1 $\alpha$ and BSA (carrier protein) encapsulated in C6 polymer microspheres using 1.5% protein particles loading with 5% trehalose content. Curve fitting of a theoretical model of diffusion controlled release (Eq. 7. 4 and 7. 5) was applied on each protein data set and is illustrated with dotted lines. Curve fit data, SDF-1 $\alpha$ : $R^2=0.9$ , $D = 1.5(\pm 0.1) \cdot 10^{-12} \text{ cm}^2/\text{sec}$ – BSA: $R^2=0.94$ , $D = 1.4(\pm 0.1) \cdot 10^{-12} \text{ cm}^2/\text{sec}$ .....	82
<b>Figure 7. 6</b> Cell metabolic activity at day 1 and day 2 after incubation in SDF-1 $\alpha$ supplemented cell culture medium, using “as received” SDF-1 $\alpha$ protein at concentrations varying from 0 - 200 ng/mL, using MTT metabolic activity assay. Values reported as % increase in metabolic activity from the values obtained from the initial cell population, without the effect of SDF-1 $\alpha$ . ....	85
<b>Figure 7. 7</b> Compared cell metabolic activity (Day 2) between ‘as received’ and ‘after storage’ SDF-1 $\alpha$ protein measured using MTT metabolic activity assay at concentrations varying from 0 to 140 ng/mL. The	



values are reported as % increase in metabolic activity from the values obtained from the initial cell population, without the effect of SDF-1 $\alpha$ .....	86
<b>Figure 7. 8</b> Cell number assay at day 2 of incubation in SDF-1 $\alpha$ supplemented cell culture medium using ‘after storage’ SDF-1 $\alpha$ , measured with QuantiFluor dsDNA assay. The values are reported as % increase of the number of cells compared to the initial cell population used.....	86
<b>Figure 7. 9</b> Bioactivity of SDF-1 $\alpha$ after release from microspheres prepared using C6 (6:1 – PEG4000 – 10kDa) copolymer. The released SDF-1 $\alpha$ was diluted to a concentration 10 ng/mL and the bioactivity obtained was compared to the bioactivity obtained from ‘after storage’ SDF-1 $\alpha$ at the same concentration (10 ng/mL). .....	87

## List of schemes

<b>Scheme 2. 1</b> Ring-opening and acyl-oxygen cleavage of glycolide ring (cG).....	16
<b>Scheme 5. 1</b> Ring opening polymerization reaction of $\epsilon$ -Caprolactone, Glycolide and PEG diol using tin(II)-2-ethylexanoate [Sn(Oct) <sub>2</sub> ] as catalyst. ....	25

## List of tables

<b>Table 5. 1</b> Summary of copolymers synthesized.....	28
<b>Table 5. 2</b> Summarized results obtained from <sup>1</sup> H NMR and GPC analysis. ....	37
<b>Table 5. 3</b> Thermal properties of all PEG4000 initiated copolymers produced with bulk ROP at 150 °C.....	42
<b>Table 5. 4</b> Thermal properties of homopolymers obtained via DSC analysis.....	43
<b>Table 5. 5</b> Thermal properties of all copolymers produced using PEG1500 as initiator.....	46
<b>Table 6. 1</b> Average diameter of the microspheres produced, determined through SEM imaging analysis. .57	
<b>Table 6. 2</b> Water uptake of the copolymers tested for degradation kinetics. ....	58
<b>Table 6. 3</b> Molar ratios of CL and PEG in respect to G determined via <sup>1</sup> H NMR composition analysis of samples from in vitro degradation analysis in distilled water with pH adjusted to pH 7.4. ....	60
<b>Table 7. 1</b> Experimental outline of release rate study using lysozyme as model protein with three trehalose concentrations (10, 40 and 60%) and two different particle loading rates (1.5 and 3%) using copolymers C5 (5:1-10 kDa-PEG 4000) (solid circle) and C6 (6:1-10 kDa-PEG 4000) (open circle). ....	69
<b>Table 7. 2</b> Encapsulation efficiency yield for all protein encapsulated in polymer microspheres in C5 and C6 copolymers.....	75
<b>Table 7. 3</b> Molecular weight (Mn) and Isoelectric point (pI) of the protein used <sup>180</sup> .....	84

## List of abbreviations

<b>ATR-FTIR</b>	attenuated total reflection-Fourier transform infrared spectroscopy
<b>BSA</b>	bovine serum albumin
<b>C</b>	caproyl unit (-OCH <sub>2</sub> CH <sub>2</sub> CH <sub>2</sub> CH <sub>2</sub> CH <sub>2</sub> CO-)
<b>C<sub>c</sub></b>	ε-caprolactone monomer units sequence
<b>C<sub>g</sub></b>	alternating ε-caprolactone-glycolide monomer units sequence
<b>CL</b>	ε-caprolactone monomer unit
<b>D</b>	diffusion coefficient
<b>Đ</b>	polymer dispersity
<b>DBU</b>	1,8-Diazabicyclo[5.4.0]undec-7-ene
<b>DCM</b>	methylene chloride
<b>DNA</b>	deoxyribonucleic acid
<b>dn/dc</b>	refractive index increment
<b>dRI</b>	differential refractive index
<b>DSC</b>	differential scanning calorimetry
<b>E</b>	encapsulation efficiency
<b>EDTA</b>	ethylenediaminetetraacetic acid
<b>Et<sub>2</sub>O</b>	diethyl ether
<b>FBS</b>	fetal bovine serum
<b>G'</b>	glycolyl unit (-OCH <sub>2</sub> CO-)
<b>G<sub>a</sub></b>	glycolyl-glycolyl-caproyl sequence
<b>G<sub>b</sub></b>	caproyl-glycolyl-glycolyl sequence
<b>G<sub>c</sub></b>	caproyl-glycolyl-caproyl sequence
<b>G<sub>g</sub></b>	glycolyl-glycolyl-glycolyl sequence
<b>cG</b>	glycolide ring
<b>G</b>	glycolide monomer unit (-OCH <sub>2</sub> CO-OCH <sub>2</sub> CO-)
<b>GPC</b>	gel permeation chromatography
<b>HCl</b>	hydrochloric acid
<b>I</b>	fluorescence intensity
<b>k</b>	molar ratio [C]/[G]
<b>L<sub>c</sub></b>	experimental average length of caproyl units sequence
<b>L<sub>g</sub></b>	experimental average length of glycolyl units sequence
<b>L<sub>c</sub><sup>R</sup></b>	theoretical average length of caproyl units sequence
<b>L<sub>g</sub><sup>R</sup></b>	theoretical average length of glycolyl units sequence
<b>m<sub>dry</sub></b>	mass of dry microspheres
<b>M<sub>n</sub></b>	number average molecular weight
<b>MTT</b>	3-(4,5-Dimethylthiazol-2-yl)-2,5-Diphenyltetrazolium Bromide
<b>MW</b>	molecular weight
<b>M<sub>0</sub></b>	total amount of drug encapsulated
<b>M<sub>t</sub></b>	cumulative amount of drug released at time t
<b>M<sub>w</sub></b>	weight average molecular weight
<b>m<sub>wet</sub></b>	mass of wet microspheres
<b>n</b>	number of repeating units
<b>NMR</b>	nuclear magnetic resonance
<b>PBS</b>	phosphate buffer saline

<b>P/S</b>	penicillin-streptomycin
<b>PCL</b>	poly( $\epsilon$ -Caprolactone)
<b>PDI</b>	polydispersity index
<b>PEG</b>	poly(ethylene glycol)
<b>PG</b>	poly(glycolide) blocks
<b>PGA</b>	poly(glycolide) homopolymer
<b>PLA</b>	poly(lactic acid)
<b>PLGA</b>	poly(lactic-co-glycolic acid)
<b>pI</b>	isoelectric point
<b>R</b>	degree of randomness
<b>ROP</b>	ring opening polymerization
<b>r</b>	radius of microsphere
<b>SCLC</b>	small cell lung cancer cells
<b>SDF-1<math>\alpha</math></b>	stromal cell-derived factor-1-alpha
<b>Sn(Oct)<sub>2</sub></b>	tin (II) 2-ethylhexanoate
<b>T<sub>g</sub></b>	glass transition temperature
<b>TE</b>	tris-EDTA buffer
<b>THF</b>	tetrahydrofuran
<b>T<sub>m</sub></b>	melting temperature
<b>WU</b>	water uptake
<b>X</b>	crystallinity
<b>V</b>	volume of spherical particle
<b><math>\Delta H_m</math></b>	enthalpy of melting
<b><math>\Delta H_{m,0}</math></b>	enthalpy of melting of 100% crystalline polymer

## **Chapter 1. Introduction**

### **1. 1 Background**

Therapeutic protein drugs have been receiving increasing attention by the pharmaceutical industry. Therapeutic protein drugs have shown great bioactivity and potential to replace conventional small molecule drugs in the treatment of several chronic diseases.<sup>1</sup> Due to their low oral bioavailability and short half-lives after administration, advanced and more sophisticated delivery approaches are needed to utilize their full potential.<sup>2</sup>

Topical injections or infusions are currently the most popular administration route for protein therapeutics.<sup>3</sup> However, under frequent injection regimes and high local protein drug concentrations, tissue reaction and hypersensitivity often occur.<sup>3,4</sup> An injectable controlled delivery system has been hypothesized to improve the efficacy of this delivery method and utilize the full protein bioactivity potential.

Biodegradable microspheres formulations have been extensively explored for applications of localized drug delivery and can provide effective drug protection during storage and release. Their small size and thus ready injectability as well as the tunable polymer properties that can influence the degradation and release kinetics make this device particularly advantageous for protein delivery.<sup>5</sup> Currently, the most commonly used biodegradable polymer for microspheres formation is poly(lactide-co-glycolide) (PLGA). PLGA has a glass transition temperature that is greater than body temperature and thus is mechanically irritating to the tissue.<sup>6</sup> In an effort to reduce tissue irritation, low melting point di-block copolymers of trimethylene carbonate and  $\epsilon$ -caprolactone initiated with poly(ethylene glycol) (PEG) have previously been prepared and shown to provide effective long term and highly bioactive growth factor delivery.<sup>7</sup> However, the degradation rate of these polymers was too long to be clinically useful.

This current study aimed to accelerate the degradation rate by synthesizing a low melting amphiphilic tri-block copolymer with limited crystallinity at body temperature and enhanced

hydrolytic lability. Copolymerized,  $\epsilon$ -caprolactone (CL) and glycolide (G) monomers with PEG diol were prepared using bulk ring-opening polymerization (ROP). The introduction of glycolide monomer had significant contribution to the reduction of the copolymer's crystallinity and degradation rate due to its greater hydrolytic lability compared to  $\epsilon$ -caprolactone.<sup>8</sup> PEG was introduced in effort to enhance the hydrophilicity of the copolymer, which could further enhance the degradation kinetics and improve its biocompatibility.<sup>9</sup>

Microsphere formulation was focused on creating a non-invasive local administration of the therapeutic chemokine protein stromal derived factor-1-alpha (SDF-1 $\alpha$ ). SDF-1 $\alpha$  is of interest because it has been found to facilitate stem cell recruitment and engraftment in ischemic sites.<sup>10,11</sup> Exogenous administration of SDF-1 $\alpha$  could benefit various clinical conditions and its susceptible nature and fragile structure makes it an excellent protein molecule to demonstrate the feasibility of the designed device.

## **1. 2 Scope**

The main aim of this study was to synthesize a copolymer that will have such thermal and physicochemical properties that could be utilized for the formation of injectable microspheres for localized protein drug delivery. Considering the characteristics required for a successful injectable system, low crystallinity and complete degradation were two of the main objectives of this research.<sup>12</sup> A random copolymer structure was particularly important for these two primary objectives to be addressed. A ring opening polymerization reaction was optimized in order to obtain random structures and high yields of P(CL-G)-PEG-P(CL-G) triblock copolymers, and copolymer composition variables were adjusted to achieve optimal copolymer thermal properties. The copolymers with the most suitable properties were evaluated for their ability to form shape stable microspheres at room temperature with soft and no tissue-irritating texture at body temperature. Degradation rate and pH of the internal and external environment of the microspheres was used to

further assess the suitability of the copolymers for protein encapsulation purposes. Protein encapsulation ability and ability of the microsphere matrix to control protein release rate was evaluated using a suitable model protein. A final SDF-1 $\alpha$  encapsulation and release experiment was performed based on the results from the release experiment using model protein. Lastly, the bioactivity of the released SDF-1 $\alpha$  protein was assessed using appropriate cell-based assays and was compared to the bioactivity of the SDF-1 $\alpha$  protein before encapsulation and release.

## **Chapter 2. Literature review**

### **2. 1 Therapeutic protein delivery**

Protein therapeutics show extremely specific and potent action against numerous diverse clinical conditions such as autoimmune diseases, tissue degeneration, ischemia, mental disorders, cardiovascular conditions, cancer and others.<sup>1</sup> Their type and action can vary from antibodies, enzymes, hormones and growth factors. Their numerous functions involve regulation of body biochemistry and control of chemical transport within the body.<sup>13</sup> They are highly specific in their actions *in vivo*, minimizing the side effects typically seen with small molecular weight drugs. For this reason, they are usually well tolerated and exhibit minimal immunogenicity when exogenously administered.<sup>14</sup>

#### **2. 1. 1 Protein structure-activity**

The specific function of proteins is mainly governed by their unique three-dimensional shape. Proteins are built of a long linear chain of amino acids sequences connected by peptide bonds. A combination of a set of 20 amino acids make up all existing protein molecules.<sup>15</sup> The specific sequence of amino acids, the length, and the intermolecular forces between amino acids along the polymer chain provide proteins with their unique shape and function.<sup>16</sup> Disulfide covalent bonds, hydrogen bonds, hydrophobic, electrostatic or van der Waals interactions within the same protein molecule contribute to the specific three-dimensional shape and folding patterns of proteins.<sup>16</sup> Most of these forces are relatively weak and can be easily disrupted by pH, ionic, or temperature strain causing changes in the protein molecule shape.<sup>16,17</sup> Their complex three-dimensional architecture is extremely critical for their highly specific and potent biochemical activity.<sup>1,18</sup> Any loss of those fundamental characteristics can make the protein inactive and possibly immunogenic *in vivo*.<sup>14</sup> This fragile nature significantly limits their application, and although therapeutic proteins

possess many significant advantages over conventional drugs, their full potential has still to be realized.

### **2. 1. 2 Issues in protein delivery**

The significance and contribution of protein therapeutics in the treatment of many clinical conditions has been validated by analyzing their mode of secretion and action when naturally produced *in vivo*.<sup>13</sup> A variety of protein factors are known to participate in various functions with respect to cell activity in the near proximity of the site from which they are secreted.<sup>19</sup> Specific stimuli, such as hypoxic shock, inflammation or injury, trigger the local expression of those proteins in very low concentrations that has shown to regulate specific interactions.<sup>20</sup> Although short term exposure in very limited concentrations to the therapeutic protein can be adequate to provide complete therapeutic ability in many acute conditions, localized activity and long-term exposure is necessary to provide an effective therapeutic level in many chronic conditions.<sup>21–24</sup> The main limitation of long-term exposure is that most of these proteins have very short half-lives in body fluids after secretion.<sup>25</sup> Therefore, it is very difficult to retain an effective concentration for prolonged time periods, as most of the potent therapeutic proteins stay bioactive for a few minutes to hours after production or administration.<sup>1,26,27</sup> Thus, exogenous administration regimens, which typically consist of multiple injections and very high concentrations of the bioactive molecules, have been investigated for long-term protein exposure. However, this administration strategy poses problems with patient compliance and possible complications due to non-clinical setting of administration.

Although this administration approach may cause immediate and local increase of protein concentration, a large portion of the protein's bioactivity may be eliminated before it can be utilized due to protein degradation.<sup>2</sup> There are some inherent protein properties, such as their large molecular size and susceptibility to undergo denaturation *in vivo* that set limitations to their administration through other conventional routes.<sup>18,28</sup> The most common administration routes, such



as nasal, oral, rectal, pulmonary and transdermal have shown poor bioactivity due to transport barriers limiting protein movement into the tissue or blood stream as well as enzymatic degradation in the tissues covering those organs.<sup>18,29,30</sup>

Oral administration possesses distinct advantages that make this route the most convenient and easy for patients to comply with their administration regimen.<sup>31</sup> The popularity of this method also has to do with the variety of oral formulations available and the ease to produce them with minimal cost. The limitations that make this method unsuitable for protein delivery is the enzymatic activity in the gastrointestinal tract that leads to proteolytic degradation of the administered protein drug.<sup>32</sup> Poor absorption and depleted bioactivity levels as low as 1% have been noted using the oral administration of proteins.<sup>31</sup> Nasal and rectal routes exhibit similar limitations due to enzymatic activity while respiratory membranes exhibit limited permeability to large molecules such as proteins.<sup>33</sup>

The parenteral (i.e. intravenous, subcutaneous or intramuscular injection) route has been the predominant method of choice for protein delivery due to the ease of administration, and the poor bioavailability of other routes.<sup>34</sup> Intravenous injections often lack targetability and show poor localization to the site of interest. Due to susceptibility to enzymatic degradation and short half-lives shortly after introduction *in vivo*, limited accumulation of the protein to the site of action is usually noted. Since most clinical conditions require long-term protein exposure to achieve a therapeutic level, frequent doses are necessary to maintain the minimum therapeutic concentration.<sup>28,35,36</sup> Such an administration scheme involves painful procedures over extended periods of time ranging from several days to months while constant medical supervision is required. This process incurs a high cost of treatment and a difficulty of the patients in complying with this frequent injections regimen. It has been recognized that great benefit would be provided by a controlled release system that could reduce the number of injections needed, protect protein molecules during release and improve the current protein delivery approach.

## 2. 2 Protein controlled release

Considering conventional administration methods, drug concentration profiles follow a pattern that has peaks and valleys within the therapeutic window between the minimum effective and minimum toxic concentration (MEC and MTC respectively) (Figure 2. 1).<sup>37</sup>

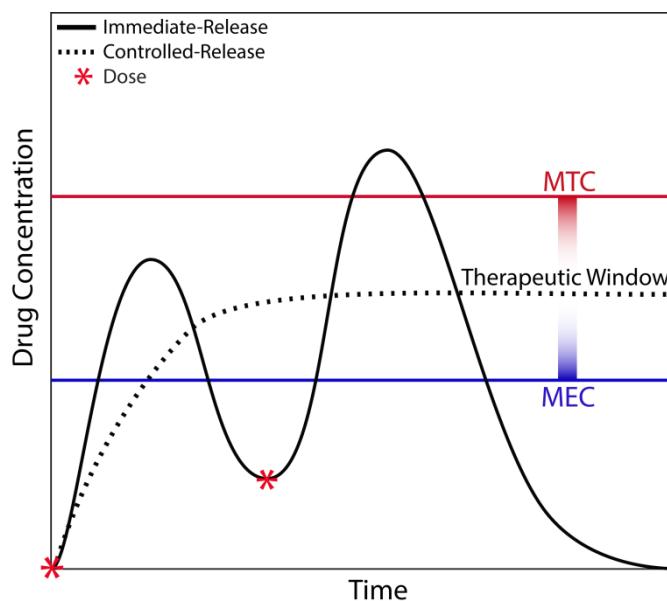


**Figure 2. 1** Illustration of the drug concentration curve after dosage and therapeutic window margins (MTC: minimum toxic concentration; MEC: minimum effective concentration).

To achieve a controlled concentration within this range using conventional drug administration systems, frequent doses with precise intervals must be provided for several days or weeks. Controlled release systems, on the other hand, can maintain the drug concentration within the therapeutic window minimizing the doses required. This way, possible side effects caused by high drug concentrations are eliminated, and maximum drug efficiency can be achieved.<sup>2</sup> A similar release approach would significantly benefit protein delivery by addressing issues such as the need for the release of bioactive molecules for prolonged periods with highly controlled concentrations.<sup>38</sup> Enhanced efficacy of localized administration could also be achieved using controlled release systems. Protein encapsulation into polymer matrices can provide a protective barrier between the

sensitive protein molecules and hostile external environments.<sup>39</sup> This way the bioavailability and stability of the protein is better retained until its release. .<sup>12,40,41</sup>

### **2. 2. 1 Protein encapsulation**

Protein encapsulation into polymer matrices has been developed to provide control over protein release as well as improve protein stability prior to being released. The encapsulation practice is capable of enhancing protein stability by minimizing its molecular mobility.<sup>22,42</sup> Constrained protein chain mobility minimizes the occurrence of chemical degradation due to deamidation, isomerization, oxidation, cleavage of disulfide bridges and  $\beta$ -elimination.<sup>43</sup> Protein chain mobility and flexibility are also highly influenced by water content, which has been well documented for its critical role in the degradation of biopharmaceuticals.<sup>44</sup>

Despite the potential advantages, protein encapsulation has always been extremely complex and challenging. The sensitivity of proteins towards chemical and physical stresses makes the formulation of consistent systems with stable dosage delivery and proven clinical safety extremely challenging. Unlike most conventional drugs that have relatively stable structures, proteins need more careful handling and sophisticated encapsulation methods to achieve similar structural integrity.<sup>13</sup>

Thus, protein controlled release studies mainly regard the development of effective encapsulation methods that involve minimum stresses against protein molecules that will retain most of its stability. The encapsulation practices, the forms and individual polymer and protein properties are parameters that need to be considered before designing a protein controlled delivery system. For example, the high temperatures applied in spray-drying are sufficient to hydrolyze peptide bonds, which can occur at temperatures as low as 80 to 100 °C.<sup>45</sup> Additionally, long-term exposure to aqueous environments, moisture, or aqueous-organic interfaces can also irreversibly affect protein

integrity.<sup>46</sup> Encapsulation into suitable and compatible polymer systems using mild encapsulation practices may be capable of protecting the protein drug against such physicochemical forces.<sup>14,39</sup>

### **2. 2. 2 Biodegradable polymers in protein delivery**

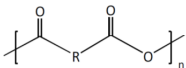
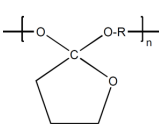
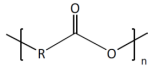
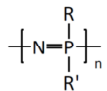
The necessity of local delivery for prolonged times may be addressed by using suitable injectable polymer depots that will continuously release the loaded protein drug after injection.<sup>41</sup> The release rate and mechanism are mainly governed by the specific properties of the polymers used, the properties of the loaded protein, as well as the biology of the site of injection.<sup>47</sup> All these parameters should be considered when designing a controlled delivery system.

The physical properties of the polymer system used as the protein delivery vehicle can be finely adjusted to provide comfortable and benign *in vivo* behavior after injection. It is considered necessary for the injectable systems to be able to provide a soft response to the natural activity of the host tissue. Rigid and brittle textures combined with shear stresses at the injection site can cause severe mechanical tissue irritation that could induce inflammation and a foreign body response.<sup>48</sup>

Aiming at eliminating the need for redundant surgical operations and other invasive treatment methods, biodegradable and biocompatible polymers with tunable properties and forms have emerged in the protein delivery area. Compared to non-biodegradable polymers, these materials prevail in injectable and implantable systems as there is no need for additional invasive procedure for the removal of the device after drug release. After the therapeutic purpose is complete, hydrolytic or enzymatic degradation mechanisms break the polymer down into products that can be excreted in the urine or feces, or that can be further broken down via metabolic biochemical pathways.<sup>49</sup> Biodegradable polymers have found application in the delivery of small low molecular weight drugs as well as large molecules such as proteins, hormones or other biotherapeutics.<sup>50,51</sup>

Several forms of biodegradable synthetic or natural polymers have been studied. The compatibility of the encapsulated protein within the polymer matrix is a major consideration when designing the delivery device. It is essential for the polymers to be able to retain the pharmacological properties of the loaded protein during encapsulation, storage and release and not to produce any substances that could be harmful or toxic to the surrounding tissues or which denature the loaded protein.<sup>52</sup> Some of the classes of biopolymers that have been investigated for protein delivery are natural collagen, alginate, hyaluronic acid and gelatin and synthetic poly(esters), poly(anhydrides), poly(saccharides) and poly(anhydrides) with the aliphatic polyesters holding a large portion of the popularity and applications (Table 2. 1).<sup>53</sup>

**Table 2. 1** Common polymers in controlled protein delivery, general structures, and some proteins explored.<sup>17,42,51,54</sup>

Class	Type	General Structure	Examples	Proteins released
Synthetic	Poly(anhydrides)			Insulin <sup>55,56</sup> , myoglobin <sup>57,58</sup> , lysozyme <sup>59</sup> , albumin <sup>60</sup> -immunoglobulin <sup>61</sup> , LHRH analogue <sup>62</sup> , Lysozyme <sup>63</sup> , Albumin <sup>63</sup> , VEGF <sup>63</sup>
	Poly(ortho esters)			
	Poly(esters)		Poly(lactic acid) (PLA)	HSA <sup>64</sup> , insulin <sup>65</sup> , LHRH <sup>66</sup> , albumin <sup>67</sup> , BMP <sup>68</sup>
			Poly(lactic-co-glycolic acid) (PLGA)	IL-2 <sup>69</sup> , insulin <sup>70-72</sup> , BSA <sup>73,74</sup> , myoglobin <sup>75</sup> , BPM-2 <sup>76</sup> , VEGF <sup>77</sup>
			Poly(caprolactone) (PCL)	BSA <sup>78</sup>
	Poly(phosphazenes)			<sup>79</sup> , Insulin <sup>135</sup>
Natural	Proteins		Albumin gelatin	Insulin, IIF-2, IFNα <sup>80</sup> , albumin <sup>81</sup> , IFN-γ <sup>82</sup> , FGF <sup>83</sup>
			collagen	TGF-β <sub>1</sub> <sup>84</sup> , NGF <sup>85</sup> , insulin <sup>86,87</sup>
	Poly(saccharides)		Starch cellulose chitosan dextran alginic acid	IFNα, albumin, Lysozyme, Immunoglobulin <sup>88</sup>

### **2. 2. 3 Microsphere delivery systems**

Biodegradable polymers are predominantly applied in systems that need to be implanted or injected as they do not require invasive procedures and revisions after implantation.<sup>89</sup> Various types of biodegradable microparticles have been explored as injectable depots for protein delivery. The type, chemistry and form of the polymers used can vary to fulfill the needs of each particular protein and release rate required.

#### **2. 2. 3. 1 Microparticles**

Microparticles or microcapsules have been one of the most successful candidates for protein drugs. Microparticles offer prolonged and adjustable release profiles. Special attention has been paid to this type of delivery device as it can be formed using a variety of fabrication methods and a variety of natural and synthetic polymers.<sup>41,90,91</sup> Their small size and injectability in combination with the ability to effectively control drug release rates, by adjusting the size, surface, porosity or chemical composition, have made this formulation extremely popular for localized drug delivery to a variety of body sites.<sup>92 93,94</sup>

The number of fabrication methods allows for a proper encapsulation of sensitive molecules with minimum structural and bioactivity changes. Spray drying,<sup>95</sup> double emulsion<sup>96,97</sup>, electrospraying,<sup>94</sup> and solvent extraction/evaporation<sup>98,99</sup> techniques are some of the methods that have been utilized to prepare protein-loaded microspheres. The method used must retain the biological and structural stability of the protein drug while having a good encapsulation efficiency ( $E \geq 80\%$ ) and high yield of microparticles to be practically applicable for larger laboratory or industrial production. Most of these techniques result in solid particles with solid dispersion of protein particles evenly distributed in the polymer matrices of the microspheres.<sup>100</sup> The ability of the encapsulation of protein molecules in their solid state has been shown to provide great stability and protection over protein

denaturation during storage and delivery. Enhanced bioactivity has been observed in solid encapsulated proteins compared to solution administration forms.<sup>101,102</sup> Polymer matrix encapsulation also provides an effective barrier from external conditions that might affect protein stability such as moisture and ionic activity.

Poly(lactic-co-glycolic acid) (PLGA), poly(glycolic acid) (PGA) and poly(lactic acid) (PLA) are the most commonly studied synthetic polymers used for microspheres. PLGA has been the gold standard for injectable microspheres formulations, probably because many implantable devices containing polymers made using lactic and glycolic acid have been approved by the FDA, and thus a significant number of toxicological, histological, chemical and biodegradation data are available for these materials.<sup>103</sup>

Although PLGA has already found commercial application as a drug and peptide carrier, protein delivery is still a challenge.<sup>41</sup> The release of the encapsulated drugs is mainly governed by hydrolytic degradation of the PLGA polymer. The hydrolytic degradation mechanism produces glycolic and lactic acid monomers and oligomers.<sup>103</sup> These acidic degradation products may need a long time to diffuse out of the device. As a result, the pH of the microclimate inside the polymer bulk as well as the external environment of the matrix is lowered, and microclimate pH's of from 1.5 to 4.8 have been reported.<sup>104</sup> These conditions can accelerate the degradation process and affect the integrity of the loaded drug causing its denaturation. Such low pH values can also trigger inflammation of the surrounding tissue and cause significant losses in the mechanical strength of the device.<sup>14,1057</sup> Moreover, the crystalline and brittle texture of PLGA often causes irritation in the local injection site.<sup>7</sup> Approaches such as copolymerization with hydrophilic copolymers have been explored in order to limit the acidic degradation effects while exploiting all the beneficial characteristics of the homopolymers.<sup>49,106,107</sup>

### **2. 2. 3. 2 Protein release mechanisms**

For drugs encapsulated in polymer vehicles, the physicochemical properties of the polymer matrix and the compatibility with the properties of the drug influence the release mechanism.<sup>108</sup> Diffusion, swelling and osmotic pressure forces, drug/polymer and drug/water miscibility and thermodynamics of the drug/polymer system are some of the factors that must be considered when designing a drug delivery system. Degradation of the biodegradable vehicle can also significantly influence the release rate from the vehicle.<sup>51</sup>

Hydrophilic drug release from delivery systems made from hydrolytically degradable polymers such as PLGA, usually follow a triphasic release scheme (Figure 2.2).<sup>109,110</sup> The initial burst phase, which can last a few hours, one day or even several days, is attributed to the drug that is exposed at the surface of the device. After the initial burst phase, a lag phase follows where a slower drug release is observed, which is due to the diffusion of the water into the bulk of the polymer device. Slow polymer erosion might also take place in this phase. The third and last phase exhibits a quick release due to polymer erosion and both polymer and drug are continuously released.<sup>41,47</sup> Although this profile is very common, there are formulations with less distinct triphasic release profile and instead only one or two of these phases might be noted during release.<sup>111</sup>



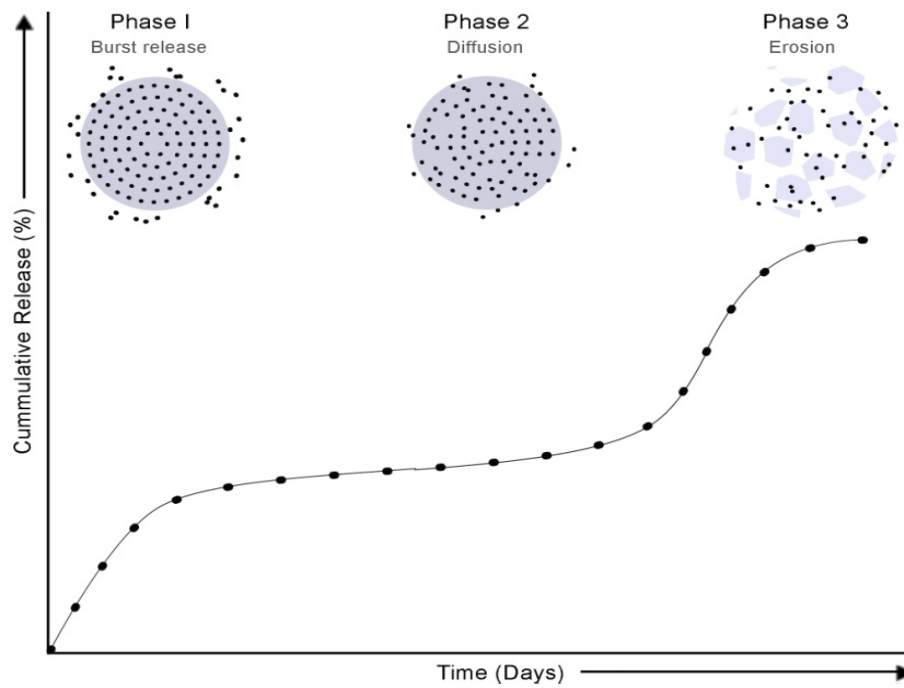


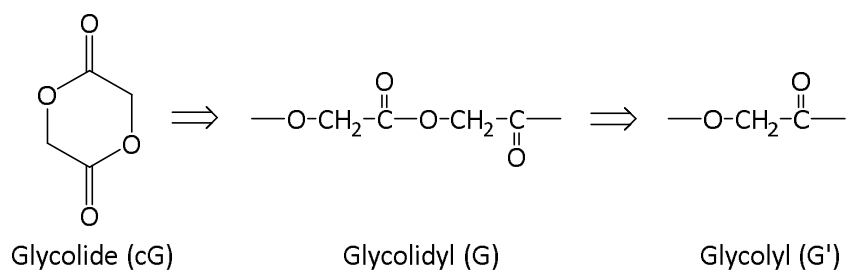
**Figure 2. 2** Representative triphasic release profile from PLGA microspheres. Phase I shows high burst release, phase II shows the diffusion-controlled release and phase III shows the fast release rate due to the polymer matrix erosion.<sup>47</sup>

## 2. 3 Effect of copolymerization on polymer properties

Ring-opening polymerization (ROP) is a very versatile synthetic route for copolymers of cyclic esters and lactones that has sensitive reaction equilibrium, depending on the thermodynamics and reactivities of the individual monomers involved.<sup>112,113</sup> Bulk ROP reactions are particularly affected by temperature and reaction time and such factors are often modified appropriately to optimize the polymerization product.<sup>114</sup>

Copolymerization of monomers with different properties and reactivities requires optimization in order to achieve effective polymerization degrees with suitable composition and molecular weight control.<sup>113</sup> It is also essential that the chemical and thermal stability of the monomers and the obtained copolymers are taken into consideration and appropriate measures taken while optimizing the conditions of a polymerization reaction.

In the copolymerization of  $\epsilon$ -caprolactone (CL) and glycolide (cG) two transesterification modes of glycolide in the copolymer take place.<sup>115</sup> The first mode involves bond cleavage between glycolidyl units (G) originating from different diglycolyl molecules, which results in the formation of CL-G sequences with an even number of glycolyl units (G'). In contrast, during second mode transesterification (Scheme 2. 1) cleavage of glycolidyl units (G) originating from the same diglycolyl molecule occurs which leads to the formation of CL-G sequences with an odd number of glycolyl units (G') as well as CL-G'-CL chain sequences. This effect is reflected in the  $^1\text{H}$  NMR spectra of the copolymers and can be utilized to determine the microstructure of the copolymer chain as well as the degree of randomness.<sup>115-117</sup>



**Scheme 2. 1** Ring-opening and acyl-oxygen cleavage of glycolide ring (cG).

Analysis of the proton NMR of the copolymerized  $\epsilon$ -caprolactone and glycolide indicated that their characteristic proton peaks differed significantly from those in their homopolymers. The resonance of the methylene protons adjacent to the carbonyl group is sensitive to microstructural changes in the copolymer chain.<sup>117</sup>

Kasperczyk et al. have extensively studied the microstructures of lactone copolymers and have also analyzed the microstructures obtained from bulk polymerization of glycolide with  $\epsilon$ -caprolactone. They were able to perform a detailed microstructural analysis and determine the degree of randomness from both proton and carbon NMR spectroscopy.<sup>115,116,118</sup>

The same analytical procedure has also been established by Dobrzynski et al., in a comparative study of the monomer reactivities.<sup>115,116</sup>  $^{13}\text{C}$  and  $^1\text{H}$  NMR spectroscopy were used to study the microstructural changes and the sequences of the monomer units. These studies were used for the assignment of the monomer unit sequences to the individual peaks observed in each  $^1\text{H}$  NMR spectrum obtained.

The secondary transesterification can be particularly beneficial for copolymers of glycolide. Glycolide oligomers and homopolymers as well as their poly(glycolyl) blocks in copolymerized formulations have very poor solubility in all organic solvents and exhibit high crystallinity with a melting point at 220 °C.<sup>117,119</sup> High concentrations of alternating monomer units and random sequences in the copolymer can result in more amorphous structures and eliminate the crystallinity of PG segments

completely. Random structures are also beneficial to the crystallization efficiency of the other components in the copolymer as glycolyl units hinder the ability of the polymer chain to form perfect crystals.<sup>116,118</sup>

In terms of degradation ability, glycolide homopolymers exhibit much faster degradation rates than do  $\epsilon$ -caprolactone homopolymers.<sup>115,119</sup> Therefore, an even distribution of glycolide monomer units within the copolymer blocks will increase the degradation rate of the copolymer. This faster degradation results from a higher hydrolytic susceptibility of the glycolidyl units and from the reduction in the crystallinity of those segments.<sup>49</sup>

The exact monomer sequence in the copolymer formed is sensitive to the monomer ratios and their individual reactivities.<sup>113</sup> Furthermore, the reactivity of ring monomers highly depends on their thermodynamic equilibrium between their closed ring monomer state and the open polymerization state.<sup>113</sup> Thermodynamic studies have shown that a higher number of acyl units in a ring monomer pushes the equilibrium towards the cyclic monomer state as it is characterized by low strain. In copolymerizations, even small difference in reactivities can propagate during polymerization and form more blocky structures. This can be controlled by changing the conditions of polymerization that affect the thermodynamic equilibrium of the individual monomers.<sup>113,114</sup>

However, thermodynamic polymerizability does not absolutely correlate with the monomer's reactivity. In order to evaluate polymerizability both polymerization and back depropagation reactions should be considered, with the latter being more dependent on the ring monomer strain than its thermodynamic properties.<sup>114</sup>

## 2. 4 SDF-1 $\alpha$ protein

Stromal cell-derived factor-1 $\alpha$  (SDF-1 $\alpha$ ) was selected to demonstrate the feasibility of this delivery strategy. SDF-1 $\alpha$  is a small (molecular weight = 10.6 kDa, isoelectric point = 9.9) chemokine protein that is locally and constitutively secreted to regulate numerous physiological processes *in vivo*. SDF-1 $\alpha$  can be found in several organs but undergoes rapid proteolytic degradations and therefore has a very short half-life *in vivo* that has been estimated at  $25.8 \pm 4.6$  min by Misra et al.<sup>120–122</sup>

The upregulation of SDF-1 $\alpha$  has been recently correlated with the occurrence of ischemic injury. It has been shown to be an important pro-angiogenic and anti-apoptotic chemokine that plays a significant role in cell survival and recruitment after ischemic injuries.<sup>123</sup> Increased expression in ischemic brain, kidney, heart and skeletal muscle of ischemic limb indicates the molecular mechanism that induces its expression. It has been determined that hypoxia inducible factor-1 (HIF- $\alpha$ ) acts as the signaling protein for the secretion of chemokine SDF-1 $\alpha$  and its receptor CXCR4.<sup>11,124</sup> The amount of SDF-1 $\alpha$  produced is proportional to the amplitude of hypoxic factors expressed and rapidly increases immediately after the loss of blood supply.<sup>11</sup>

The most important role of this pro-angiogenic chemokine is to act as a chemoattractant for cell migration, homing and engraftment.<sup>125</sup> It has also been shown to regulate cell proliferation, anti-apoptotic activity and contribute to the stabilization of new vessels during neovascularization by recruiting bone marrow-derived stem cells.<sup>123,126</sup> Epithelial progenitor cells (EPCs), known for their ability to repair damaged tissue, have been found to be recruited to ischemic sites driven by SDF-1 $\alpha$ /CXCR4 signaling. However, the success of this mechanism relies on the retention of both signaling and progenitor cells at the site of injury.<sup>123</sup>

SDF-1 $\alpha$  is naturally produced by cells in local ischemic sites after their occurrence of injury and remains upregulated for up to a week.<sup>127</sup> The maximum concentration of SDF-1 $\alpha$  has been mainly reported at 24 hours post-injury with a decreasing tendency thereafter.<sup>10,127,128</sup> Some studies have

reported secretion of this chemokine for up to 4 weeks, but in the majority of studies the concentration after seven days is significantly limited so as to be undetectable.<sup>129–131</sup> The bioactivity levels of SDF-1 $\alpha$  has been extensively studied *in vitro*, using cell migration assays on mesenchymal stem cells (MSCs).<sup>132–134</sup> In the majority of the studies, the concentrations that exhibited highest bioactivity were determined to be between 10 to 200 ng/mL, with 100 ng/mL providing the maximum efficacy.<sup>128,135–138</sup> It is proposed that prolonged delivery within this therapeutic window for a target period of 2 to 3 weeks could promote significant angiogenic function and tissue regeneration.

The administration of SDF-1 $\alpha$  protein as a potential therapy to enhance angiogenesis has been proposed for the treatment of a number of diseases, including ischemia and severe inflammation. Co-delivery with progenitor cells has also been also proposed in order to enhance the efficacy of this approach. However its potential, it exhibits a limited half-life in plasma, undergoing significant enzymatic degradation, which prohibits an efficacious accumulation and therapeutic activity.<sup>120</sup> Concerns regarding its short half-life due to proteolytic degradation *in vivo* are addressed by exploring advanced delivery vehicles that could sustainably release and protect SDF-1 $\alpha$  after delivery. Furthermore, encapsulation can provide protection against ischemic environments that can become particularly hostile for such proteins as they exhibit higher enzymatic activity due to inflammation and pH that are often slightly acidic (pH~6).<sup>139</sup> Controlled and sustained release of SDF-1 $\alpha$  has been suggested and explored in the present study in order to protect SDF-1 $\alpha$  from external forces and retain its bioactivity. Localized delivery with an injectable microsphere system may further enhance the efficacy of this approach.

### Chapter 3. Proposed approach

Protein delivery via injectable polymer systems has already been the subject of several studies. However, most of the polymers examined had only partially successful, if not insufficient, results. The prevalent systems have been PLGA microsphere based, having been studied for delivery of growth factors and other proteins.<sup>69,75,103</sup> However, because of the limitations of using PLGA another promising material that has been studied for the formulation of appropriate microspheres has been a triblock copolymer composed of poly(trimethylene carbonate-co- $\epsilon$ -caprolactone)-block-poly(ethylene glycol)-block-poly(trimethylene carbonate-co- $\epsilon$ -caprolactone), which exhibited no alteration of pH during its degradation. Unfortunately, the hydrolytic degradation rate of this copolymer was very slow, being greater than one year.<sup>7</sup>

A possible solution to current microsphere material limitations was explored in this research endeavor. The limitations were addressed by the design of a polymer matrix with suitable properties and compatibility with the physicochemical properties of the protein, which would ensure retention of the protein's bioactivity. Such a synthetic drug delivery vehicle should have similar mechanical behavior with the native surrounding tissue to avoid irritation. Simultaneously, it must possess sufficient structural stability to protect the delivered cells during storage, injection, and sustained release at the targeted tissues.<sup>140–142</sup> The need for such a new composition of materials was addressed by using two monomers used to prepare polymers with extensive clinical histories, glycolide and  $\epsilon$ -caprolactone, along with poly(ethylene glycol).<sup>49,143,144</sup>

An assortment of low molecular weight (6.5-25 kDa) copolymers was prepared from PEG, glycolide (G) and  $\epsilon$ -caprolactone (CL). Each of the three homopolymer structures used in this study individually contributed to the final formulation requirements. Thus, polymer architectures were achieved with a suitable degradation rate for the application, a melting point close to body temperature, a low crystallinity percentage allowing for appropriate release rates, and the ability to form stable microspheres transferable by injection through a carrier gel into any site of the patient's body. Major

issues and limitations of current microspheres materials addressed in this study were (i) acidic degradation products, (ii) slow degradation, (iii) brittle texture at body temperature, and (iv) slow or incomplete protein release.

PEG is highly hydrophilic and has excellent biocompatibility with limited *in vivo* response.<sup>145,146</sup> Due to its hydrophilic nature it tends to become oriented at the surface of microspheres when immersed in a polar solvent such as water. This configuration holds several advantages for *in vivo* applications and most importantly it has been found to reduce the likelihood of immune responses after implantation.<sup>147</sup> The incorporation of PEG in drug delivery systems has been applied either by copolymer formulations or as a coating agent. Coating has been shown to inhibit opsonization but also enhances water solubility of the materials.<sup>148</sup> It is well established that polymer mixtures with PEG show reduced protein adsorption and limited non-specific interactions *in vivo* that could induce an immune response.<sup>149</sup> In this current study, PEG plays also an important role in the handling ability of the materials as it provides additional crystallinity and stability at room temperatures yet due to its hydrophilic nature it forms soft materials with low melting temperature and crystallinity after injection at 37 °C. This room temperature crystallinity also accommodates an easy formulation and good stability of the microspheres while increasing water penetration within the hydrophobic P(CL-G) regions. Enhanced hydrophilicity could improve the degradation rate and, subsequently, the rate of protein release. Furthermore, PEG minimizes ionic interactions by steric stabilization that limits protein aggregation within the particles.<sup>150</sup> Two different molecular weights of PEG were explored in this study: 4000 and 1500 Da. Both PEG grades were solid at room temperature but softened upon implantation, providing handling ability at room temperature but a soft and non-irritating texture at physiologic temperature in water.

Poly( $\epsilon$ -caprolactone) (PCL) is a high crystalline polymer that also allows for easy handling at room temperature. It is highly biocompatible and exhibits good biodegradability, although at a relatively slow rate that for microsphere formulations can range from several months to a year depending on



the size of the microspheres and the molecular weight of the polymer.<sup>151,152</sup> The low melting point (60 °C) and the low glass transition temperature (-60 °C) make it a superb microsphere material candidate.<sup>153,154</sup> The slow degradation of PCL can be significantly increased by copolymerizing caprolactone with glycolide. Poly(glycolide) (PGA) is characterized by much faster degradation rates.<sup>113</sup> When copolymerized with caprolactone, glycolide would also interfere PCL block interactions, hindering their crystallization ability. This effect reduces the melting point and the degree of crystallinity while enhancing the water permeability of the copolymer.<sup>155,156</sup> All these factors will shorten degradation times via hydrolysis. Slow diffusion and accumulation of glycolic acid during hydrolytic degradation could potentially create an acidic microclimate environment inside the microspheres. However, the efficient wettability of the copolymer due to the presence of PEG may provide a potential diffusion-based control of the copolymer's degradation products. The amphiphilic nature of the copolymer was proposed to provide effective dispersion of the microparticles in aqueous medium. Moreover, the hydrophilic PEG blocks would improve the water solubility of the degradation products providing for their effective clearance from the degrading microparticle.

A previously employed electrospraying technique was used to fabricate the microparticles.<sup>7</sup> Electrospraying gives the ability to generate high yields of polymer microparticles with narrow and well controlled size distribution.<sup>157</sup> The principle of this formulation technique is based on the ability of an electric field to change the interfacial area at a droplet formation process.<sup>158</sup> During the droplet formation of a dense polymer solution flowing out of a nozzle tip, an applied charge at the end of the nozzle can electrostatically force the meniscus to form a jet of droplets.<sup>159</sup> The voltage intensity can influence the size of the droplets produced.<sup>157</sup> The resulted droplets are collected in a cold collector solution grounded with an aluminum plaque immersed in the solution and connected to the grounding electrode (Figure 3. 1). Specific parameters including the polymer solution concentration, the intensity of the voltage applied, the distance of the tip of nozzle from the collector solution and the flow rate of the solution can be modified to control the size of the microparticles produced.<sup>160</sup> For protein and drug encapsulation, solid particles of the active substance can be dispersed in the

polymer solution prior to electrospraying. Very high encapsulation efficiencies with values varying from 65 to 90 % have been reported in the majority of the studies using electrospraying as encapsulation method.<sup>157,158,161</sup>

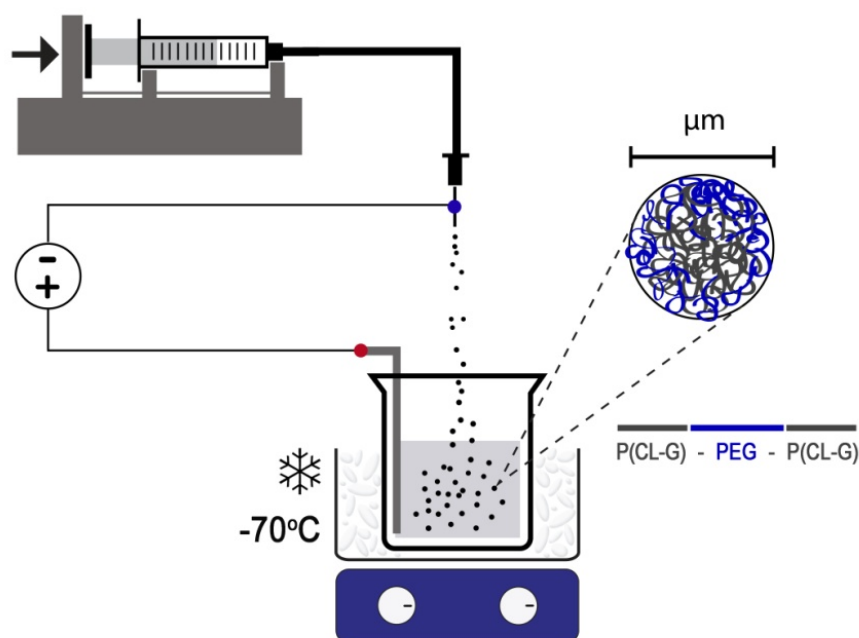


**Figure 3. 1** Electrospraying apparatus for fabrication of microspheres.

Among the advantages of this fabrication method, the most important are the lack of aqueous-organic interfaces and physicochemical stress (temperature, pressure, pH, etc.) that could compromise the stability of the protein. In addition, a small amount of organic solvents is needed during the formulation process and the solid-state protein particles encapsulation has shown improved protein stability during storage and release.<sup>162</sup>

## Chapter 4. Objectives

The main objective of this study was to prepare polymer microspheres for SDF-1 $\alpha$  encapsulation and delivery by injection. The polymers to be used require important features to allow for effective release of the bioactive therapeutic protein as well as physical properties that would facilitate their biodegradability with minimum adverse effects. A previously established electrospraying technique was used to prepare protein loaded microspheres possessing an average microsphere diameter small enough to be injectable yet sufficiently large to provide control over protein release.

Thus, the specific objectives were as follows:

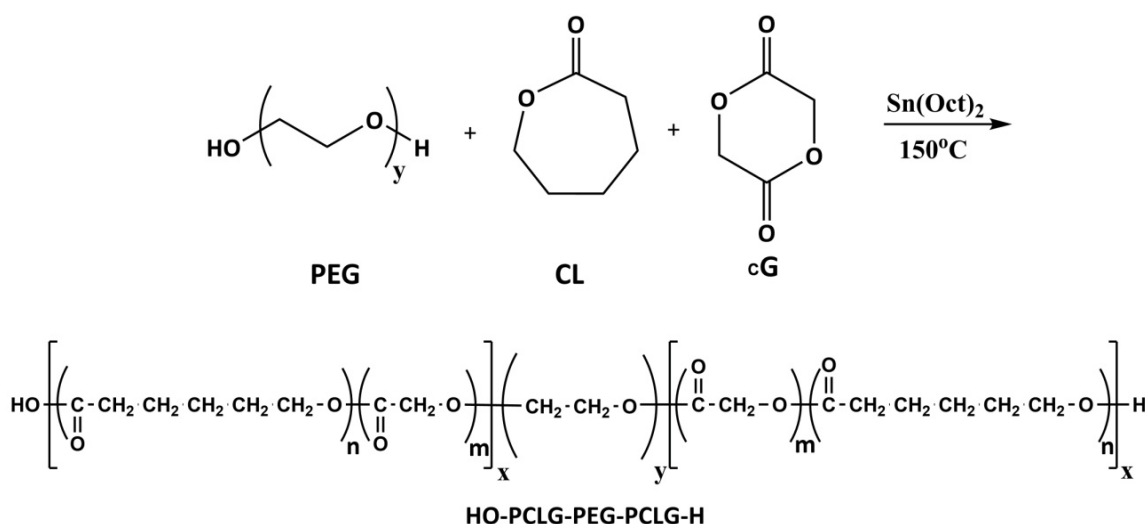
1. To synthesize PEG-P(CL-G)<sub>2</sub> amphiphilic copolymers exhibiting low crystallinity above 37 °C, that are soft at body temperature yet possess good handling ability at room temperature.
2. To use these polymers to prepare microspheres using an electrospraying technique.
3. To achieve a microsphere degradation time of from 6 to 8 weeks, with minimum acidic degradation product accumulation within the microspheres.
4. To study the *in vitro* release of lysozyme model protein and assess the effect of varying parameters (loading rate, additives and so on) on the kinetics of release.
5. To assess the feasibility of this delivery strategy using a therapeutically relevant protein SDF-1 $\alpha$ .

## Chapter 5. Tri-block copolymer synthesis

### 5. 1 Introduction

The aim was to synthesize copolymers that would be suitable for the fabrication of injectable microspheres. A successful candidate for this application would have a melting close to body temperature and minimum crystallinity above 37 °C. To impede the crystallization of the copolymers a random monomer distribution was necessary. This random distribution would also facilitate the degradation of the copolymers.

ABA tri-block copolymers were prepared using the one step ring opening polymerization (ROP) of  $\epsilon$ -caprolactone (CL) and glycolide (G) monomers with either PEG 4000 or PEG 1500 diols as initiators and tin(II)-2-ethylhexanoate ( $\text{Sn}(\text{Oct})_2$ ) as the catalyst (Scheme 5. 1). The CL-G blocks were targeted to be identical in length with CL:G molar ratios varying from 1:1 to 12:1. The total target molecular weights ranged between 6.5 and 25 kDa while the molar ratio of the total monomers to PEG (M:PEG) for both PEG4000 and PEG1500 initiated copolymers was around 52.4:1.



**Scheme 5. 1** Ring opening polymerization reaction of  $\epsilon$ -caprolactone, glycolide and PEG diol using tin(II)-2-ethylhexanoate [ $\text{Sn}(\text{Oct})_2$ ] as catalyst.

## 5. 2 Materials

Poly(ethylene glycol) diol (Mn 4000 Da) (PEG4000) and poly(ethylene glycol) diol (Mn 1500 Da) (M.W.1500Da) (PEG1500),  $\epsilon$ -caprolactone (CL), 1,8-diazabicyclo[5.4.0]undec-7-en (DBU) catalyst (98%) and anhydrous toluene were purchased from Acros Organics, USA. Unless otherwise described, poly(ethylene glycol) diols were used after drying at 40 °C under vacuum for 12 h. Hydrochloric acid, acetic acid, dichloromethane (DCM), methanol and diethyl ether were from Fisher Scientific, Canada. Tin(II)-2-ethylhexanoate [Sn(Oct)<sub>2</sub>], 96% was purchased from Alfa Aesar, USA and glycolide was purchased from Altasorb, USA. The chloroform-d, 99.8%, was from Sigma-Aldrich, Canada.

## 5. 3 Methods

### 5. 3. 1 Bulk ring-opening polymerization

Polymerization was carried out in oven-dried glass ampoules with appropriate amounts of monomers and PEG weighed directly into the ampoule. The empty ampoules were filled with argon gas prior to weighing. After addition of the monomers and PEG, the ampoules were capped with aluminum foil and placed in an oven at 110 °C until all components were melted. At that point, the ampoule was taken out of the 110 °C oven and an appropriate volume of the catalyst solution was added directly to the melted mixture of PEG and monomers. A concentration of 1 mmol of catalyst for each mol of monomer was used in the polymerizations. To facilitate catalyst addition, a tin(II)-2-ethylhexanoate catalyst solution (dilution factor = 1:3.5) in dry toluene was prepared. Argon gas was immediately gently blown into the ampoule. A polymer vacuum tube was then attached on top of the ampoule and a vacuum of approximately 4 kPa applied. The contents were mixed on a vortex mixer under vacuum, which also allowed the toluene introduced with the catalyst solution to evaporate. The ampoule was then flame sealed, and placed at 150 °C in an oven for 2.5 h. Vortex mixing was applied every 20 min to ensure an even monomer distribution during the polymerization reaction. Vortex time was kept very short (5 s) to prevent significant temperature drop while the ampoule was out of

the oven. After polymerization, the glass ampoule was snapped open and the polymerization reaction was stopped by dissolving all contents in cold DCM.

### **5. 3. 2 Copolymer composition variables**

The molar ratio of the two monomers used greatly influenced the physicochemical properties of the polymer. In order to find an optimum composition with the required thermal properties, different monomer molar ratios of CL and G were evaluated. The feed monomer ratios were expressed as molar CL:G ratios. Although CL was the dominant monomer in most of the copolymers produced, ratios studied ranged from 1:1 to 12:1 for CL:G, respectively for PEG4000 initiated polymers with total MW of 10 kDa.

The total molecular weight can be used to control the amphiphilicity and thermal properties of the copolymers. For the purpose of this study the molecular weight of the hydrophilic part (PEG) and the CL:G ratio of the hydrophobic part were kept constant at 4000 Da and 3:1, respectively, and only the total molecular weight of the copolymers was varied in order to adjust the copolymer's hydrophilicity. Four different total molecular weights were produced: 6.5, 10, 15, 20 and 25 kDa.

Another parameter varied was the molecular weight of the PEG initiator. Two different number average molecular weights were used: 4000 and 1500 kDa. Three different CL:G ratios were studied in these series, specifically 1:1, 3:1 and 6:1. The reaction time was appropriately adjusted in order to obtain hydrophobic CL-G blocks at each side of the PEG diols with a molecular weight of 3 kDa. Thus, only the molecular weight of the hydrophilic PEG and the CL:G ratio was varied.

Additional experiments were carried out with the use of PEG 1500 as initiator to synthesize copolymers with higher molecular weights to analyze the effect of total molecular weight. CL-G blocks with molecular weights of 5 and 10 kDa sides were produced.

The compositions of the copolymers produced are summarized in Table 5. 1. All samples were analyzed via proton nuclear magnetic resonance spectroscopy ( $^1\text{H}$  NMR). The effects of composition on thermal properties and percentage crystallinity of the prepared copolymers were evaluated using a differential scanning calorimeter (DSC).

**Table 5. 1** Summary of copolymers synthesized.

No	MW of PEG (Da)	CL:G	Mn target (kDa)	Polymerization conditions
C1	4000	1:1	10.0	150 °C, 2.5 h
C2	4000	2:1	10.0	150 °C, 2.5 h
C3	4000	3:1	10.0	150 °C, 2.5 h
C4	4000	4:1	10.0	150 °C, 2.5 h
C5	4000	5:1	10.0	150 °C, 2.5 h
C6	4000	6:1	10.0	150 °C, 2.5 h
C7	4000	8:1	10.0	150 °C, 2.5 h
C8	4000	10:1	10.0	150 °C, 2.5 h
C9	4000	12:1	10.0	150 °C, 2.5 h
C10	4000	3:1	6.5	150 °C, 2.5 h
C11	4000	3:1	15.0	150 °C, 2.5 h
C12	4000	3:1	20.0	150 °C, 2.5 h
C13	4000	3:1	25.0	150 °C, 2.5 h
C14	1500	1:1	7.5	150 °C, 2.5 h
C15	1500	3:1	7.5	150 °C, 2.5 h
C16	1500	6:1	7.5	150 °C, 2.5 h
C17	4000	1:1	10.0	110 °C, 24 h
C18	4000	2:1	10.0	110 °C, 24 h
C19	4000	3:1	10.0	110 °C, 24 h
C20	4000	1:1	10.0	130 °C, 6 h
C21	4000	2:1	10.0	130 °C, 6 h
C22	4000	3:1	10.0	130 °C, 6 h
C23	1500	3:1	11.5	150 °C, 2.5 h
C24	1500	3:1	21.5	150 °C, 2.5 h
C25	4000	3:1	10.0	Solution, 25 °C, HCl/Et <sub>2</sub> O
C26	4000	1:1	10.0	Solution, 25 °C, DBU
C27	4000	3:1	10.0	Solution, 25 °C, DBU

### 5. 3. 3 Purification

To purify the prepared copolymers from unreacted monomers and the tin catalyst, the polymer in DCM solution was poured into – 20 °C methanol to precipitate the polymer. The mixture was kept at

-20 °C overnight and was then centrifuged at 3200 rpm for 5 minutes.<sup>1</sup> The supernatant was decanted and the process was repeated once more. The obtained purified polymer was dried at 50 °C under vacuum overnight and then air dried at ambient temperature for two more days.

### **5. 3. 4 Molecular weight fractionation**

Readily water soluble oligomers were removed by mixing the dry copolymer with distilled water at room temperature at a concentration of 25% w/v. The two phases were gently mixed using a spatula to form a wet paste. The aqueous phase was decanted and the process was repeated. The remaining polymer was then lyophilized and used for subsequent analysis.

### **5. 3. 5 Optimization of bulk polymerization**

The polymerization was conducted at three different temperatures, 110, 130 and 150 °C, to study the effect of temperature on the monomer and polymer stability, the resulting copolymer distribution, and the control on molecular weight and composition. The duration of the polymerization reaction varied accordingly to ensure complete monomer conversion and high yield.

### **5. 3. 6 Other polymerization methods explored**

#### ***5. 3. 6. 1 Polymerization in solution using DBU organic catalyst***

Synthesis of selected polymer compositions produced above was also performed using an organic catalyst. 1,8-Diazabicyclo[5.4.0]undec-7-ene (DBU) organic catalyst was used at concentrations of 0.5 and 1% of total monomer moles. Monomer feed ratios of 3:1 and 1:1, a final total molecular weight of 10 kDa, and PEG 4000 as initiator, were used to evaluate the efficiency of DBU as a polymerization catalyst at ambient temperature.



The reaction took place in 20 mL flame-dried screw-capped glass vials containing magnetic stirrers, and stirred on a stirring plate at 300 rpm. Both of the monomers and the initiator were dissolved in DCM at a concentration of 25% w/v under an argon atmosphere prior to the incorporation of the catalyst and stirred constantly. Typically, 1% w/w DBU catalyst per monomer is required for the ring opening polymerization of lactones and cyclic esters.<sup>163,164</sup> A dilute DBU solution (5% v/v) in DCM was used to transfer the catalyst drop-wise into the monomer/PEG solution under stirring. After incorporation of the catalyst, argon gas was gently blown into the vial and the vial screw capped. Argon gas was constantly blown into the vial while the vial was open. Samples from the polymerization mixture were taken at 2, 4, 6, 8, and 24 h. The samples were subjected to <sup>1</sup>H NMR analysis for composition assessment and analyzed via DSC for determination of thermal properties.

#### **5. 3. 6. 2 Polymerization in solution using HCl-Et<sub>2</sub>O system as catalyst**

Polymerization in solution with HCl as a catalyst was also used in an effort to avoid the use of the organometallic catalyst. Furthermore, because HCl catalyzed ring opening polymerization can be carried out at reduced reaction temperatures, an attempt was made to obtain the same copolymer compositions at room temperature as with the organometallic catalyst at elevated temperatures. For these reactions, the PEG (M<sub>n</sub> = 4000 g/mol) initiator needed to be completely dry as water can act as a competing initiator and the monomers are more susceptible to hydrolysis in the presence of HCl. PEG diol was dissolved in 50 mL toluene within a 100 mL flat bottom round reaction flask. The solution was azeotropically distilled under atmospheric pressure to remove water from the PEG. The toluene was then also removed by distillation. The CL and G were introduced into the flask and dry DCM was added. The reaction was initiated by the addition of 1.0 M HCl in diethyl ether (5 mL, 5 mmol) and stirring was applied at 200 rpm at room temperature overnight. After 24 h, the reaction mixture was poured into hexane to precipitate the polymer. After separation, the polymer was dissolved in DCM and precipitated in cold methanol (-18 °C). The precipitated mixture was

centrifuged at 3000 rpm for 5 min and the supernatant was decanted to isolate the polymer, which was then analyzed via  $^1\text{H}$  NMR.

### 5.3.7 Polymer characterization

#### 5.3.7.1 $^1\text{H}$ Nuclear magnetic resonance spectroscopy ( $^1\text{H}$ NMR)

The composition and molecular weight of the copolymers were determined from  $^1\text{H}$  NMR spectra obtained on a Bruker Avance-400, operating at 400 MHz. The polymers were dissolved in deuterated chloroform at a concentration of 10 mg/mL, and tetramethylsilane (TMS) peak was used as internal reference. The solution was placed in NMR tubes and analyzed at room temperature. The spectral data were analyzed using ACD lab software.

The total molecular weight of the copolymer ( $\text{MW}_{\text{total}}$ ) was determined using the  $^1\text{H}$  NMR spectra integrations of PEG methoxy protons ( $I_{\text{PEG}}$ ) compared to the integrations of the methylene protons of G ( $I_{\text{G}}$ ) and CL ( $I_{\text{CL}}$ ) monomer units that are adjacent to the carbonyl group. The values  $I_{\text{PEG}}$ ,  $I_{\text{G}}$  and  $I_{\text{CL}}$  correspond to 4 H, 4 H and 2 H per monomer unit, respectively, and the calculations were carried out as follows. The number ( $n$ ) of ethylene glycol (EG), G and CL units were determined using the equations,

$$n_{\text{EG}} = \frac{\text{MW}_{\text{PEG}}}{\text{MW}_{\text{EG}}} \quad \text{Eq. 5.1}$$

$$n_{\text{G}} = \frac{n_{\text{PEG}} \cdot I_{\text{G}}}{I_{\text{PEG}}} \quad \text{Eq. 5.2}$$

and,

$$n_{\text{CL}} = \frac{n_{\text{PEG}} \cdot 2I_{\text{CL}}}{I_{\text{PEG}}} \quad \text{Eq. 5.3}$$

in which,  $\text{MW}_{\text{PEG}}$  and  $\text{MW}_{\text{EG}}$  are the molecular weights of PEG and ethylene glycol unit, respectively.

Using the  $n$  values obtained above and the MW of the monomers, the segmental molecular weights  $\text{MW}_{\text{G},s}$ ,  $\text{MW}_{\text{CL},s}$  were calculated for G and CL, respectively using Equations 5.4 and 5.5.

$$MW_{G,s} = n_G \cdot MW_G \quad \text{Eq. 5. 4}$$

and

$$MW_{CL,s} = n_{CL} \cdot MW_{CL} \quad \text{Eq. 5. 5}$$

where,  $MW_G=116.07$  g/mol and  $MW_{CL}=114.14$  g/mol.

Finally, the total molecular weight of the copolymer was obtained from the equation:

$$MW_{total} = MW_{G,s} + MW_{CL,s} + MW_{PEG} \quad \text{Eq. 5. 6}$$

The integrations of the alkyl methylene and methoxy protons of CL were used as confirmation for the  $I_{CL}$  methylene integrations.

### 5. 3. 7. 2 Degree of randomness

The monomer distribution of the copolymer blocks was analyzed by  $^1H$  NMR spectroscopy. The average length of the caproyl and glycolyl sequences and the degree of randomness (R) were calculated as reported by Dobrzynski et al.<sup>116</sup> Briefly, the experimental lengths of the two sequences were calculated from Equations 5. 7 and 5. 8:

$$L_C = ([Cc] + [Cg])/[Cg] \quad \text{Eq. 5. 7}$$

$$L_G = \frac{L_C}{k} \quad \text{Eq. 5. 8}$$

where  $L_C$  and  $L_G$  is the experimental average lengths of caproyl ( $-OCH_2CH_2CH_2CH_2CH_2CO-$ ) and glycolyl ( $-OCH_2CO-$ ) sequences, respectively.  $[Cc]$  is the integration of Cc peak and  $[Cg]$  represents the integration of the Cg peak, shown in Figure 5. 1.  $k$  is the molar ratio of caproyl to glycolyl unit (Equation 5. 9).

$$k = [C]/[G] \quad \text{Eq. 5. 9}$$

The lengths of the caproyl and glycolyl units in randomly structured copolymers were calculated from Equations 5. 10 and 5. 11:

$$L_G^R = \frac{k+1}{k} \quad \text{Eq. 5. 10}$$

$$L_C^R = k + 1 \quad \text{Eq. 5. 11}$$

And finally, the degree of randomness was then obtained from Equation 5. 12:

$$R = \frac{L_G^R}{L_G} = \frac{L_C^R}{L_C} \quad \text{Eq. 5. 12}$$

The degree of randomness for completely random chains is 1 and is 0 for diblock copolymers. A high concentration of alternating monomer sequences is implied when R is greater than 1.

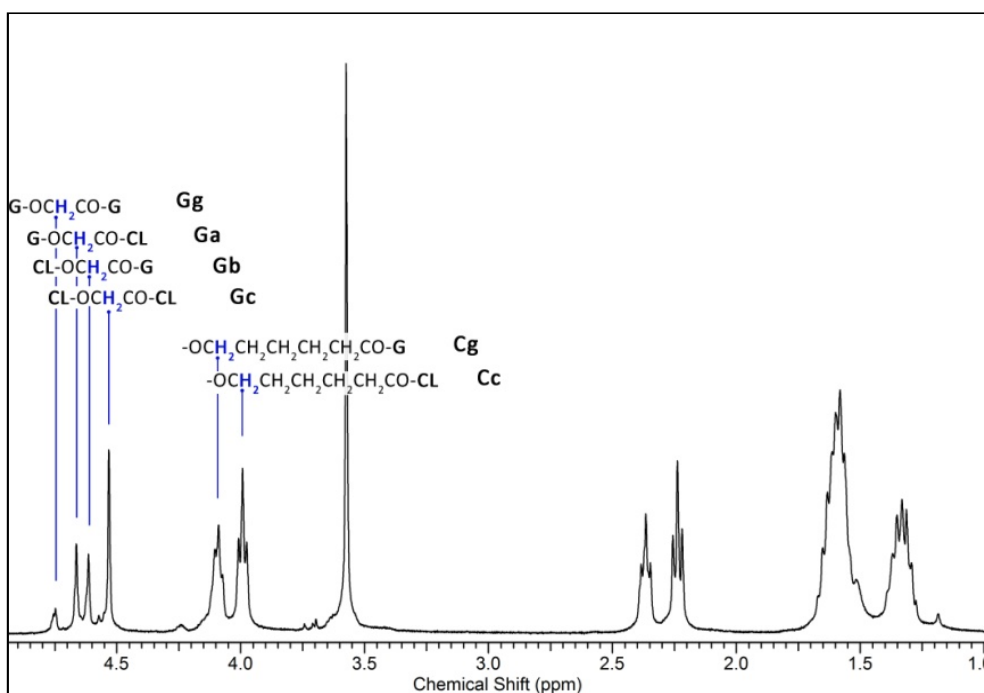


**Figure 5. 1** Representative  $^1\text{H}$  NMR spectra and microstructure analysis of copolymer C15 (3:1 - PEG1500 - 7.5 kDa).

### 5. 3. 7. 3 Differential scanning calorimetry

The thermal properties of the copolymers were measured using a Mettler Toledo DSC 1 differential scanning calorimeter. 10 mg of the sample were measured into aluminum pans. A heating/cooling/heating sequence from -80 °C to 260 °C at a 10 °C/min rate for both cooling and heating cycles was used. Melting ( $T_m$ ) and glass transition ( $T_g$ ) temperatures were determined from the second heating cycle of the sequence. The enthalpy of fusion ( $\Delta H_m$ ) was calculated from the area of the endothermic melting peak integrated using the instrument's software and the value was used to calculate the percentage crystallinity of the copolymers.

The percentage crystallinity (% X) at 37 °C was calculated as the enthalpy of melting of the sample divided by the enthalpy of melting of pure 100% crystalline poly( $\epsilon$ -caprolactone) ( $\Delta H_{m,PCL} = 139.6$  J/g) (Eq. 5. 13).<sup>7</sup> For crystallinity that was assigned to poly(glycolidyl) blocks (PG) (~220 °C), the heat of melting of pure 100% crystalline PG homopolymer ( $\Delta H_{m,PG} = 206.6$  J/g)<sup>165</sup>:

$$\%X = 100 \times \frac{\Delta H_m}{\Delta H_{m,o}} \quad \text{Eq. 5. 13}$$

where  $\Delta H_{m,o}$  is the enthalpy of melting of the pure crystalline homopolymer.

To subtract the crystallinity corresponding to the PEG segment, which will disappear after hydration of the polymer in use, thermographs of hydrated samples were also obtained. The hydration of the samples was performed using approximately 50 mg of dry copolymer immersed in 0.5 mL distilled water for 24 h. The water was removed and the samples blotted dry before weighing the samples.

### 5. 3. 7. 4 Gel permeation chromatography

For the determination of the number average molecular weight ( $M_n$ ) and the dispersity  $\mathcal{D}$ , of the polymers, gel permeation chromatography (GPC) was performed. The GPC instrument consisted of a Waters 2690 separation module equipped with four Waters Styragel HR columns connected in series.

Refraction index and multi-angle light scattering detectors were used. The light scattering detector was a Wyatt Technology DAWN EOS. HPLC grade tetrahydrofuran (THF) was used as the mobile phase with the flow rate set at 1 mL/min. Samples consisted of 5 mg/mL polymer solution in THF. The increment of refractive index (dn/dc) value used for analyzing the light scattering detector data was determined using the Wyatt Optilab rEX differential refractive index (dRI) instrument. The same HPLC grade THF was used as the solvent for the preparation of five polymer solutions at concentrations ranging from 0.2 to 10 mg/mL. The dRI detector wavelength was set at 690 nm, as in the GPC instrument. Five different concentrations of each copolymer were used to determine the dRI increments with concentration, from which was determined the slope that represents the dn/dc value.

#### **5. 3. 7. 5 Attenuated total reflection-Fourier transform infrared spectroscopy (ATR-FTIR)**

Attenuated total reflection-Fourier transform infrared spectroscopy (ATR-FTIR) was used as a solvent-free structural analysis for insoluble fractions of the copolymers synthesized. To study the structural differences between soluble and insoluble fractions, the two phases were separated and analyzed using a Nicolet 6700 ATR-FTIR spectrometer (Thermo Fisher Scientific, Canada). A small amount of the copolymers was placed in 10 mL vials with 5 mL DCM. The copolymers remained in the DCM at room temperature for 24 h until all the soluble portions had dissolved. The poorly soluble fraction of the copolymer formed a separate phase at the bottom of the vial. The two phases were separated and transferred to two clean vials, in which they were thoroughly dried prior to ATR-FTIR analysis. The spectra over the range of 4000 to 400  $\text{cm}^{-1}$  were collected at room temperature.

## 5. 4 Results and discussion

### 5. 4. 1 Polymer characterization

#### 5. 4. 1. 1 Composition analysis

The efficiency of all the polymerization reactions was evaluated using  $^1\text{H}$  NMR spectroscopy. From the spectra, the molecular weight and composition of the copolymers were calculated and the chain monomer distribution analyzed to obtain the degree of randomness within the CL-G regions.

The final caproyl:glycolidyl ratio (CL:G) in the copolymers was obtained from the integrations of the peaks assigned to the methylene groups of glycolidyl ( $-\text{OCH}_2\text{COOCH}_2\text{CO}-$ ) and caproyl units ( $-\text{OCH}_2\text{CH}_2\text{CH}_2\text{CH}_2\text{CH}_2\text{CO}-$ ). In the majority of the copolymers produced, the molecular weight and the final molar ratio obtained from their NMR spectra were in agreement with the feed ratios (Table 5. 2)

The number average molecular weights of the CL:G blocks were determined as described above. The integration  $I_{\text{PEG}}$  of the PEG methoxy protons peak at  $\delta$  3.65 ppm was compared to the integrations  $I_{\text{CL}}$  and  $I_{\text{G}}$  of the methylene groups of CL and G' appearing at  $\delta$  4.00-4.30 ppm and  $\delta$  4.55-4.85 ppm, respectively (Figure 5. 2).

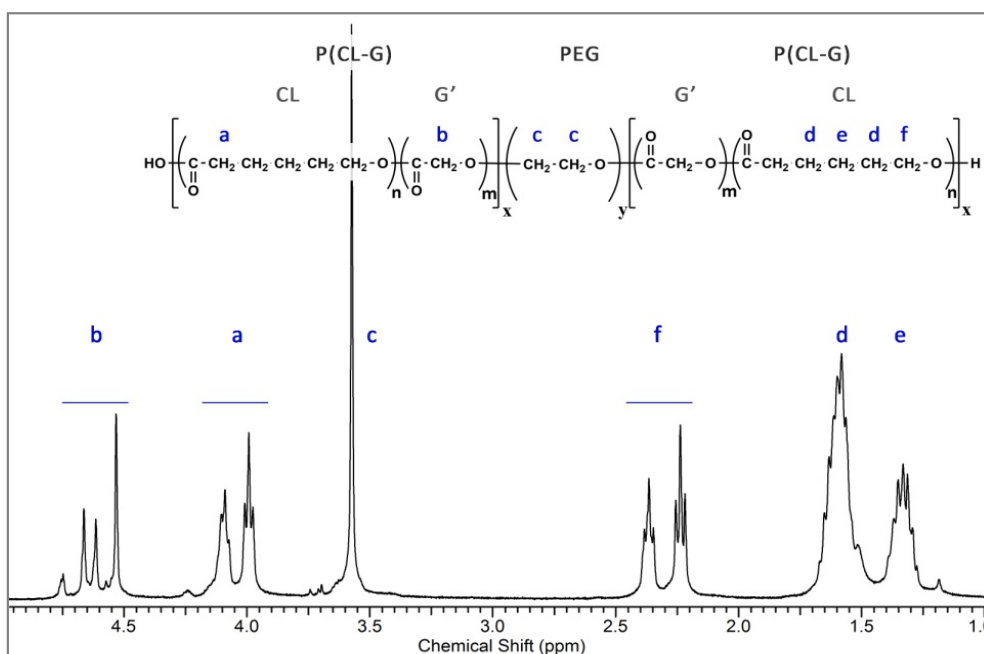


**Figure 5. 2**  $^1\text{H}$  NMR peak assignments on a spectrum obtained from copolymer C15 (3:1- PEG1500-7.5 kDa).

The multiple peaks at 1.2 - 2.5 ppm were assigned to the methylene and methoxy protons of  $\epsilon$ -caprolactone, as shown in Figure 5. 2.<sup>116,118</sup> The protons of the two equivalent methylene groups of the caproyl unit (d) appeared as multiple peaks at 1.5-1.7 ppm while methylene e appeared at 1.25-1.45 ppm and methoxy protons f at 2.20-2.45 ppm. The integrations of the peaks at 3.5-4.5 ppm were used for all the calculations performed.

For composition analysis the ratios of the caproyl (CL) to glycolidyl (G) monomer units was measured and reported as CL:G ratios. The degree of randomness was calculated as described in paragraph 5.3.7.2. All results are summarized in Table 5. 2.

**Table 5. 2** Summarized results obtained from <sup>1</sup>H NMR and GPC analysis.

No	M <sub>n</sub> PEG (Da)	Polymerization conditions	CL:G	M <sub>n</sub> target (kDa)	CL:G	M <sub>n</sub> NMR (kDa)	M <sub>n</sub> GPC (kDa)	$\bar{D}$	R
C1	4000	150 °C, 2.5 h	1:1	10	1.2:1	10.9	8.7	1.01	0.89
C2	4000	150 °C, 2.5 h	2:1	10	2.0:1	9.3	8.8	1.07	0.88
C3	4000	150 °C, 2.5 h	3:1	10	2.9:1	12.3	11.6	1.12	1.30
C4	4000	150 °C, 2.5 h	4:1	10	4.1:1	10.4	12.7	1.10	1.27
C5	4000	150 °C, 2.5 h	5:1	10	5.0:1	10.4	13.2	1.09	1.28
C6	4000	150 °C, 2.5 h	6:1	10	5.9:1	9.6	12.5	1.11	1.54
C7	4000	150 °C, 2.5 h	8:1	10	6.9:1	11.0	12.1	1.06	1.40
C8	4000	150 °C, 2.5 h	10:1	10	9.1:1	13.0	12.7	1.15	0.97
C9	4000	150 °C, 2.5 h	12:1	10	10.7:1	14.2	13.5	1.02	1.00
C10	4000	150 °C, 2.5 h	3:1	6.5	3.0:1	6.1	6.3	1.21	1.10
C11	4000	150 °C, 2.5 h	3:1	15	2.8:1	18.2	17.3	1.14	1.36
C12	4000	150 °C, 2.5 h	3:1	20	2.5:1	26.0	22.2	1.19	1.28
C13	4000	150 °C, 2.5 h	3:1	25	2.6:1	27.6	26.3	1.24	1.17
C14	1500	150 °C, 2.5 h	1:1	7.5	1.1:1	8.7	8.9	1.13	1.00
C15	1500	150 °C, 2.5 h	3:1	7.5	3.0:1	7.6	8.0	1.11	1.32
C16	1500	150 °C, 2.5 h	6:1	7.5	6.0:1	8.2	8.1	1.11	1.22
C17	4000	110 °C, 24 h	1:1	10	1.0:1	9.8	6.3	1.01	0.78
C18	4000	110 °C, 24 h	2:1	10	2.3:1	10.3	6.7	1.11	0.86
C19	4000	110 °C, 24 h	3:1	10	3.2:1	9.9	6.4	1.13	1.13
C20	4000	130 °C, 6 h	1:1	10	0.9:1	10.7	8.5	1.11	0.68
C21	4000	130 °C, 6 h	2:1	10	2.1:1	12.0	10.0	1.12	0.94
C22	4000	130 °C, 6 h	3:1	10	2.9:1	11.2	10.3	1.15	1.15
C23	1500	150 °C, 2.5 h	3:1	11.5	2.9:1	12.1	12.0	1.02	1.24
C24	1500	150 °C, 2.5 h	3:1	21.5	2.7:1	24.2	20.2	1.14	1.68
C25	4000	HCl/Et <sub>2</sub> O	3:1	10	-	-	-	-	-
C26	4000	DBU	1:1	10	-	-	-	-	-
C27	4000	DBU	3:1	10	-	-	-	-	-

\*  $\bar{D}$  = Mw/Mn

\*\*R→0: block, R→1:random, R→2:alternate



#### **5. 4. 1. 2 Molecular weight and dispersity**

The refractive index increment determined was  $0.064(\pm 0.04)$  for PEG 4000 initiated copolymers and  $0.042(\pm 0.04)$  for PEG1500 initiated copolymers. Using these values, the molecular weight and molecular weight distribution of the polymers as measured via GPC. All polymers produced with the bulk ROP reaction resulted in narrow molecular weight distributions. The dispersities ( $\mathcal{D}$ ) were close to 1 and the obtained number average and weight average molecular weights ( $M_n$  and  $M_w$ , respectively) were close to the feed values and those calculated from the  $^1\text{H}$  NMR analysis (Table 5. 2).

The copolymers that possessed longer PG blocks according to NMR and FTIR analysis exhibited limited solubility in the GPC solvent. The solubility was further reduced with further extension of the PG blocks. A variety of GPC solvents were used to achieve sufficient solubility of those samples but poor solubility of the PG blocks in all solvents resulted in incomplete solubility and formation of cloudy solutions. Filtration of the samples prior to GPC measurement resulted in decreased GPC signals and lower  $M_n$  and  $M_w$  values than expected based on the molecular weight calculated from the NMR analysis and monomer consumption.

#### **5. 4. 2 Effect of temperature on ring opening polymerization**

In bulk ROP polymerization, temperature and time of reaction are very important factors in controlling the molecular weight and the microstructure of the obtained copolymers. Cyclic esters and their oligomers are unstable in processes that involve high temperatures in the presence of oxygen and water.<sup>112</sup> In order to obtain a high yield and minimum monomer or product degradation the reaction temperature for the ROP needs to be optimized. For complete monomer conversion 24, 6 and 2.5 h at 110, 130 and 150 °C, respectively, were required. All three polymerization temperatures led to copolymers with good control over molecular weight and CL:G ratio in

agreement with the feed values, while dispersity values measured by GPC were close to 1 (Table 5. 2).

Different monomer reactivities resulted in different copolymer microstructures. Monomer reactivity shifts caused by changing the reaction temperature further exacerbated the microstructural variations. The higher polymerization kinetics of glycolide compared to  $\epsilon$ -caprolactone,<sup>113</sup> resulted in faster monomer conversions creating longer PG blocks while  $\epsilon$ -CL required a longer time to reach maximum conversion at the same temperature. When the reaction temperature increased to 130 °C, the conversion rates were better balanced for both monomers while solubility issues and blocky structures still remained at high glycolide ratios due to the formation of the aforementioned PG blocks. The best balance between monomer reactivities was reached at 150 °C, where random microstructures and good molecular weight control was achieved within 2.5 h reaction time.

The secondary cleavage of G is accelerated at higher polymerization temperatures, which can be inferred by the decrease of long glycolidyl sequences (Gg) and the increase in the number of alternate sequences (Gc) as seen in the <sup>1</sup>H NMR spectra obtained from the copolymers produced at 150 °C (Figure 5. 3). Although increasing the temperature was effective in providing enhanced random structures for most copolymers, nonetheless, similar monomer feed rates (1:1 and 2:1) still formed longer PG blocks regardless of the polymerization temperature used. The formation of long PG blocks was also confirmed by DSC and FTIR-ATR analysis.

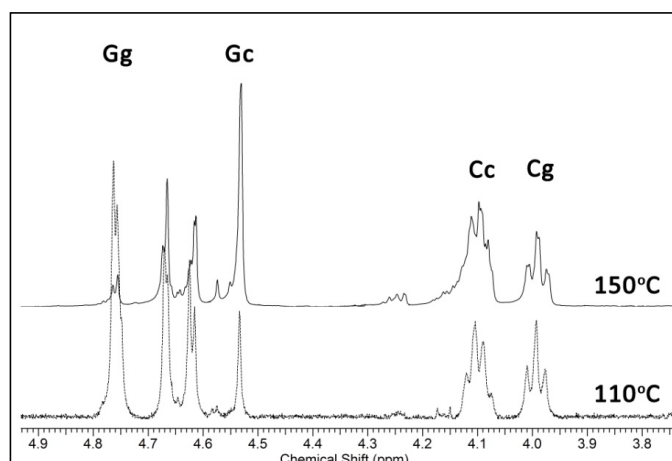


**Figure 5. 3** Section of  $^1\text{H}$  NMR spectra of PEG 4000 initiated copolymers with 3:1 CL:G molar ratio and total molecular weight 10 kDa (3:1 - PEG4000 – 10 kDa) , produced at different temperatures, 150 °C (C3) and 110 °C (C19). Glycolide peaks can be seen at 4.8-4.5 ppm.

#### 5. 4. 3 Structural analysis using ATR-FTIR

Polymers that contained longer glycolide blocks within the copolymer sequence also had poor solubility in most organic solvents and hence their analysis was challenging. When mixed with organic solvents they formed cloudy solutions that soon separated into two distinct phases. Using a solvent-free analytical method like FTIR-ATR spectroscopy, information was obtained that helped to explain the solubility differences through structural analysis.

In all spectra of both soluble and insoluble fractions of the copolymers, strong absorption bands were noted in the regions between  $1760$  and  $1740\text{ cm}^{-1}$ , due to the carbonyl groups present in both glycolide and  $\epsilon$ -caprolactone monomers (Figure 5. 4). Asymmetric and symmetric stretching of -C-O- ester bonds exhibit strong bands at  $1300$ - $1100\text{ cm}^{-1}$ .<sup>166</sup> These regions of the spectrum are very useful for the characterization of the backbone structure and randomness in polyesters. Multiple small intensity peaks present between  $4000$ - $3500\text{ cm}^{-1}$  were assigned to -OH groups due to moisture in the copolymer.<sup>167</sup> Any residual -OH from unreacted PEG would exhibit a broader and more distinct peak in this region. In the spectra of the insoluble polymer fractions, characteristic peaks of the PG

homopolymer at 1500-500  $\text{cm}^{-1}$  appeared amplified, which suggested an elevated concentration of G units in the copolymer fraction (Figure 5. 4).

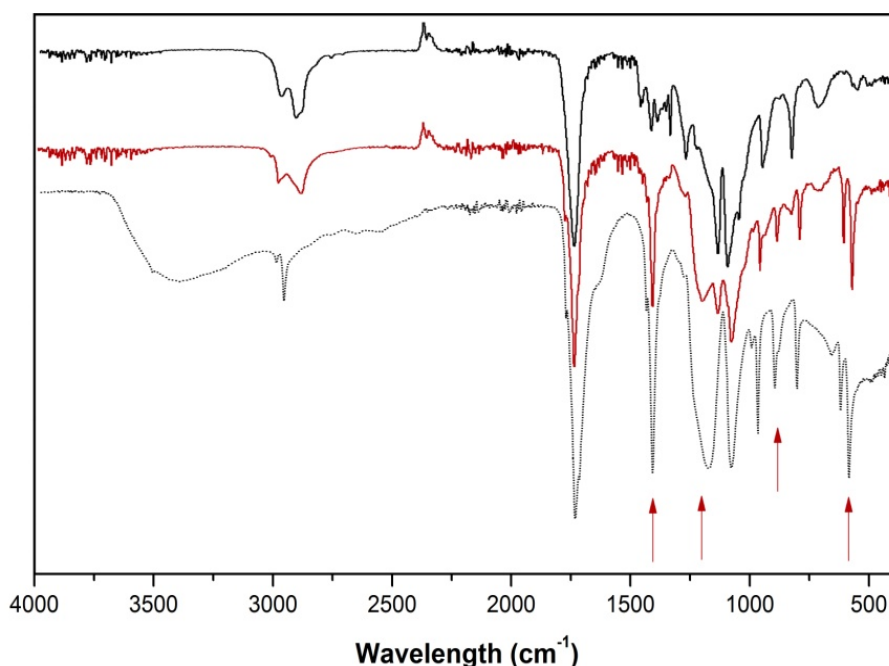


**Figure 5. 4** FTIR-ATR spectra of two polymer fractions: insoluble (red) and soluble (black) recorded using 1:1 PEG 4000 polymer polymerized at 110 °C (sample C17, Table 5. 2). The characteristic peaks of PG homopolymer (dotted spectrum) that are enhanced in the insoluble fraction are indicated with arrows.

#### 5. 4. 4 Thermal analysis

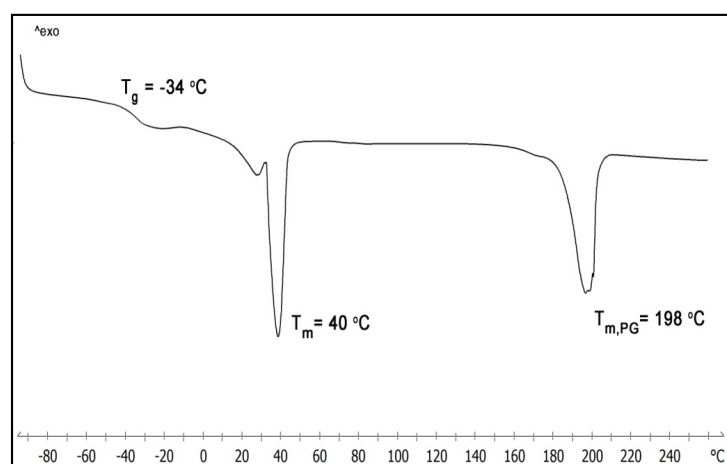
Thermal analysis revealed a low glass transition temperature ( $T_g$ ) of  $-50 \pm 10$  °C for all the copolymers (Table 5. 3). A small effect was noted for the change of monomer molar feed ratios. Starting with a  $T_g$  lower than -55 °C for the 12:1 CL:G copolymer, an increment of 2-4 degrees was noted for each mol decrease in the  $\epsilon$ -caprolactone content. Most of the materials tested exhibited all their melting events between 30-45 °C. Those copolymers that had more blocky structures exhibited an extra characteristic melting peak around 200 °C that was assigned to PG segments in the copolymer (Figure 5. 5). This melting peak of PG was exhibited only at the first heating cycle of the thermogram, for most of the samples that this event was observed, as PG blocks did not effectively undergo crystallization under the brief cooling cycle of the thermal analysis (-80 to 260 °C, 10 °C/min).

**Table 5. 3** Thermal properties of all PEG4000 initiated copolymers produced with bulk ROP at 150 °C.

No	CL:G	Mn (kDa)	T <sub>g</sub> (°C)	T <sub>m</sub> (°C)	ΔH <sub>m</sub> (J/g)	%X** (>37 °C)	T <sub>g</sub> (°C)	T <sub>m</sub> (°C)	ΔH <sub>m</sub> (J/g)	%X** (>37 °C)
DRY							HYDRATED			
C1*	1:1	10	-34	34-44	33.4	24.4	-35	34-43	10.6	9.5
C2*	2:1	10	-40	35-43	36.8	26.0	-45	36-43	14.8	12.6
C3	3:1	10	-45	36-43	33.1	23.7	-38	36-43	16.3	13.7
C4	4:1	10	-49	38-42	30.2	21.7	-50	38-42	8.9	6.3
C5	5:1	10	-50	39-44	35.5	25.4	-52	39-43	9.5	6.8
C6	6:1	10	-54	39-44	40.8	29.2	-55	40-45	9.8	7.0
C7	8:1	10	-55	37-44	30.6	21.9	-57	38-45	25.1	8.7
C8	10:1	10	-56	39-45	30.9	22.1	-59	40-46	24.8	6.6
C9	12:1	10	-57	38-46	44.7	32.0	-59	37-45	25.2	10.0
C10	3:1	6.5	-43	32-40	28.1	20.1	-45	32-40	8.4	6.0
C11	3:1	15	-47	33-41	34	24.3	-50	37-43	14.0	10.0
C12*	3:1	20	-43	35-42	22	24.0	-44	31-41	12.1	14.3
C13*	3:1	25	-46	35-41	17.8	20.7	-47	31-40	8.0	11.2

\*Exhibited additional melting peak at T<sub>m,PG</sub> = ~195-210°C

\*\*Total crystallinity %X= %X<sub>PCL</sub> + %X<sub>PG</sub>, observed at T > 37 °C. Calculated using the ΔH<sub>m</sub> of 100% crystalline PCL (ΔH<sub>m,0</sub>=139.6 J/g) and PG (ΔH<sub>m,0</sub>=206.6 J/g).<sup>7,119</sup>

**Figure 5. 5** DSC thermogram (1<sup>st</sup> heating cycle) of dry sample C1 (Table 5. 3). T<sub>m,PG</sub> at 198 °C was attributed to the melting of PG blocks formed at high G content copolymers.

Although most of the materials exhibited a single melting temperature with onset close to 37 °C, some of the compositions exhibited double endothermic peaks at the same temperature range that in some cases overlapped. The double peak or peak shoulder phenomenon could be easily explained by assignment of the peaks to the individual melting temperatures of PEG and PCL segments (Table 5. 4). However, such an assignment could not be confirmed as either the phenomenon or the ratio of the peaks was not consistent with the compositional changes. Since both endothermic peaks were

equally affected by compositional changes, secondary crystallization of PCL probably took place,<sup>168</sup> which would explain the secondary endothermic peak.

**Table 5. 4** Thermal properties of homopolymers obtained via DSC analysis.

Pure homopolymer	T <sub>g</sub> (°C)	T <sub>m</sub> (°C)
PEG 4000	-22	59-64
PEG 1500	-55	48-52
PCL	-60	56-60
PG	35-40	220-225

The melting onset was affected by the CL:G ratio as well as the molecular weight of the initiator used. The onset temperature gradually increased with increasing CL ratio, ranging from 34 °C up to 38 °C for the C1 (1:1) and C9 (12:1) in dry copolymers, respectively. An individual melting peak for the PEG segments was expected around 53 - 56 °C for PEG 4000 and 43 - 45 °C for PEG 1500, but due to proximity of the melting temperatures and the fact that copolymerization hinders the complete crystallization of the individual blocks, the melting peaks of the homopolymerized segments were depressed and often overlapped forming a single melting event for PEG and PCL. To support this explanation, polymers were tested both in their dry and hydrated states. The hydration reduced or eliminated the crystallinity of hydrophilic PEG blocks while the hydrophobic blocks retained most of their crystallinity and thermal properties. The overall crystallinity was significantly reduced after hydration. Moreover, an increase in crystallinity was noted when the PEG ratio in the copolymer was increased. All these findings indicated that most of the crystalline segments of the copolymer were from the crystallization of the PEG segments.

Polymers with similar amounts of  $\epsilon$ -caprolactone and glycolide exhibited a second melting point around 200 °C, which was attributed to the melting temperature of PG blocks formed. In an equal monomer feed ratio a more random structure would be expected, but due to faster polymerization kinetics of glycolide compared to  $\epsilon$ -caprolactone, blocks of PG are formed before CL incorporation and interchange.<sup>114</sup> These copolymers also exhibited low solubility in all the organic solvents

examined, which further supported the presence of insoluble PG blocks that inhibited the overall solubility of the polymer.<sup>119</sup> Increased overall crystallinity was also observed for these samples above 40 °C.

An exothermic crystallization peak was noted at  $10 \pm 5$  °C for most copolymers. In addition, cold crystallization ( $T_{cc}$ ) was noted during the heating cycle in some of the copolymers (Figure 5. 6). Cold crystallization is very common in copolymers with random structures or homopolymers and copolymers with bulky side groups.<sup>169</sup> The random structures can act as effective barriers to prevent the completion of the crystallization process during cooling under specific cooling rates. This leads to the appearance of a second crystallization peak when temperatures reach values higher than the polymer's  $T_g$  and the polymer chains regain enough mobility during a subsequent heating cycle.

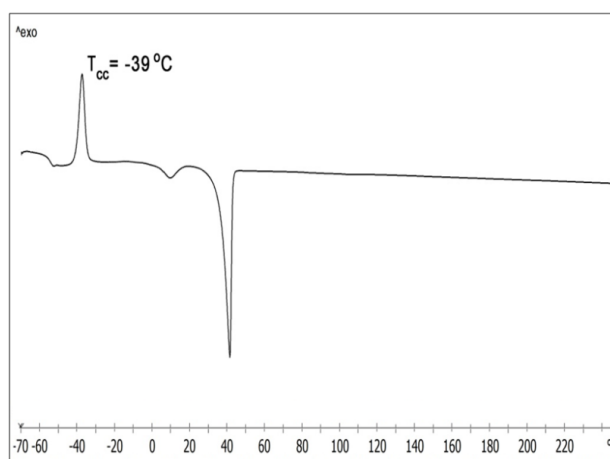


**Figure 5. 6** DSC thermogram (2<sup>nd</sup> heating cycle) of sample C5 (Table 5. 3) exhibiting a cold crystallization ( $T_{cc}$ ) at -38 °C.

## 5. 4. 5 Polymer composition parameters

### 5. 4. 5. 1 *Effect of monomer ratio*

Monomer ratio was used to finely tune the thermal properties of the copolymers produced. Copolymers were prepared starting from an equimolar CL:G feed and reaching up to a ratio of 12:1. The copolymers were characterized using  $^1\text{H}$  NMR, DSC and GPC analysis. The polymerization conditions were kept at 150 °C for 2.5 h for all copolymers in this series.

Due to the lower polymerization activity and ring strain of  $\epsilon$ -caprolactone compared to glycolide,<sup>113</sup> higher CL feed molar ratios could not be completely converted into polymer and incorporated in the copolymer within the polymerization reaction time used. Thus, the resulting copolymers with CL feed ratios larger than 6:1, samples C7, C8 and C9, exhibited incomplete conversion and a final composition ratio of one or two ratio units less than the feed (Table 5. 2)

The thermal properties of the copolymers gradually changed with the variation in the monomer ratio. Only two compositions (1:1 and 2:1) at 10 kDa total molecular weight exhibited a melting peak attributed to PG blocks, confirming the <sup>1</sup>H NMR results showing that random microstructures were mainly produced at 150 °C. All copolymers exhibited melting temperatures lower than 50 °C with most compositions ranging between 35 to 45 °C (Table 5. 3) In hydrated samples, the heat of melting calculated from the melting peak at 35-45 °C was reduced by 50 to 70% for all copolymers compared to the corresponding dry samples. This drop of crystallinity was attributed to the elimination of crystal regions of the most hydrophilic components of the copolymer, PEG segments.

#### **5. 4. 5. 2 Effect of initiator**

Substitution of the PEG 4000 initiator with PEG 1500 eliminated the crystallinity of the copolymers attributed to CL and PEG regions (Table 5. 5). Glass transition temperatures were close to -47 °C and no other peaks for both 3:1 and 1:1 copolymers were observed. At 6:1 CL:G ratio a melting peak appeared between 25-31 °C and the  $T_g$  dropped to values close to -55 °C. Increasing the molecular weight of the CL-G segments minimally affected the polymerization reaction and similar compositional and overall molecular weight results were obtained. Thermal properties were significantly altered by increasing the total molecular weight. A distinct endothermic peak was noted in the DSC thermographs at  $200 \pm 2$  °C while  $T_g$  was close to -35 °C. The exotherm peak at such high temperatures was from the crystallinity of PG blocks present within the copolymer backbone. Although the crystallinity observed was low, the PG segments gave the copolymers a much more



rigid and stiff texture with crystallinity that would not be easily eliminated *in vivo* and could potentially irritate the surrounding tissue.

**Table 5. 5** Thermal properties of all copolymers produced using PEG1500 as initiator.

No	PEG	CL:G	Mn target	T <sub>g</sub> (°C)	T <sub>m</sub> (°C)	ΔH <sub>m</sub> (J/g)	%X	T <sub>g</sub> (°C)	T <sub>m</sub> (°C)	ΔH <sub>m</sub> (J/g)	%X
				DRY				HYDRATED			
C14	1500	1:1	7500	-35	-	-	-	-	-	-	-
C15	1500	3:1	7500	-47	-	-	-	-	-	-	-
C16	1500	6:1	7500	-55	24-29	31.4	22.5	-55	25-31	8.4	6.1
C23	1500	3:1	11500	-31	194-211	6.4	3.1	-33	197-211	0.5	<1%
C24	1500	3:1	21500	-37	205-215	9.4	1.0	-43	190-210	1.0	<1%

#### 5. 4. 5. 3 Effect of total molecular weight

A decrease in the yield of the polymerization reaction was observed with increasing target total molecular weight. As CL has reduced reaction activity than G, the time required for total monomer conversion increased. Therefore, for higher molecular weights under the same polymerization conditions, less polymer was produced and in terms of composition analysis CL did not reach full conversion after 2.5 h. Increasing the total molecular weight of the copolymer by lengthening the molecular weight of the CL-G segments did not affect the degree of randomness as the peaks of block to alternating G-C remained practically unaltered. On the other hand, thermal properties measured with DSC showed that increasing the molecular weight of the CL-G segments resulted in increasing concentrations of PG in the copolymer. This was made clear by the exothermic melting peak at 200 °C that was observed in the thermographs of copolymers with total molecular weight higher than 15 kDa shown in Figure 5. 7. The crystallinity close to body temperature that was assigned to PCL and PEG segments seemed to gradually decrease as the total molecular weight increased. This was explained by the fact that the majority of the crystallinity observed at this region was due to crystals from the PEG segment and its ratio was reduced at higher molecular weights.

This explanation was further supported by the thermal analysis of the hydrated samples for which 80% of the exothermic peak's heat of melting at 30-40 °C was eliminated after hydration for 24 h.

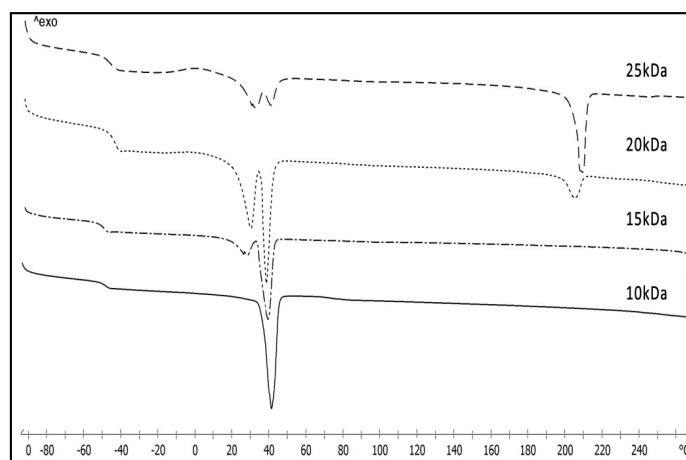


**Figure 5. 7** DSC thermograms (1<sup>st</sup> heating cycle) of PEG4000 initiated copolymers with 3:1 CL:G molar ratio in various Mn from 10 to 25 kDa. [C3: 10 kDa, C11: 15 kDa, C12: 20 kDa and C13:25 kDa at Table 5. 2].

#### 5. 4. 6 Other polymerizations explored

Polymers produced in solution using either DBU or HCl-Et<sub>2</sub>O catalysts showed relatively fast G and very slow CL conversion. Poor solubility due to the formation of PG blocks resulted in weak signals obtained in <sup>1</sup>H NMR analysis. To assess the formation of PG, DSC analysis was used. A melting endotherm was observed at 220 °C (*T<sub>m</sub>* of PG homopolymer) as shown in Figure 5. 8. A second melting peak was observed at 58 °C, which was attributed to the crystalline PEG 4000 used.

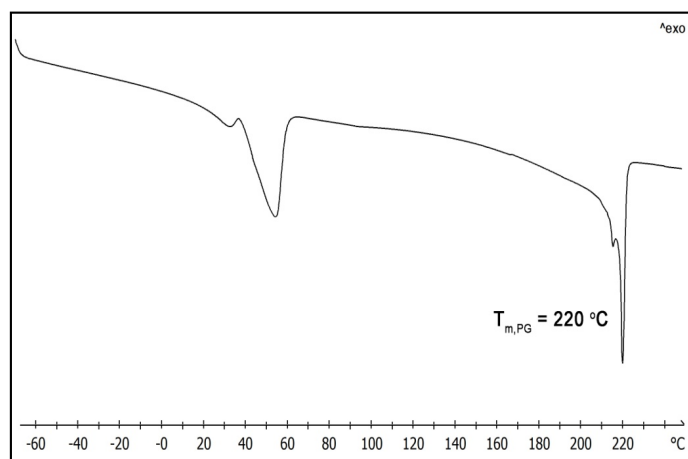


**Figure 5. 8** DSC thermograms (1<sup>st</sup> heating cycle) of C27 copolymer (3:1 - 10 kDa - PEG4000) synthesized using DBU catalyst. The characteristic endothermic attributed to the PG blocks melting can be seen at 220 °C.

The high activity of DBU catalyst makes it a very effective catalyzing agent for the synthesis of block copolymers with well-controlled size distribution and molecular weight.<sup>163</sup> However, it is very difficult to obtain random structures in copolymerization reactions due to the large difference in reactivity of the monomers used.<sup>114</sup> In this case, glycolide was found to be readily polymerized while  $\epsilon$ -CL needed more time for full conversion.

Overall, alternative methods of catalyzing the polymerization reaction at room temperature proved ineffective at producing random structures of copolymerized  $\epsilon$ -caprolactone and glycolide and, thus, cannot be considered as a polymerization method for the specific compositions required in this study. Hence, we confirmed that, of the catalysts examined, only  $\text{Sn}(\text{Oct})_2$  was successful at producing random copolymer blocks using the one-step polymerization reaction. A sequential polymerization reaction with gradual interchanging monomer addition could potentially prove effective in the synthesis of P(CL-G) random blocks using DBU.

## 5. 5 Conclusion

Tri-block copolymers were successfully synthesized with random microstructures obtained for those having higher  $\epsilon$ -caprolactone ratios compared to glycolide. The ROP reaction was appropriately optimized in order to consistently obtain random copolymers with good molecular weight control. This was achieved by performing the reaction at the highest temperature studied (150 °C). Because of the need to have a random copolymer, materials prepared at this temperature were used for all subsequent studies. The thermal properties of the copolymers prepared allowed for easy handling at room temperature, but also provided for soft particles with minimum crystallinity (< 8%) upon hydration at 37 °C. The percentage crystallinity above 37 °C and the handling properties of the materials were used to evaluate their applicability for microsphere formation for protein delivery. Thermal properties and hydrophilicity can also highly affect degradation and release rates and were effectively tuned by altering the molar ratio of the hydrophilic PEG block and the hydrophobic CL-G blocks in the copolymer. The materials with the most promising characteristics for this particular application were selected to be formulated into microspheres and were subjected to degradation analysis.

## Chapter 6. Microspheres: Preparation and degradation

### 6.1 Introduction

As discussed earlier, specific thermal and handling properties are required for the materials to be successfully formulated into injectable microspheres for the release of SDF-1 $\alpha$  protein. A polymer composition with minimal crystallinity at body temperature and low molecular weight could be readily degraded *in vivo* and would be less likely to induce tissue irritation due to crystallinity.<sup>8</sup> A sustained yet complete protein delivery must be achieved during the degradation period with minimal loss in protein stability.

Based on the handling properties of the dry copolymers at room temperature and the thermal properties of the hydrated copolymers above 37 °C, materials that exhibited high crystallinity above 37 °C were excluded from consideration. From the remaining materials those with a total molecular weight of 10 kDa were selected so that complete degradation would be achieved within the desired period of time. Consequently, four of the copolymers C4 (4:1-PEG4000-10 kDa), C5 (5:1-PEG4000-10 kDa), C6 (6:1-PEG4000-10 kDa), and C16 (6:1-PEG1500-7.5 kDa) were chosen to be studied for their ability to form stable microspheres and evaluated for their hydrolytic degradation properties.

### 6.2 Materials

Dichloromethane (DCM), ethanol, NaOH 1N solution, phosphate buffered saline (PBS) powder concentrate were purchased from Fisher Scientific, Canada. Lysosensor yellow/blue and SNARF-1 dextrans 10,000 MW, pH sensitive fluorescent dyes were obtained from Thermo Fisher Scientific, Canada. The chloroform-d used in <sup>1</sup>H NMR analyses was from Sigma-Aldrich, Canada.

## 6. 3 Methods

### 6. 3. 1 Electrospraying of microspheres

The electrospraying apparatus used for the preparation of the polymer microspheres consisted of a syringe pump, a high voltage generator, a stirring plate and a cold ethanol bath that served as the collector of the microspheres as described earlier in paragraph 3 (Figure 3. 1). The positive electrode of the high voltage generator was attached to the syringe needle containing the polymer solution while the ethanol bath was grounded using a piece of aluminum plaque connected to the second electrode of the circuit. The piece of the aluminum plaque was immersed into the ethanol and fixed close to the walls of the beaker to keep mixing undisturbed.

The tip of a 20 gauge needle was cut and filed to create a round flat end for more uniform round particles and better control of the flow. A concentrated polymer solution (0.7 g/mL) in DCM was injected through the flat tip needle syringe using a syringe pump set at 0.5 mL/min. The microspheres formed were collected in a 250 mL beaker filled with cold ethanol (collector bath). The collector bath was immersed in dry ice to keep the temperature close to -70 °C, well below the  $T_g$  of the copolymers ( $-50 \pm 5$  °C). This allowed for quick solidification of the droplets into stabilized glassy amorphous polymer particles upon contact with the cold ethanol. The bath was constantly stirred at 400 rpm and small dry ice pieces added several times to the ethanol bath throughout the process to maintain the temperature. The flow of the polymer solution was paused every 200  $\mu$ L to allow for the formed particles to harden and settle to the bottom of the beaker. This way, microsphere aggregation was less likely to occur. The voltage applied was 7 kV and the current was set at 0.1 mA. The distance from the tip of the needle to the surface of the collector solution and the ground electrode was 7 cm.

The microspheres were kept in the ethanol bath at -80 °C in a freezer for 48 h to extract the DCM from the microspheres into the ethanol. The suspended microspheres were then transferred to a -20 °C freezer, above the polymer's glass transition temperature, to allow for polymer crystallization. The

suspension remained at this temperature for a minimum of 24 h to ensure that crystallization was complete before proceeding to size separation.

### **6. 3. 2 Microspheres size separation**

For size separation and isolation of the microspheres from the ethanol, the suspended microspheres were sieved through appropriate pore sized sieves to obtain a size distribution between 45 and 100  $\mu\text{m}$ . Sieving and further handling were carried out in a cold room to prevent softening of the microspheres during processing that could lower the final yield. All sieves and equipment were cooled to  $-80\text{ }^{\circ}\text{C}$  for an hour before use. The microspheres were retrieved from the sieves using cold ethanol and remained for several days in a ventilated fridge ( $4\text{ }^{\circ}\text{C}$ ) to dry completely. The suspension of microspheres was briefly sonicated using a Fisher Scientific 100 probe sonicator to break any aggregates formed during the preparation and solvent extraction periods. Samples were kept in a dry ice bath before and during sonication to prevent warming.  $^1\text{H}$  NMR analysis was used to determine whether the microspheres were free from solvents.

### **6. 3. 3 Mean microsphere diameter determination**

The average diameter of the microspheres was determined from Scanning Electron Microscopy (SEM) images using Adobe Photoshop CS6 image software. The scale on the SEM images was used to calibrate the integrated scale of the software to the corresponding number of pixels. Using the pixels-to-length calibrated scale we were able to determine the diameter of the particles in the pictures. An average was calculated in triplicate for a total number of 100 microspheres from images taken with the same magnification factor ( $\times 100$ ).

#### 6. 3. 4 Water uptake

To measure the ability of the copolymers to absorb water, polymers were heat molded into 1.5 cm square thin films (3 mm), immersed in an aqueous environment at 37 °C, and their weight variation with time monitored. To create the films, 100 mg ( $m_{dry}$ ) of the copolymer was placed in a square mold and into a 100 °C oven for 10 min to melt flat at the bottom of the mold. The molds were quickly transferred to a desiccator and remained there to cool at room temperature and crystallize before being removed from the mold. The weight of the dry film was recorded at room temperature and then placed dry in a 37 °C incubator for 2 h.

Phosphate-buffered saline pH 7.4 at 37 °C was added to the film and the samples were incubated for 6 h. After 6 h, the buffer was removed and the excess moisture was blotted off the surface of the film. The weight was recorded again at room temperature ( $m_{wet}$ ) and the samples were dried overnight in an oven at 110 °C. After drying, the films were transferred to a desiccator to cool to room temperature and the weight of the dry film was recorded. The water uptake (WU) was calculated as,

$$WU = \frac{m_{wet} - m_{dry}}{m_{dry}} \times 100\% \quad \text{Eq. 6. 1}$$

#### 6. 3. 5 Hydrolytic degradation of microspheres

For the hydrolytic degradation study, approximately 20 mg of dry microspheres were placed in 40 pre-weighed 1 mL glass vials ( $n = 4$  for each time point). 1 mL of distilled water was then added to the vials. The added water had a pH of 7.4 which was adjusted with a 0.01N NaOH solution. The vials were then placed in a 37 °C incubator and mixed gently on a rocking platform mixer. The incubation medium was refreshed daily and analyzed for pH change using an Accumet AR15 Fischer Scientific pH meter. At predetermined time points, four vials of each sample were centrifuged at 1500 rpm for 5



min. The incubation medium was removed and the vials were lyophilized to obtain the remaining dry mass weight. Pure PCL and PCL-PEG-PCL microspheres of similar molecular weights and size distribution were tested as negative controls. The dried material was then subjected to  $^1\text{H}$  NMR and GPC analysis for composition and molecular weight changes, respectively. Selected samples were analyzed via Differential Scanning Calorimetry (DSC) for changes in their thermal properties during degradation.

### **6. 3. 6 Microenvironmental pH of degrading microspheres**

Lysosensor yellow/blue and SNARF-1 pH sensitive fluorescent dyes with dual emission and dual excitation properties, were used for the ratiometric determination of the microclimate pH distribution inside degrading microspheres of C5 and C6 copolymers. Both of the fluorescent dyes used for this study were conjugated on 10,000 Da solid dextran obtained from Fisher Scientific, Canada.

Two different batches of microspheres were fabricated for each dye under the same encapsulation method. Each dye was co-lyophilized with a small amount of PBS buffer solution at pH 7.4 (10% w/v). The lyophilized powder was dispersed in DCM at a concentration of 4% w/v, vortexed for 2 min and gently pulse sonicated using Fischer Scientific 100 probe sonicator for 1 min while kept in an ice bath to get small uniform sized particles. Appropriate amounts of polymer and DCM were added. The final polymer concentration was 0.7 g/mL in DCM. The concentration of the dyes in the dry polymer mass was 4 mg/g. The solution was subsequently electrosprayed as described in paragraph 6. 3. 1, into a cold ethanol bath to form microspheres. The microspheres were subjected to size separation (45-100  $\mu\text{m}$  sieves) and air dried at 4 °C.

20 mg of microspheres with one fluorescence dye encapsulated were incubated in 1 mL PBS buffer solutions (pH7.4) under mild agitation on a rocking platform mixer (60 cycles/minute) (n = 3 per

sample). At predetermined time intervals the incubation medium was removed and replaced with fresh buffer while at the same time a small amount of microspheres was removed for analysis. The pH of the removed incubation medium was measured each time. The analysis of the microspheres was performed with an Olympus FV1000 confocal microscope using an Ar/He laser at 488 nm and 405 nm for the excitation of SNARF-1 and LysoSensor, respectively. The intensity of the laser was set at 40 %. While focusing at the center of the microspheres, images were taken at two emission wavelengths for each dye using narrow band emission wavelength filters set at  $\pm 20$  nm from the wavelength of interest. The emission images of LysoSensor dye were taken at 450 and 520 nm and for SNARF-1 the images were taken at 580 nm and 640 nm. All microspheres selected for analysis had a diameter close to the average diameter calculated in 6. 4. 2 ( $63 \pm 5 \mu\text{m}$ ) (Table 6. 1).

The analysis provided a quantitative ratiometric method and the values obtained were concentration independent ratios.<sup>104</sup> The calibration was performed using pH-adjusted PBS buffer solutions ranging from 2.8 to 5.8 for LysoSensor and 5.5 to 8 for SNARF-1. The pH of the solutions was adjusted using 0.1M acetic acid and 0.1 NaOH solutions. LysoSensor and SNARF-1 dextrans were dissolved in the buffer solutions at concentrations of 1 and 0.2 mg/mL, respectively. The standard curve for each dye was obtained by plotting the fluorescent intensity ratios under two emission wavelengths,  $I_{450}/I_{520}$  for LysoSensor and  $I_{640}/I_{580}$  for SNARF-1, versus the pH value of the solution. The excitation wavelengths were again 405 nm and 488 nm for LysoSensor and SNARF-1, respectively.

## **6. 4 Results and discussion**

### **6. 4. 1 Microspheres preparation**

The electrospraying technique was optimized in order to achieve specific characteristics that will facilitate an effective microsphere distribution within the water-based injectable carrier. Spherical particles with smooth surface have been shown to exhibit better dispersion and limited aggregation

compared to irregularly shaped particles.<sup>34</sup> Injectability was also ensured by adjusting the microsphere size distribution to a range that could be easily administered using a conventional syringe needle size. The aim was to obtain a high yield of narrow size distribution spherical microparticles at an injectable size range of between 45-100  $\mu\text{m}$ . A variety of needle sizes, polymer solution concentrations, voltage, and flow rate values were examined in order to optimize the microsphere preparation protocol described above in section 6. 3. 1, where maximum yield and suitable size distribution was achieved. Microspheres were particularly susceptible to softening and aggregation when suspended in ethanol solution, and therefore a very low temperature of less than -10  $^{\circ}\text{C}$  was required until all DCM had been extracted. The temperature should also be retained lower than 10  $^{\circ}\text{C}$  until complete solvent evaporation.

A complete solvent extraction and evaporation was testified using  $^1\text{H}$  NMR spectroscopy. The obtained  $^1\text{H}$  NMR spectra were also used to investigate any compositional changes that may have occurred during electrospraying. The spectra of the dry initial and after microformulation polymers showed no solvent peaks or change in composition (Figure 6. 1A). Also, the  $T_m$  and  $T_g$  of the copolymers after formulation were in agreement with the initial thermographs obtained from the pure copolymers (Figure 6. 1B).

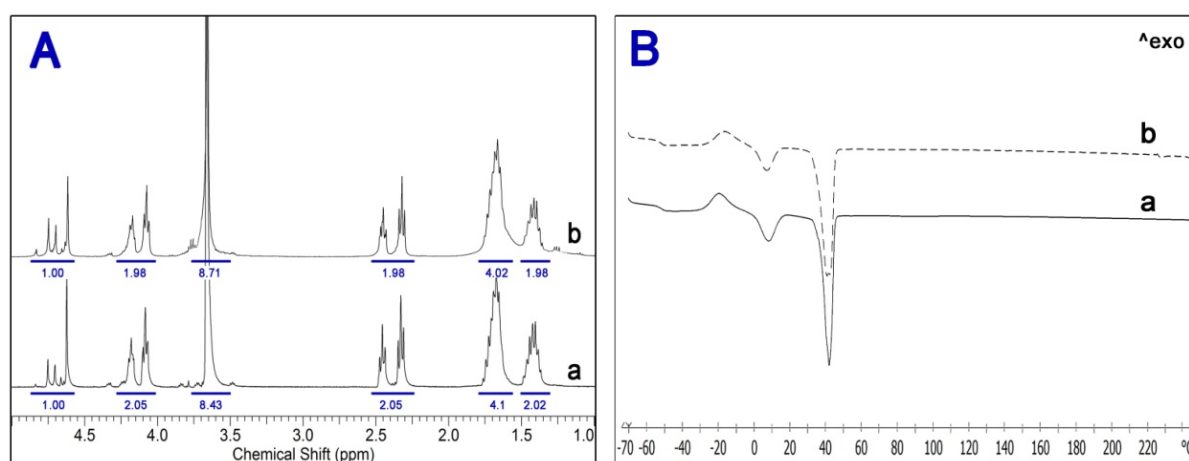


**Figure 6. 1**  $^1\text{H}$  NMR spectra (A) and DSC thermograms (1<sup>st</sup> heating cycle) (B) of dry polymer sample C4 before electrospraying (a) and after microsphere formation (b).

#### 6. 4. 2 Microsphere average diameter and morphology

The electrospraying technique and size separation produced uniform spherical particles with smooth surfaces and minimum aggregations. Images obtained by scanning electron microscopy (SEM) (Figure 6. 2) were used to calculate the average microspheres size for each of the copolymers used (Table 6. 1).

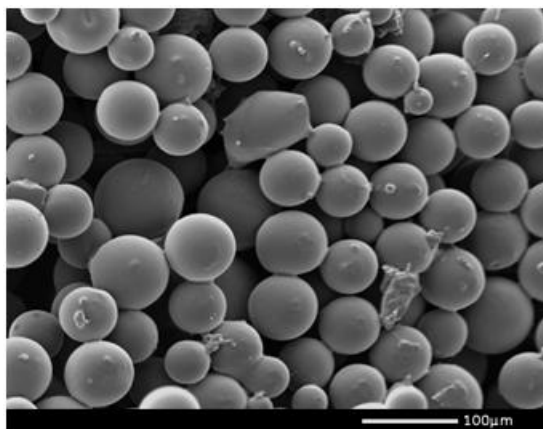


**Figure 6. 2** Scanning electron microscope (SEM) image obtained from 6:1 PEG4000 (C6) copolymer.

**Table 6. 1** Average diameter of the microspheres produced, determined through SEM imaging analysis.

Copolymer	Average diameter ( $\mu\text{m} \pm \text{SD}$ )
C4	$68.9 \pm 4.8$
C5	$65.4 \pm 2.9$
C6	$60.2 \pm 8.4$
C16	$56.4 \pm 3.1$

#### 6. 4. 3 Water uptake

The equilibrium water uptake was measured for the copolymers that were selected for their hydrolytic degradation and protein release rates. The ability of the polymer to absorb water is a determinant of the rate of hydrolytic degradation as well as the protein release kinetics. The polymer disks absorbed between 21 to 25 % w/w of water. The water uptake was higher in copolymers with lower  $\epsilon$ -caprolactone ratios, although the difference was not significant ( $F=0$ , one-way ANOVA) (Table 6. 2).

**Table 6. 2** Water uptake of the copolymers tested for degradation kinetics.

Polymer	Water uptake (% w/w $\pm$ SD)
C4	25.1 $\pm$ 0.9
C5	22.3 $\pm$ 1.2
C6	21.1 $\pm$ 0.7

#### 6. 4. 4 Hydrolytic degradation rate

A complete mass loss was observed within 8 weeks for all copolymers tested (Figure 6. 3). The PEG 1500 initiated copolymer showed rapid mass loss within 20 days of incubation. This rapid degradation was attributed to the lower molecular weight and the completely amorphous state ( $T_m \sim 25^\circ\text{C}$ ) of the samples at the incubation temperature (Table 5. 5) that helped water penetration and fast hydrolysis of the polymer.

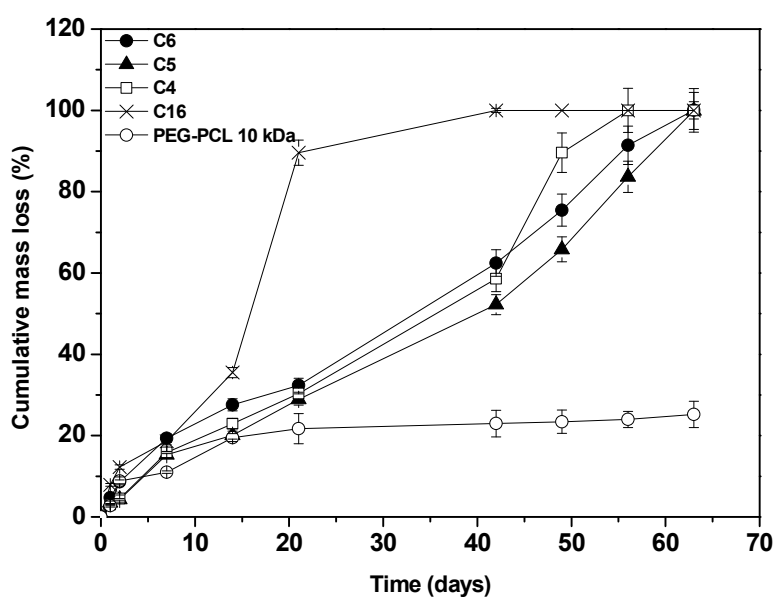


**Figure 6. 3** Cumulative mass loss obtained from in vitro hydrolytic degradation kinetics analysis on copolymer microspheres in distilled water with pH adjusted to pH 7.4. Samples C6 (6:1 – PEG4000 - 10 kDa), C5 (5:1 – PEG4000 - 10 kDa), C4 (4:1 – PEG4000 - 10 kDa), and C16 (6:1 – PEG1500 – 7.5 kDa) compared to copolymerized PEG4000 with pure PCL blocks to total 10 kDa molecular weight.  $n = 4$  per time point. Straight lines connecting the data points of each sample were used to guide the eye.

C4, C5 and C6 PEG 4000 initiated copolymers had very similar degradation rates that were affected by the CL:G ratio especially during the last weeks of the study. The rate of mass loss accelerated as the degradation progressed after week 3 with the most significant increase observed for the C4 copolymer. This increase was attributed to hydrolytic autocatalysis caused by acidic degradation products (e.g. glycolic acid). The higher glycolide content in the C4 copolymer may also have caused the burst in mass loss at the latter stage of its degradation due to the accumulation of glycolic acid in the bulk of the copolymer.

Although bulk erosion of polymers is usually characterized by continuous  $M_n$  loss but small mass loss at the initial stages of degradation, low molecular weight amphiphilic polymers can exhibit quite fast and direct mass loss from the earliest stages.<sup>8</sup> The molecular weight threshold below which polymer chains become soluble in the hydrolysis medium can be easily reached with minimum chain scissions by polymers of already low molecular weight. Consequently, simultaneous molecular weight and mass loss is usually observed in such samples, as in the samples studied herein (Figure 6. 4).

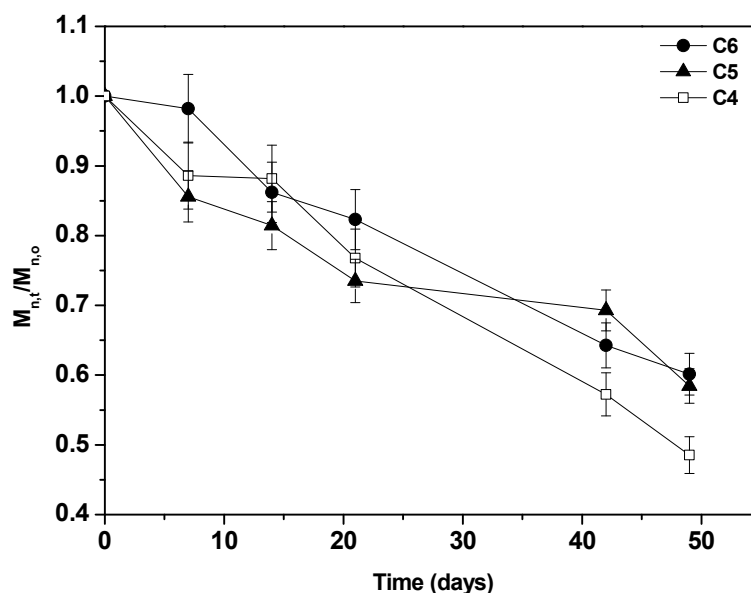


**Figure 6. 4** Cumulative  $M_n$  loss obtained from in vitro hydrolytic degradation kinetics analysis on copolymer microspheres in distilled water with pH adjusted to pH 7.4. Samples C6 (6:1 – PEG4000 - 10 kDa), C5 (5:1 – PEG4000 - 10 kDa), C4 (4:1 – PEG4000 - 10 kDa) were analyzed.  $n = 4$  per time point. Straight lines connecting the data points of each sample were used to guide the eye.

The composition analysis of degrading microspheres was studied with respect to the integration of glycolide methylene peaks (Table 6. 3). As expected, the glycolyl units showed faster degradation rates than PCL segments while PEG segments concentrations were also quickly reduced. PCL degrades very slowly and this was confirmed by the much longer retention of the PCL blocks in the copolymers. Pure PCL microspheres (control) showed only 0.25% mass loss in first weeks of incubation and did not reveal any further reduction in the timeframe of the analysis.

**Table 6. 3** Molar ratios of CL and PEG in respect to G determined via  $^1\text{H}$  NMR composition analysis of samples from in vitro degradation analysis in distilled water with pH adjusted to pH 7.4.

week	6:1		5:1		4:1	
	CL/G	PEG/G	CL/G	PEG/G	CL/G	PEG/G
0	5.92	12.71	5.11	10.30	4.13	8.43
1	5.98	10.72	5.36	9.32	4.13	7.32
2	6.05	8.89	5.40	9.05	4.22	7.17
3	5.96	8.15	5.24	8.53	4.34	7.07
6	5.98	8.10	5.98	9.71	4.51	6.60
7	6.03	9.08	6.01	9.50	-	-

The hydrolytic degradation study was carried out in distilled water with an adjusted pH of 7.4 to enable assessment of the acidic by-products formed during degradation. The incubation medium was replaced daily and its pH measured (Figure 6. 5). A rapid drop of the external pH was noted during the first days of incubation, which reached values as low as pH 4.7 at days 20 to 30 for the copolymer that was higher in G content (C4).

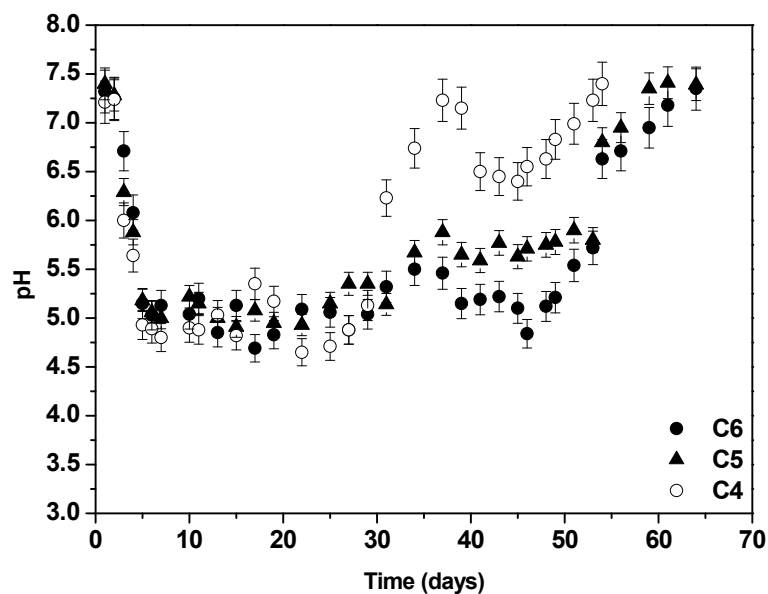


**Figure 6. 5** pH values of the external incubation medium during degradation of microspheres prepared with copolymers C6 (6:1-PEG4000-10 kDa), C5 (5:1-PEG4000-10 kDa) and C4 (4:1-PEG4000-10 kDa). The degradation took place in water with pH adjusted at pH7.4. The incubation medium (water, pH7.4) was refreshed daily. n=4 per time point.

Thermal analysis of the degrading microspheres revealed that the crystallinity of the hydrated samples decreased after one week of degradation and continued to decrease gradually as degradation progressed. The glass transition and melting temperature were retained in similar onset and endset values and only the integration of the endothermic melting peaks showed a decrease (Figure 6. 6).

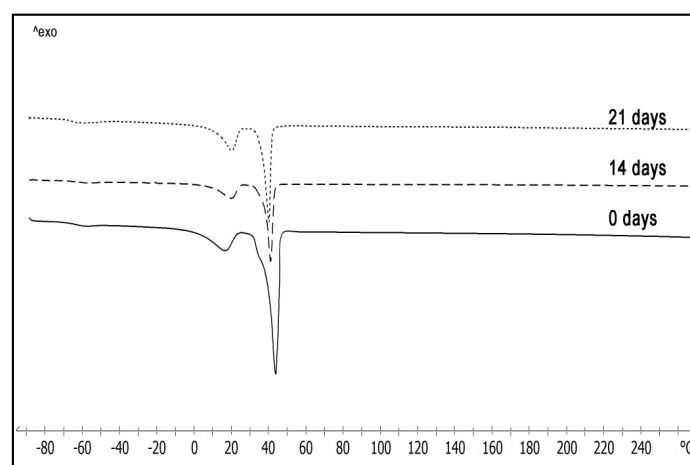


**Figure 6. 6** DSC thermographs (1<sup>st</sup> heating cycle) of copolymer C5 (5:1- PEG 4000-10 kDa) during hydrolytic degradation in water at pH 7.4. Graphs obtained from dry samples at day 0, 14 and 21 of the study.



#### 6. 4. 5 Microenvironmental and external pH of microspheres degrading in PBS pH 7.4

The microenvironmental pH study was critical to ensure the stability of the protein after encapsulation and during the polymer's degradation. The copolymers C5 and C6 that exhibited more controlled mass loss and higher pH values during degradation were selected for this study. C5 and C6 polymer microspheres with encapsulated pH-sensitive fluorescence dextrans were incubated in PBS (pH 7.4) buffer solution and studied for their microenvironmental and external pH variations with time. Two dual emission and dual excitation fluorescent dyes, Lysosensor yellow/blue and SNARF 1, were encapsulated into the microspheres to study the change of the pH in the core of the microspheres using confocal microscopy. The Lysosensor dye was used to visualize pH variation within the range 2.8 - 5.8, while SNARF-1 was sensitive to pH values between 5.8 - 8. Samples of the hydrated microspheres were collected at specific time intervals during degradation and analyzed using confocal microscopy. The intensity of the fluorescence at the center of the microspheres (Figure 6. 7) was measured at both emission wavelengths as instructed by the manufacturer for each fluorescent dye.

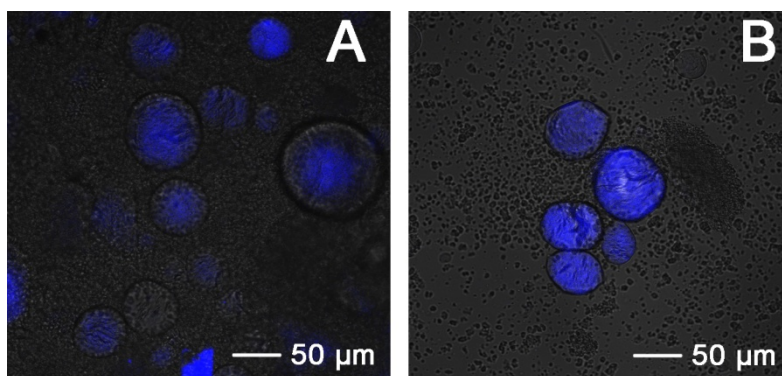


**Figure 6. 7** Fluorescence images collected at 450nm from lysosensor dextran encapsulated into 6:1-PEG4000-10 kDa (C6) microspheres at pH ~5.4, day 3 (A) and pH ~5.8, day 2 (B).

Standard curves correlating fluorescence intensity ratios and pH values were established for both of the dyes used. The ratios were concentration independent and fitted by a third order polynomial function as shown in Figure 6. 8. The concentration independence ensures the integrity of the

standard curve even after degradation or decrease of dye concentration due to release during incubation.

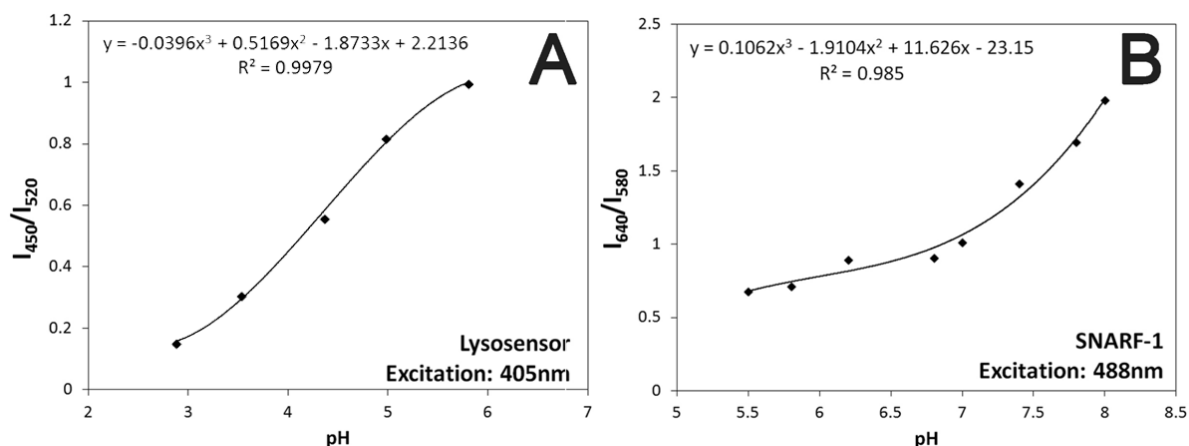


**Figure 6. 8** Standard curve of fluorescence ratio versus pH using Lysosensor (A) and SNARF-1 (B) dextran in pH-adjusted PBS buffer. The excitation of lysosensor was performed at 405nm and the emission was recorded at 450 and 520 nm, while for SNARF-1 dextran the excitation was at 488 nm and emission was recorded at 580 and 640 nm.

The fluorescence values could be obtained for up to two weeks incubation. After that point the encapsulated dextran reached concentrations below the detection limit. Within this incubation period most of the values were within the SNARF-1 detectable range and right at the upper limit of the Lysosensor dextran range. This result suggests that the degrading microspheres did not develop significant acidity that would require detection by the Lysosensor dye. The two polymer compositions exhibited very similar micro-environmental pH values, which were higher than 5.5 throughout the time of the study. The micro-environmental pH was affected by a higher glycolide content, which resulted in higher acidic during the degradation process (Figure 6. 9).

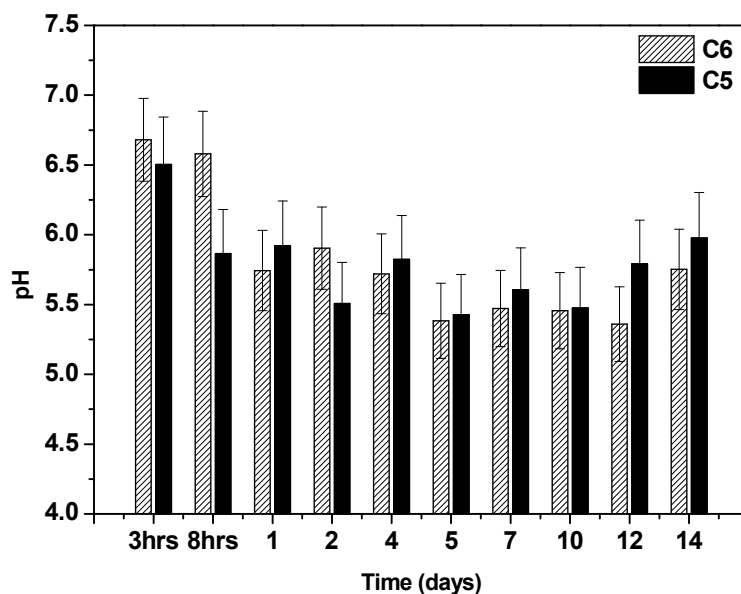


**Figure 6. 9** Microclimate pH change of degrading microspheres into PBS buffer solution (pH 7.4). Mn 10 kDa, 5:1-PEG400 (C5) and 6:1-PEG4000 (C6) polymer microspheres with encapsulated fluorescence dextran Lysosensor and SNARF-1 were analyzed using confocal microscope.

The pH of the incubation medium was also monitored using an Accumet AR15 Fischer Scientific pH meter. A rapid pH decrease was observed during the first hours of incubation; however this acidity was eliminated gradually until day 7 (Figure 6. 10). This initial pH drop could be explained by the presence of acidic impurities or oligomers in the polymer that diffused out from the polymer microspheres giving rise to the external pH increase. However, the pH value of the incubation medium never dropped below 6.7 for both of the copolymers tested, with the lowest values measured with the C5 copolymer.

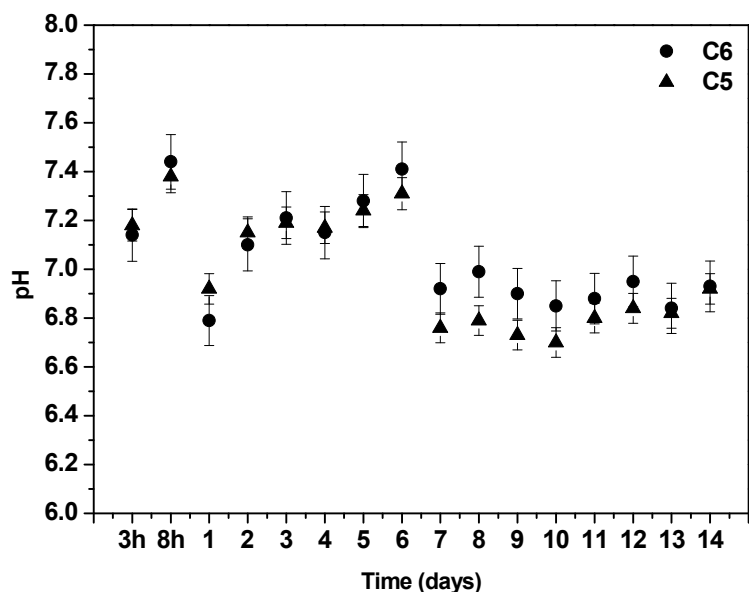


**Figure 6. 10** pH change of the incubation medium (PBS pH 7.4) during degradation of microspheres prepared using C5 (5:1 – PEG4000 – 10kDa) and C6 (6:1 – PEG4000 – 10kDa) copolymers.

## 6. 5 Conclusion

The copolymers tested were capable of producing uniformly sized microspheres with smooth surfaces that retained the thermal properties and chemical structure of the copolymers after the formulation process. Microspheres were soft at 37 °C and preserved their shape and size after incubation. Hydrolytic degradation analysis showed constant mass loss up until 8 weeks of incubation whereas complete mass loss for all the copolymers tested was observed. Higher glycolide contents enhanced degradation rates due to the higher hydrolytic susceptibility of glycolide and, subsequently, more pronounced autocatalysis at latter stages. Microenvironmental and incubation medium pH measurements revealed that there was no significant accumulation of acidic degradation by-products in the microspheres. Diffusion of acidic degradation products out of the microspheres proceeded without trouble and the microenvironmental pH remained at not significantly acidic values.

## **Chapter 7. Protein release and bioactivity**

### **7.1 Introduction**

The objective of this chapter was to assess whether the copolymer microspheres produced in this study could be used as an effective controlled protein release vehicle. To explore this potential, C5 and C6 copolymers were selected to study the encapsulation efficiency and release kinetics using lysozyme as a model therapeutic protein, as they exhibited the best degradation kinetics, external and microenvironment pH. After optimizing all parameters to achieve a sustained lysozyme release the release rate and stability of encapsulated SDF-1 $\alpha$  was investigated. As described later in this chapter, the molecular weight (MW) and isoelectric point (pI) of lysozyme (MW= 14.3 kDa, pI 11.35) were similar to those of SDF-1 $\alpha$  (MW= 10.6 kDa, pI 9.92) and thus it was a suitable model protein for this study. Bioactivity analysis was carried out to determine the extent to which SDF-1 $\alpha$  maintained structural stability during encapsulation and release.

### **7.2 Materials**

The NCI-H69 male human small cell lung carcinoma cell (SCLC) line was purchased from ATCC® (USA). RPMI-1640 (ATCC modified) cell culture medium and Pierce® BCA protein assay kit were obtained from Fisher Scientific Canada. HyClone penicillin-streptomycin solution and phosphate buffered saline 10X concentrate solution was purchased from Fisher Scientific Canada and fetal bovine serum, bovine serum albumin, and lysozyme from egg white (98%) was from Sigma-Aldrich Canada. Recombinant human SDF-1 $\alpha$  (CXCL12) and a human SDF-1 $\alpha$  ELISA kit were both purchased from PeproTech Inc., USA. For cell proliferation evaluation, MTT assay reagent was used from Invitrogen®, Fisher Scientific, Canada. For measuring DNA content in cell culture a QuantiFluor® dsDNA kit was purchased from Promega.

## **7. 3 Methods**

### **7. 3. 1 Protein particles preparation and size reduction**

The average diameter of the microspheres obtained after size separation process was 45-100  $\mu\text{m}$ , which is in the injectable size range while sufficiently large to control the release of the loaded proteins. Since microspheres are relatively small, the encapsulated particles should be reduced in size to allow for uniform distribution within the polymer matrix. In addition, small sized particles would create smaller pores upon release that will help sustain water diffusion and protein release. A target of 2  $\mu\text{m}$  as an average particle size was sought for this purpose.

One of the main challenges in processing proteins is avoiding dehydration stress, which can be particularly harmful to protein stability. Various excipients and additives such as maltose, sucrose and trehalose have been used to enhance protein stability under lyophilization and spray drying processing.<sup>92</sup> Hydrogen bonding with these excipients upon drying has been found to prevent protein denaturation.<sup>170</sup> In this study, trehalose was used as a bulking and stabilizing agent in the preparation of protein particles. Different trehalose concentrations were evaluated for their ability to form small particles in the size range of 2  $\mu\text{m}$  required.

The size reduction protocol was optimized using lysozyme as a model protein. Three different compositions, 10%, 40% and 60% of trehalose in lysozyme, were co-dissolved using PBS pH 7.4 buffer solution at a concentration of 5 % w/v. The solution was frozen in liquid nitrogen and lyophilized. The lyophilized particles were ground in a small agate mortar and pestle and sieved through Fisherbrand U.S Standard a No.325 (45  $\mu\text{m}$ ) sieve and then a No.500 (25  $\mu\text{m}$ ) sieve. The sieved particles were transferred into a clean centrifuge tube and dispersed in DCM at a concentration of 4 % w/v. Vortex was then applied to the suspension for 2 min at maximum speed. The tube was placed in an ice bath for 5 min to cool. The protein suspension was then sonicated using a probe sonicator Fischer Scientific 100 sonic dismembrator at intensity 2 (9 Watts) in 1:2 pulses (1 sec pulse:2 sec pause) for 1 min while the protein tube was kept in the ice bath to prevent heating induced by sonication. A Zeis

Axio M1 microscope was used to measure the size of the protein particles and SEM images were also obtained. The final protein suspension in DCM was subsequently used for the encapsulation of the protein into the polymer matrix.

### **7. 3. 2 Protein encapsulation in polymer microspheres**

The encapsulation of the protein in the polymer matrix was carried out using the microsphere electro spraying procedure described in paragraph 6. 3. 1. The protein particles obtained after the size reduction described in section 7. 3. 1 were mixed with appropriate amounts of C5 and C6 copolymers in DCM to obtain a final polymer concentration of 0.7 g/mL (protocol described in paragraph 6. 3. 1). The amount of polymer added to the suspension was adjusted accordingly for microspheres with varying protein particles loading. A brief sonication for 10 seconds in pulses was applied to effectively disperse the protein particles in the polymer solution. The solution was transferred into a 1 mL syringe and electro sprayed into cold ethanol. The voltage was set at 7 kV and the current at 0.1 mA. The flow rate of the solution was adjusted at 0.5 mL/min. The microspheres obtained were subjected to size separation (as described in section 6. 3. 2) and the 45-100  $\mu$ m size fraction was used to study lysozyme release.

### **7. 3. 3 Protein encapsulation efficiency**

The amount of the encapsulated protein was measured by dissolving 10 mg of protein-loaded microspheres in 1 mL DCM. The solution was vortexed for 2 min at maximum speed and centrifuged at 500,000 rpm for 5 min. The supernatant was removed and the precipitated protein particles were air-dried. The dry particles were dissolved in a PBS pH 7.4 buffer solution and the protein content was measured using Pierce® BCA assay at 562 nm with an EnSpire 2300 microplate reader (Perkin Elmer). The analysis was carried out in triplicate. A seven-point calibration curve was established to

calculate the protein content (m) and the encapsulation efficiency was calculated in respect to the feed protein weight ( $m_o$ ) during encapsulation. The encapsulation efficiency (E) was calculated from equation 7. 1:

$$E = \frac{m}{m_o} \times 100\% \quad \text{Eq. 7. 1}$$

#### 7. 3. 4 Lysozyme release

Lysozyme was used as the model protein and the protein release mechanism was studied from the microspheres produced. Protein particles loadings of 1.5 and 3 % in dry polymer mass and trehalose content (10, 40 and 60 %) were evaluated for their effect on protein release rate. Copolymers with 5:1 and 6:1 CL:G monomer ratios were also tested to see the effect of the polymer composition and crystallinity on protein release.

The experimental scheme followed is illustrated in Table 7. 1. Briefly, two different protein particle loadings (1.5 and 3 % w/w) were studied using the C5 copolymer ( $T_{m,hydrated} = 39^\circ\text{C}$ ,  $X_{hydrated} = 6.8\%$ ). Particles with 40 and 10% w/w trehalose in lysozyme were evaluated using both loading rates while particles with 60% trehalose were tested only at 3% particle loading. To assess the effect of different polymer compositions, the release from C6 polymer ( $T_{m,hydrated} = 40^\circ\text{C}$ ,  $X_{hydrated} = 7.0\%$ ) microspheres was studied using 1.5 % loading extent with particles containing 10% trehalose in lysozyme. The experiment was performed in triplicate for all conditions tested (i.e. polymer composition, trehalose content and protein particle loading).

**Table 7. 1** Experimental outline of release rate study using lysozyme as model protein with three trehalose concentrations (10, 40 and 60%) and two different particle loading rates (1.5 and 3%) using copolymers C5 (5:1-10 kDa-PEG 4000) (solid circle) and C6 (6:1-10 kDa-PEG 4000) (open circle). n = 3 per formulation.

	60% trehalose	40% trehalose	10% trehalose
Loading 1.5%		●	●○
Loading 3%	●	●	●



Triplicates of 25 mg and 50 mg of dry microspheres of 3 % and 1.5 % particle loadings, respectively, were incubated in 1 mL PBS pH 7.4 at 37 °C under mild agitation on a rocking platform at a mixing frequency of 60 cycles/min. The release medium was removed for lysozyme content analysis at each sampling time and replaced with fresh PBS. The protein content of the release medium was quantified using a Pierce® BCA assay kit. The absorbance was measured at 562 nm in an EnSpire microplate spectrometer (Perkin Elmer). A calibration curve was generated using seven lysozyme concentrations.

### **7. 3. 5 SDF-1 $\alpha$ protein particles preparation**

SDF-1 $\alpha$  was aliquoted into 4  $\mu$ g aliquots and stored in distilled water with 0.1 % BSA at -80 °C according to the storage protocol provided by the company. A 2  $\mu$ g aliquot was directly used for bioactivity assay described below in paragraph 7. 3. 8.

The solid SDF-1 $\alpha$  particles were prepared using BSA as carrier protein and trehalose as stabilizing agent. The three components, i.e. SDF-1 $\alpha$ , BSA, and trehalose, were all mixed in a 5 mL tube at a weight ratio of 0.1:94.9:5, respectively. The solid mixture was dissolved in a PBS pH 7.4 buffer solution at a concentration of 5 % w/v, frozen in liquid nitrogen, and lyophilized. After lyophilization, DCM was added so that concentration of the mixture was 4 % w/v and vortex was applied for 2 min. The tube was placed in an ice bath and 10 x 1 s sonication was applied using probe sonicator Fisher Scientific 100 sonic dismembrator at intensity 2 (9 Watts) . The average particle size of the protein mixture was evaluated using a M1 Zeiss Axio Imager and AxioVision Rel. 4.7 software. The bioactivity of the SDF-1 $\alpha$  after the size reduction process was validated using a cell-based assay as described below in section 7. 3. 8.

### **7. 3. 6 SDF-1 $\alpha$ encapsulation**

Based on the results obtained from the preliminary release experiments using lysozyme protein, polymer C6 and protein particle loading 1.5% w/w showed the most controlled protein release. This formulation was therefore used for the SDF-1 $\alpha$  release study. The SDF-1 $\alpha$  particles were prepared as described in paragraph 7. 3. 5. The final protein suspension in DCM was mixed with the appropriate amount of polymer until the protein particles to polymer ratio was 1.5% w/w. The mixture was diluted with the addition of DCM until the polymer concentration was 0.7 g/mL. Subsequently, the solution was electrosprayed as described in section 6. 3. 1. The microspheres obtained were subjected to size separation as described in section 6. 3. 2 and the 45-100  $\mu$ m size fraction was used to study the release of SDF-1 $\alpha$ .

### **7. 3. 7 SDF-1 $\alpha$ release**

The release experiment was performed ( $n = 3$ ) as outlined in paragraph 7. 3. 4 for lysozyme release. The protein particle loading was 1.5% wt. per dry polymer and 5% wt. trehalose was added in protein particles as stabilizing agent. The amount of SDF-1 $\alpha$  released was quantified in the release PBS medium using an SDF-1 $\alpha$  ELISA kit according to the instructions provided by the company. The color development was measured at 405 nm using the EnSpire 2300 microplate reader (Perkin Elmer). An identical release experiment was carried out in RPMI-1640 cell culture medium ( $n = 3$ ) supplemented with 2% penicillin-streptomycin antibiotics (P/S) mixture and 1% fetal bovine serum (FBS). The release medium from eight time points (day 1, 2, 3, 4, 7, 12, 15, and 26) of this experiment were used to study the SDF-1 $\alpha$  bioactivity as described next.

### **7. 3. 8 SDF-1 $\alpha$ bioactivity**

The bioactivity of the SDF-1 $\alpha$  was assessed upon receipt, after 2 weeks of storage, after size reduction, and after release, using a cell-based assay. Small cell lung cancer cells (SCLC) NCI-H69 were used for this study as it has been previously reported that SDF-1 $\alpha$  shows to significantly enhance their proliferation ability.<sup>171</sup> This proliferation ability was utilized to quantify the stability of the protein through processing steps, encapsulation and release. An MTT assay was used to measure the change in the metabolic activity of the cells, which can be correlated to the number of viable cells in the sample via a calibration curve. A QuantiFluor dsDNA assay was performed to determine the total number of cells present regardless of their viability.

Cell proliferation was measured after 1 and 2 days of culture in SDF-1 $\alpha$  supplemented medium using either the MTT or DNA assay (section 7. 3. 11). Triplicates of 25,000 cells/well were placed in the wells of a 96 well plate with 100  $\mu$ L low FBS medium (98% RPMI-1640, 1% FBS, 1%, P/S) and supplemented with SDF-1 $\alpha$  in concentrations varying from 0 to 200 ng/mL. Three wells served as controls with no SDF-1 $\alpha$  added. An 8-point cell number standard curve was generated for each time point with cell densities varying from 0 to 200,000 cells/well.

For the bioactivity of the released SDF-1 $\alpha$ , the release experiment was performed in RPMI-1640 cell culture medium as described in paragraph 7. 3. 7. Release samples from nine time points of the release experiment were diluted to a final concentration of 10 ng/mL using fresh RPMI-1640 medium supplemented with 1 % P/S and 1 % FBS. The solution was filtered through sterile filters and the cells were then thoroughly suspended at a cell density of 25,000 cells/100  $\mu$ L in the diluted release medium. Triplicates of 100  $\mu$ L of cell suspension were placed in a 96-well plate (25,000 cells/well) and incubated at 37 °C. An MTT metabolic activity assay was performed at day 2 of incubation.

### **7. 3. 9 Cell expansion**

The small cell lung carcinoma cells (SCLCs, NCI-H69) were purchased from ATCC®, USA and were expanded according to the protocol provided. Briefly, cells were thawed at 37 °C and removed from the cryopreservation medium. The cells were cultured in a T-150 cell culture flask with RPMI-1640 medium supplemented with 10% FBS and 1% penicillin-streptomycin (P/S) antibiotics mixture (complete medium). The flask was horizontally incubated at 37 °C and a small amount of fresh medium was added every 2 days. Subculture was performed every 7 days in 1:2 subcultivation ratio. SCLCs grow in suspended loosely packed aggregates and no trypsinization was required for cell passaging. Any cells attached at the bottom of the flask were easily detached by gentle shaking of the flask in a horizontal position.

### **7. 3. 10 Cell counting**

SCLC counting can easily lack accuracy due to the aggregates formed during expansion. Breaking cell aggregates should be avoided to exclude any potential negative implication on their viability, although this was absolutely necessary for most of the assays used in this study to ensure accurate and reproducible results. The cells formed loosely packed clusters and passage through a large gauge syringe needle was sufficient to effectively break most aggregates without affecting viability. Two passages through 18 gauge needles were able to give good countable cell suspension and high viability and the same protocol was followed throughout all proliferation assays.

### **7. 3. 11 Cell viability assays**

An MTT colorimetric assay was used to measure the metabolic activity of the cells after incubation in SDF-1 $\alpha$  protein. The MTT assay is based on measuring metabolic activity via the 3-(4,5-dimethylthiazol-2-yl)-2,5-diphenyltetrazolium bromide (MTT) reagent conversion to formazan dye.

The amount of formazan dye formed can be assigned to the number of metabolically active cells in the culture.

In order to confirm the correlation between metabolic activity and cell population, a second quantification method was used. The QuantiFluor dsDNA assay is a fluorescence double standard DNA binding dye that allows for very low DNA content quantifications. The assay was performed according to the protocol provided by the company. Briefly, tris-EDTA TE buffer in nuclease free water was used as diluent for the fluorescent dye, samples and standard solutions. A seven-point standard curve was generated by serial dilutions of the standard DNA vial provided. All unknown samples were diluted at 1:100 dilution factor to a total volume 100  $\mu$ L in TE buffer and placed in a 96-well plate. A 100  $\mu$ L dye working solution was then added and the plates were incubated for 5 min while protected from light. The fluorescence was measured in an EnSpire 2300 Perkin Elmer microplate reader at 504 nm and 531 nm excitation and emission wavelengths, respectively.

## **7. 4 Results and discussion**

### **7. 4. 1 Protein particles**

Particle reduction of the lysozyme protein required more extensive processing procedures as it proved to be quite resilient to break up. Nonetheless, reduced sized particles containing 60 % trehalose were achieved with an average diameter of  $2.4 \pm 1.6 \mu\text{m}$  content (Figure 7. 1). A change in trehalose content minimally affected the size reduction ability, which was only influenced by the processing time using vortex or sonication mixing. BSA containing SDF-1 $\alpha$  (0.1 %) was more susceptible to size reduction and therefore processing was abbreviated to eliminate losses during processing. The average BSA/SDF-1 $\alpha$  size obtained was  $1.2 \pm 0.5 \mu\text{m}$ .

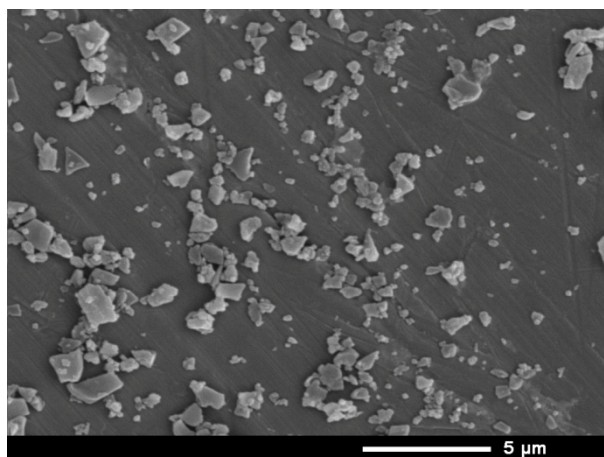


**Figure 7. 1** Lysozyme protein particles with 40% trehalose. Image taken using scanning electron microscopy (SEM)

#### 7. 4. 2 Encapsulation efficiency

Encapsulation efficiency of the lysozyme protein within the C5 and C6 copolymers was calculated and greater than 75 % of the protein was consistently retained during the solvent extraction and drying processes (Table 7. 2).

**Table 7. 2** Encapsulation efficiency yield for all protein encapsulated in polymer microspheres in C5 and C6 copolymers.

Polymer	<sup>a</sup> Trehalose (%)	<sup>b</sup> Loading (%)	Encapsulation efficiency (%)
C5/Lysozyme	10	3	87.2 ± 4.6
	40	3	74.5 ± 3.1
	60	3	86.5 ± 0.9
	60	1.5	76.2 ± 2.8
C6/Lysozyme	10	1.5	84.5 ± 5.8
C6/BSA	5	1.5	80.3 ± 2.1
C6/SDF-1α	5	1.5	87.3 ± 4.1

<sup>a</sup> % wt. of protein particles mixture

<sup>b</sup> % wt. of polymer

### 7.4.3 Lysozyme release

The aim of this experiment was to understand the effect of parameters such as trehalose content (10%, 40% and 60% w/w), CL:G ratio (5:1 and 6:1, or C5 and C6, respectively) and protein particle loading extent (1.5 % and 3 % w/w) on protein release kinetics using lysozyme as a model protein.

An initial burst release of 20-30 % of the lysozyme during the first hours of incubation was observed for all formulations with a small decrease noted when the particle loading was 1.5 %. Polymer composition and loading rate affected the release kinetics while different trehalose ratios had minimal impact on the release rate (Figure 7. 2). Trehalose content has been shown to greatly influence protein osmotic driven release from polymer microspheres.<sup>94,108,170,172</sup> This mechanism was assumed to have a contribution in this delivery approach and hence, different trehalose concentrations were studied. The influence of trehalose on the release rate would allow for better understanding the release mechanism and the influence of osmotic forces developed. As illustrated in Figure 7. 2, different trehalose contents had no significant impact on protein release profiles. This result suggests that osmotic forces were possibly limited or were not further enhanced from trehalose content and this variable did not significantly affect the release kinetics. The amount of PBS salts (11% wt. of the protein particles) present could effectively contribute to the osmotic driven release. This factor was consistent in all formulations studied and therefore an effect could not be noted.

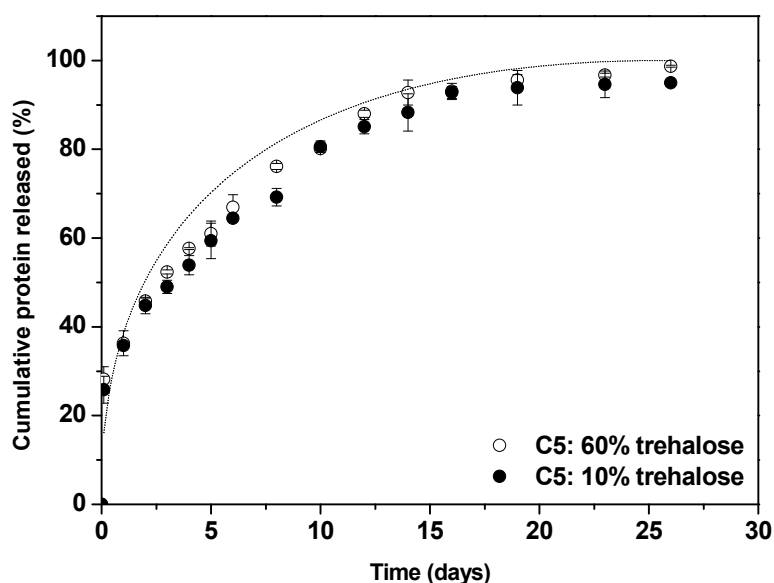


**Figure 7. 2** Release profiles of lysozyme from C5 (5:1-PEG4000-10 kDa) polymer microspheres prepared with the same protein particle loading rates (3%) as a function of trehalose content of 10 and 60%. Curve fitting of a theoretical model of diffusion controlled release was applied on each data set and is illustrated with dotted lines. Curve fit data, C5, 60% trehalose:  $R^2=0.91$ ,  $D = 1.81(\pm 0.26) \cdot 10^{-12} \text{ cm}^2/\text{sec}$  – C5, 10% trehalose:  $R^2=0.91$ ,  $D = 1.82(\pm 0.26) \cdot 10^{-12} \text{ cm}^2/\text{sec}$ .

As analyzed earlier in paragraph 6. 4. 3, the materials showed a high affinity for water uptake, which suggested that the release of rather hydrophilic proteins could be highly controlled by a diffusion mechanism. To explore this hypothesis, appropriate mathematical models for diffusion controlled release were tested. Considering that microparticles were spherical with solid protein particles uniformly dispersed throughout the polymer matrix, and degradation rate of the material was completed beyond the extent of the release, the potential of diffusion controlled release rate can be analyzed using the following solution for release from a spherical geometry under non-steady state conditions:<sup>173,174</sup>

$$\frac{M_t}{M_0} = 1 - \frac{6}{\pi^2} \sum_{n=1}^{\infty} \frac{1}{n^2} \exp\left(-\frac{n^2 \pi^2 D t}{r^2}\right) \quad \text{Eq. 7. 2}$$

where  $M_t$  and  $M_0$  are the cumulative amount of solute released at time  $t$  and the total amount of drug sorbed, respectively, while  $D$  denotes the diffusion coefficient of the drug and indicates the



drug diffusion ability through the polymer matrix and  $r$  represents the radius of the spherical device. The new average radius of the hydrated microspheres was calculated using the average dry microsphere diameter calculated in paragraph 6. 4. 2 for each copolymer and the volume change after water uptake (determined in paragraph 6. 4. 3). Equation 7. 3, that represents the volume of spherical particle, was used to calculate the new average radius after hydration:

$$V = \frac{4}{3}\pi r^3 \quad \text{Eq. 7. 3}$$

The equation was applied for dry microsphere volume ( $V_{\text{dry}}$ ) and the volume after hydration ( $V_{\text{hydr}}$ ), where  $V_{\text{hydr}}$  was calculated from the water uptake determined in paragraph 6. 4. 3 with the density of the copolymer considered as 1.13 g/mL (average density value of PCL and PEG homopolymers).<sup>9,49</sup> The new values obtained were 35.5  $\mu\text{m}$  for C5 and 32.7  $\mu\text{m}$  for C6 copolymer microspheres, respectively. The new average radius was used in diffusion coefficient calculations explained below.

Two simplified forms of this model (Eq. 7. 2) can apply. For early time approximation, which holds over the initial portion of the curve where  $M_t/M_0 < 0.4$ , the equation can be approximated by equations 7. 4 and 7. 5 below<sup>173,174</sup>:

$$\frac{M_t}{M_0} = 6\sqrt{\frac{Dt}{r^2\pi}} - 3\frac{Dt}{r^2} \quad \text{Eq. 7. 4}$$

and for later times the following approximation can be used,

$$\frac{M_t}{M_0} = 1 - \frac{6}{\pi^2} \exp\left(\frac{-\pi^2 Dt}{r^2}\right) \quad \text{Eq. 7. 5}$$

which is valid for  $M_t/M_0 > 0.6$ .

Equations 7. 4 and 7. 5 exhibited a rather close fit to the experimental data, regardless of the trehalose content and particle loading ratio used. An average R-square of  $0.90 \pm 0.01$  was exhibited

for samples with 1.5% particle loading and  $0.95 \pm 0.02$  for the 3% protein particle loaded microspheres. The diffusion coefficient was determined to be of an average  $D = 1.9(\pm 0.2) \cdot 10^{-12}$  cm<sup>2</sup>/sec for the 1.5% loaded microspheres and  $D = 1.8(\pm 0.2) \cdot 10^{-12}$  cm<sup>2</sup>/sec for the 3% loaded samples tested.

Although diffusion influenced protein release rate, other parameters may contribute to a combination of release forces and should be explored for their effect on the lysozyme release profile. In terms of protein particle loading, it was observed that an increase in loading rate provided a rather small effect on the rate of release. A smaller more delayed initial burst release which was noted at lower protein particle loading was attributed to a reduction in the surface-resident particles that are readily dissolved upon hydration. Additionally, more controlled and slower release were noted with the 1.5% loaded microspheres compared to the 3% loaded microspheres after the initial burst release (Figure 7. 3). This result could be due to the enhanced concentration of highly hydrophilic components (e.g. trehalose, PBS salts) that provide better water penetration compared to the more hydrophobic and slowly hydrated regions of the polymer.

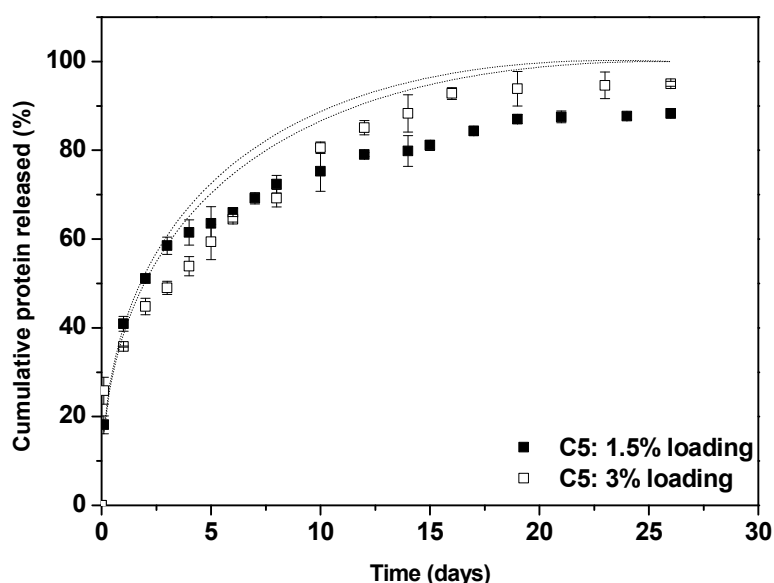


**Figure 7. 3** Release profiles of lysozyme from C5 (5:1 - PEG4000 - 10 kDa) copolymer microspheres as a function of loading rate 1.5 and 3%. Trehalose content in the protein particles was 10% for both of the samples. Curve fitting of a theoretical

model of diffusion controlled release was applied on each data set and is illustrated with dotted lines. Curve fit data, C5, 1.5% loading:  $R^2=0.87$ ,  $D = 1.98(\pm 0.23) \cdot 10^{-12} \text{ cm}^2/\text{sec}$  – C5, 3% loading:  $R^2=0.91$ ,  $D = 1.82(\pm 0.26) \cdot 10^{-12} \text{ cm}^2/\text{sec}$ .

Since diffusion shows to have some control on the release mechanism the extent of polymer hydration would highly affect protein release profiles. As discussed above in section 6. 4. 3 in regards to water uptake of the polymers, water absorption is highly influenced by polymer crystallinity and chemical hydrophilicity. Hence, a lower initial burst release was observed for the polymer C6, which had a higher CL content, shown to increase both crystallinity and hydrophobicity of the materials (Figure 7. 4) and exhibiting a more limited and slower hydration.

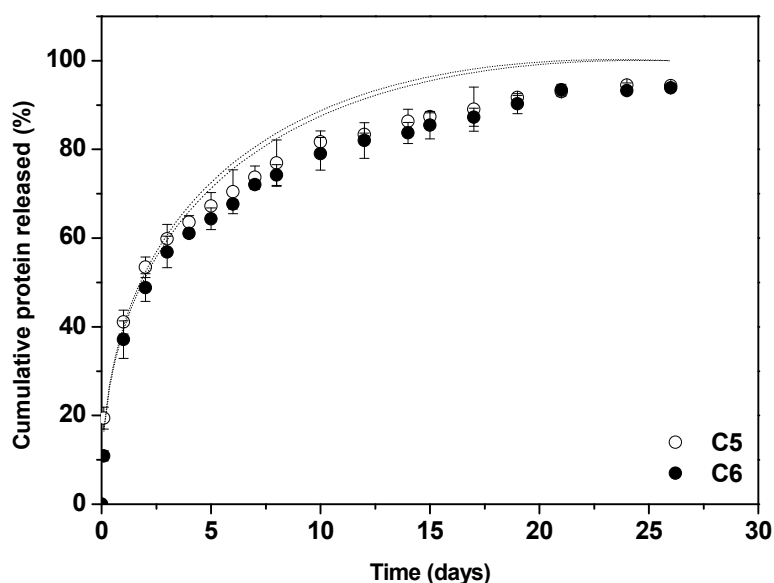


**Figure 7. 4** Release profiles of lysozyme from C5 (5:1-PEG4000-10 kDa) and C6 (5:1-PEG4000-10 kDa) microspheres prepared with the same loading rate (1.5%) and same trehalose content (10%) as a function of polymer composition and crystallinity. Curve fitting of a theoretical model of diffusion controlled release was applied on each data set and is illustrated with dotted lines. Curve fit data, C5:  $R^2=0.87$ ,  $D = 1.98(\pm 0.23) \cdot 10^{-12} \text{ cm}^2/\text{sec}$  – C6:  $R^2=0.90$ ,  $D = 1.89(\pm 0.20) \cdot 10^{-12} \text{ cm}^2/\text{sec}$ .

Based on the results obtained from the preliminary release study of lysozyme, the following release mechanism is proposed. Following immersion of the microspheres into an aqueous environment, the surface-resident protein particles are dissolved and released into the incubation medium.<sup>108</sup> At the same time, water penetrates the polymer microspheres and gradually reduces the crystalline regions

within the polymer network. Encapsulated protein particles undergo dissolution upon contact with the water penetrating the amorphous regions of the microspheres and osmotic pressure is likely developed contributing to the release of the protein.<sup>172</sup> The elimination of crystallinity combined with high water uptake eventually creates soft hydrated gel-like viscous microparticles that act as permeable matrices controlling protein drug diffusion out of the microparticles. The initial accelerated phase of the protein release (1 – 6 days) is followed by a slower lag phase (7 – 20 days) where the copolymers have probably reached a significant level of degradation (~20-30% mass loss, Fig. 6. 3) that can affect the degree of water diffusion within the microspheres and protein release control. Higher protein particle loading (3%) may also have significantly enhanced the hydrolytic degradation rate due to higher concentration of hygroscopic factors (i.e. trehalose, PBS salts) into the polymer matrix.

The proposed release mechanism highly depends on the dimensions of the device. In microsphere formulations size and porosity of the particles can increase free surface available for interactions as well as water absorption rates.<sup>96,175</sup> Polymer degradation as well as protein-polymer and protein-protein interactions could also contribute to the release profiles, but any specific effect of these parameters was not observable in the release profiles.

#### **7. 4. 4 SDF-1 $\alpha$ release**

Utilizing the data obtained from the preliminary lysozyme release experiments it was concluded that the 6:1 copolymer (C6) with 1.5% loading showed the lowest initial burst release and almost 90% of the loaded lysozyme was effectively released within three weeks (Figure 7. 2). For the SDF-1 $\alpha$  protein encapsulation, the C6 (6:1) copolymer was therefore used and the amount of trehalose was decreased to 5% w/w. Trehalose has been shown to effectively protect the protein's structure and stability during lyophilization and spray drying processes at concentrations as low as 2%.<sup>92</sup> The final composition of the protein particles was 0.1% SDF: 84% BSA: 5% trehalose: 11% PBS buffer salts.

Both SDF-1 $\alpha$  and BSA were quantified in the release medium. Both proteins followed a similar release profile featuring an initial burst release and a more sustained release phase after one week of incubation (Figure 7. 5). The release profiles were significantly similar to the profiles obtained from lysozyme studies regardless the molecular weight of the individual proteins (Table 7. 3) encapsulated (SDF-1 $\alpha$  and BSA). Mathematical models of diffusion release were also applied and R-square values from the curve fits were 0.91 and 0.94 for SDF-1 $\alpha$  and BSA, respectively (Figure 7. 5). The diffusion coefficients were  $D = 1.5(\pm 0.1) \cdot 10^{-12} \text{ m}^2/\text{sec}$  for SDF-1 $\alpha$  and  $D = 1.4(\pm 0.1) \cdot 10^{-12} \text{ cm}^2/\text{sec}$  for BSA which could indicate an overall slower release rate compared to lysozyme ( $D = 1.9(\pm 0.2) \cdot 10^{-12} \text{ cm}^2/\text{sec}$ ), if the release would be controlled exclusively by diffusion. However, as other factors, such as osmotic activity, degradation of the copolymers and polymer-protein interactions may take place along with diffusion the diffusion coefficient values represent only a theoretical consideration of the release rate.

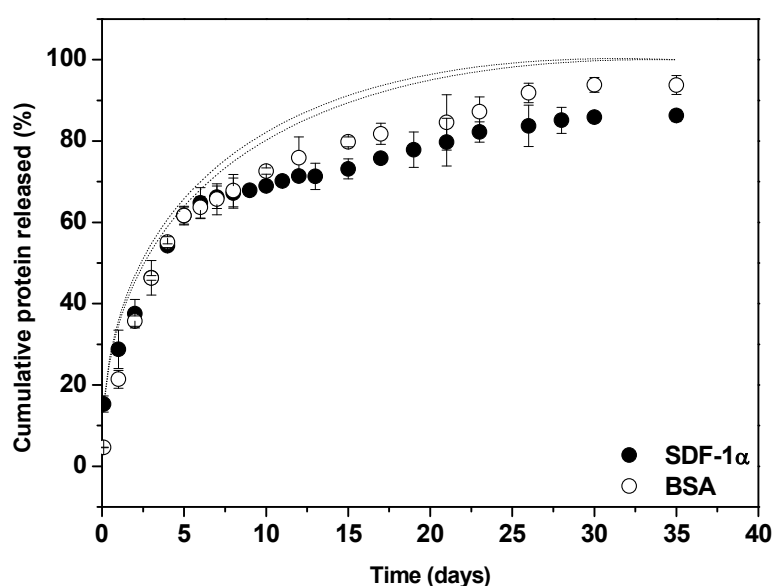


**Figure 7. 5** Release profiles of SDF-1 $\alpha$  and BSA (carrier protein) encapsulated in C6 polymer microspheres using 1.5% protein particles loading with 5% trehalose content. Curve fitting of a theoretical model of diffusion controlled release (Eq. 7. 4 and 7. 5) was applied on each protein data set and is illustrated with dotted lines. Curve fit data, SDF-1 $\alpha$ :  $R^2=0.9$ ,  $D = 1.5(\pm 0.1) \cdot 10^{-12} \text{ cm}^2/\text{sec}$  – BSA:  $R^2=0.94$ ,  $D = 1.4(\pm 0.1) \cdot 10^{-12} \text{ cm}^2/\text{sec}$ .

Due to the differences in the molecular size (Table 7. 3) of the two proteins, a slow release of the large BSA molecule compared to the small protein SDF-1 $\alpha$  was expected.<sup>175,176</sup> High molecular weight protein molecules have a larger radius and thus should diffuse more slowly.<sup>162</sup> However, despite this difference, the rate of release was minimally affected by the size of the encapsulated proteins. As release is controlled by both diffusion and osmotic pressure the release rate could be influenced by several factors related to concentrations of factor affecting osmotic activity, polymer-drug interactions,<sup>177</sup> interactions between drug molecules,<sup>178,179</sup> and heterogeneous degradation that alters water absorption or drug diffusion.<sup>6,180–182</sup> PBS salts and trehalose contents were sufficient to develop osmotic pressure through highly hydrated regions of the microspheres to the external medium that led to protein release profiles minimally influenced by the size of the protein.<sup>108,172,183</sup>

Considering the isoelectric points of the proteins used, it is also proposed that the two proteins will be differently charged and different polymer-protein electrostatic interactions will apply that may contribute to the release profiles obtained. As indicated in the degradation study of C6 (paragraph 6. 4. 4), hydrolytic degradation begun immediately at a steady after first week of incubation and accelerated after three weeks. The hydrolytic degradation mechanism of  $\alpha$ -hydroxy poly(esters) produces short polymer chain fractions with carboxylic end groups.<sup>49,179</sup> Dissociation of acidic groups as in the case of carboxylic groups to carboxylate anions ( $-\text{COO}^-$ ) creates negatively charged moieties that can attract or repulse encapsulated charged molecules.<sup>177,179</sup> Considering the average microenvironmental pH determined in paragraph 6. 4. 5 and the pI values of the proteins (Table 7. 3) we can conclude that BSA and SDF-1 $\alpha$  will be charged differently during release. BSA will be predominantly negatively charged ( $\text{pH} > \text{pI}$ ) while SDF-1 $\alpha$  will be mostly positively charged ( $\text{pH} < \text{pI}$ ).<sup>16</sup> This suggests possible attracting forces between the polymer and SDF-1 $\alpha$  protein that slows down the release of the protein from the polymer matrix while repulsive forces between the polymer and the BSA protein may enhance its release rate.

**Table 7. 3** Molecular weight (Mn) and Isoelectric point (pI) of the protein used<sup>184</sup>

Protein	M <sub>n</sub> (kDa)	pI	<sup>a</sup> Water solubility (mg/mL)
Lysozyme	14.3	11.35	10
BSA	66.5	4.9	40
SDF-1α	10.6	9.92	12 <sup>b</sup>

<sup>a</sup>values provided in the product data sheet (Sigma Aldrich, CA)<sup>b</sup>highest concentration in aqueous solution found in literature<sup>185</sup>

The effect of microclimate electrostatic forces within polymer microspheres has been extensively studied using PLGA-based materials.<sup>186</sup> PLGA microspheres with encapsulated cationic peptides has been studied for the effect of ionic strength on sustained release mechanism. Studies showed that cationic molecules can be adsorbed to the surface of anionic low molecular weight polymers and their release can be controlled by the rate of desorption.<sup>179,186–189</sup> A reverse system with a cationic polymer system of polyethyleneimine (PEI) and encapsulated anionic molecules has also been extensively studied for gene delivery through electrostatic forces.<sup>190,191</sup>

The dissolution rate of the proteins is also an important factor affecting the rate of protein diffusion out of the microspheres.<sup>192</sup> BSA is known to have very high water solubility while lysozyme and SDF-1α exhibit significantly lower solubility compared to BSA (Table 7. 3). This difference in solubility also probably contributed to the enhanced BSA release rate observed which was comparable to the rates of the smaller protein molecules, i.e. lysozyme and SDF-1α.

#### 7. 4. 5 SDF-1α bioactivity

The stability of the released protein is a crucial factor in assessing the effectiveness of this delivery approach. The bioactivity of the SDF-1α released from C6 microspheres was analyzed using a cell-based assay. The ability of this cytokine to enhance the viability and proliferation of NCI-H69 small cell lung cancer cells was measured and compared to the bioactivity of the as-received and after-storage SDF-1α. SDF-1α bioactivity level has been reported at concentrations 20-100 ng/mL.<sup>193</sup>

However, we observed linear concentration dependence from the lowest concentration tested (10 ng/mL) up to 40 ng/mL for day 2 of incubation (Figure 7. 6). A further increase in SDF-1 $\alpha$  concentration did not enhance cell proliferation while at very high protein concentrations the proliferation of the cells decreased compared to concentrations below 100 ng/mL. This can be explained by desensitization of the cell protein receptors. Prolonged exposure to solutions with high ligand concentration can cause the down-regulation of the protein-specific receptors due to endocytosis or loss in sensitivity.<sup>194</sup> For bioactivity measured at day 1 of incubation, no concentration dependence could be defined.

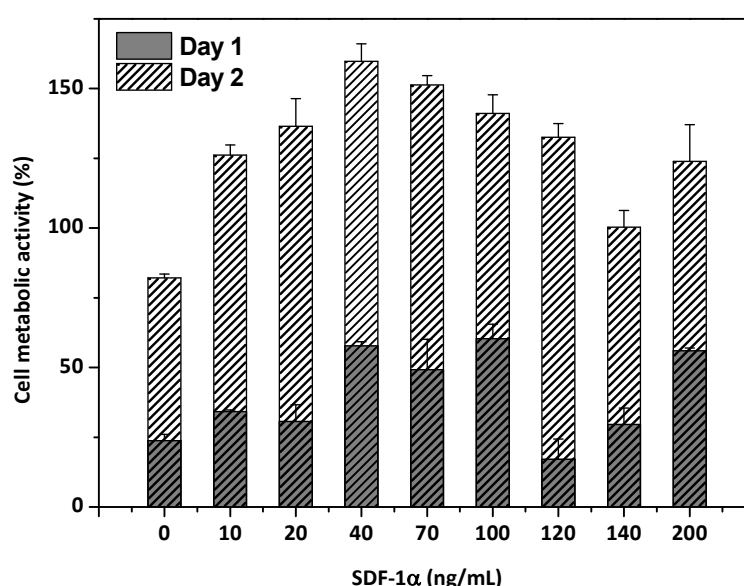


**Figure 7. 6** Cell metabolic activity at day 1 and day 2 after incubation in SDF-1 $\alpha$  supplemented cell culture medium, using “as received” SDF-1 $\alpha$  protein at concentrations varying from 0 - 200 ng/mL, using MTT metabolic activity assay. Values reported as % increase in metabolic activity from the values obtained from the initial cell population, without the effect of SDF-1 $\alpha$ .

Similar results were obtained from the evaluation of bioactivity after two weeks of storage (Figure 7. 7) at -80°C according to the manufacturer’s storage protocol. The bioactivity of the protein after storage was also confirmed using a DNA assay to assess the number of cells present regardless of their metabolic activity (Figure 7. 8). The results showed linearity at concentrations 10-40 ng/mL, which did not increase further with an increase in SDF-1 $\alpha$  concentration.



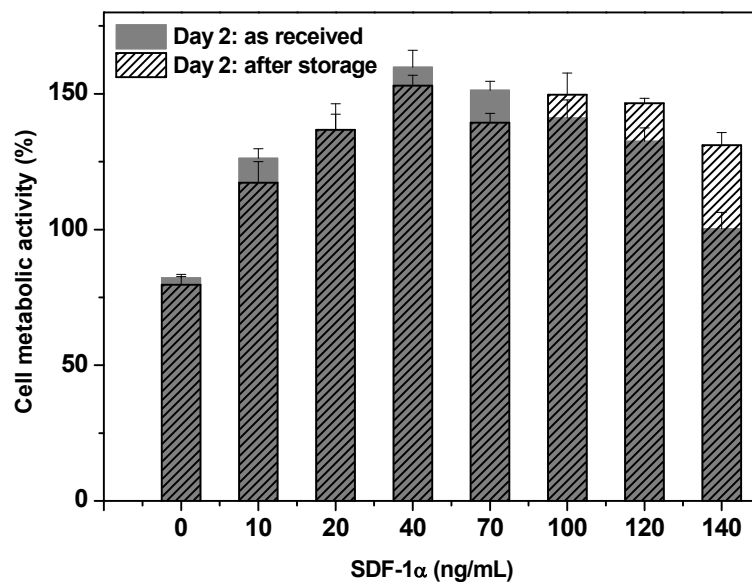


**Figure 7. 7** Compared cell metabolic activity (Day 2) between ‘as received’ and ‘after storage’ SDF-1α protein measured using MTT metabolic activity assay at concentrations varying from 0 to 140 ng/mL. The values are reported as % increase in metabolic activity from the values obtained from the initial cell population, without the effect of SDF-1α.

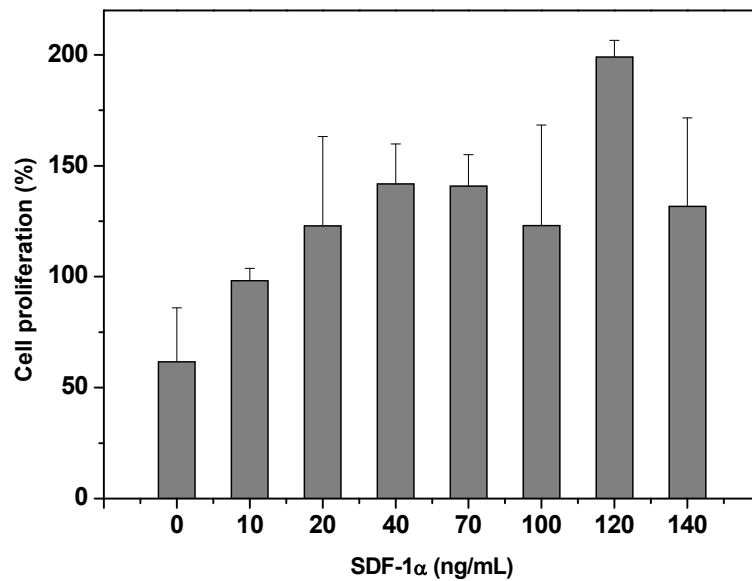


**Figure 7. 8** Cell number assay at day 2 of incubation in SDF-1α supplemented cell culture medium using ‘after storage’ SDF-1α, measured with QuantiFluor dsDNA assay. The values are reported as % increase of the number of cells compared to the initial cell population used.

The results obtained from the MTT assay of the released SDF-1α were normalized to the ‘after storage’ metabolic activity at the same SDF-1α concentration (10 ng/mL). The comparison showed

that the average bioactivity of the protein remained high during encapsulation and release, while cell proliferation was enhanced compared to the control group (0 ng/mL SDF-1 $\alpha$ ) (Figure 7. 9).

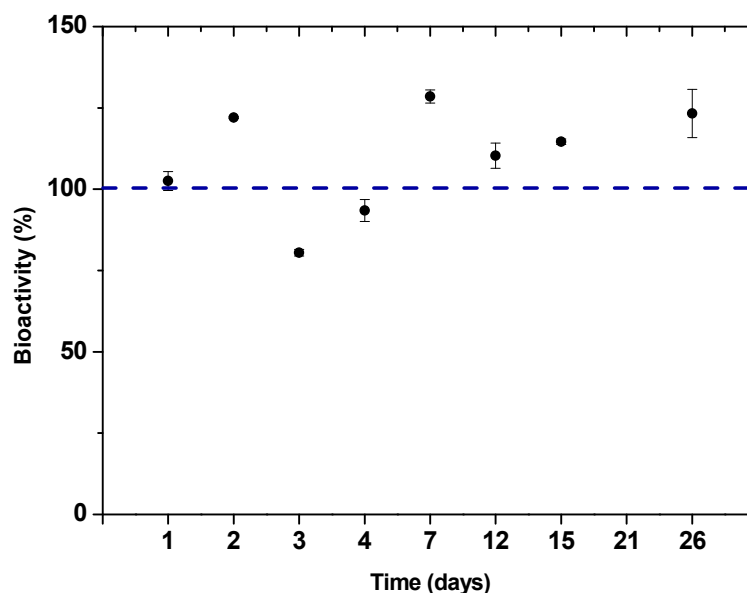


**Figure 7. 9** Bioactivity of SDF-1 $\alpha$  after release from microspheres prepared using C6 (6:1 – PEG4000 – 10kDa) copolymer. The released SDF-1 $\alpha$  was diluted to a concentration 10 ng/mL and the bioactivity obtained was compared to the bioactivity obtained from ‘after storage’ SDF-1 $\alpha$  at the same concentration (10 ng/mL).

## 7. 5 Conclusion

Tri-block copolymers initiated with PEG 4000 exhibited a prolonged protein delivery that was driven by a combination of forces including osmotic pressure and diffusion while degradation of the copolymer further affected protein release at the second release lag phase observed. The polymers tested had good water permeability that facilitated protein release in high yield. The release profiles were controlled by adjusting the polymer composition, which in turn affected overall water content of the polymer matrix. Protein particle loading also provided better control over release profiles, which was attributed to more effective distribution of the protein particles in the polymer matrix. The bioactivity study of SDF-1 $\alpha$  revealed a concentration dependence at concentrations between 10-40 ng/mL which was retained after encapsulation and release from the microspheres. Promisingly,

the formulations investigated provided sustained release profiles with excellent encapsulation efficiencies while the bioactivity of the loaded SDF-1 $\alpha$  protein was preserved at high levels.

## Chapter 8. Summary and Conclusion

Random structured triblock copolymers P(CL-G)<sub>2</sub>-PEG were successfully synthesized and characterized. A variety of compositions was produced which had melting temperatures close to 37 °C and sufficient crystallinity at room temperature to provide good handling properties. Varying the CL:G ratio it was possible to control the melting onset of PEG 4000 initiated polymers while PEG 1500 initiation polymers resulted in amorphous copolymers. Copolymers with total molecular weight higher than 15 kDa exhibited enhanced crystallinity due to the formation of long crystalline PG blocks that could potentially induce tissue irritation upon injection *in vivo*.

A linear mass loss with time and complete degradation within 8 weeks was noted for polymers with  $M_n < 10$  kDa, which was influenced by monomer ratio and the initiator used. The release of encapsulated proteins was influenced by diffusion and osmotic activity through highly hydrated polymer microspheres and the rate was controlled by the water content and degradation of the matrix. An effective and prolonged release of 3 weeks was exhibited for all proteins studied while the bioactivity of the released SDF-1 $\alpha$  was retained fully, as determined using cell-based assays.

Overall, this protein delivery vehicle was capable of effectively delivering highly bioactive SDF-1 $\alpha$ . The small size and injectability make this formulation an attractive approach for localized protein delivery. The encouraging results demonstrated in this study warrant the investigation of the *in vivo* applicability and efficacy of the formulations.

Future work recommendations:

1. A transition to higher molecular weights of the tri-block copolymers could allow for better control over release kinetics and further prolong release while further enhancing handling properties.

2. *In vivo* or *in vitro* degradation where enzymatic activity will participate in the degradation of the polymer microspheres could also provide interesting insight on the rate of biodegradation.
3. The *in vivo* efficacy of this delivery approach for protein delivery application needs to be demonstrated.

## Bibliography

1. Pisal, D. S., Kosloski, M. P. & Balu-Iyer, S. V. Delivery of therapeutic proteins. *J. Pharm. Sci.* **99**, 2557–75 (2010).
2. Sinha, V. R. & Trehan, A. Biodegradable microspheres for protein delivery. *J. Control. Release* **90**, 261–80 (2003).
3. Walle, C. Van der. Peptide and Protein Delivery. (2011).
4. *Biodrug Delivery Systems: Fundamentals, Applications and Clinical Development*. (CRC Press, 2009).
5. Sinha, V. R. & Trehan, A. Biodegradable microspheres for protein delivery. *Journal of Controlled Release* **90**, 261–280 (2003).
6. Park, T. G. Degradation of poly(lactic-co-glycolic acid) microspheres: effect of copolymer composition. *Biomaterials* **16**, 1123–1130 (1995).
7. Sukarto, A. & Amsden, B. G. Low melting point amphiphilic microspheres for delivery of bone morphogenetic protein-6 and transforming growth factor- $\beta$ 3 in a hydrogel matrix. *Journal of Controlled Release* **158**, 53–62 (2012).
8. Nair, L. S. & Laurencin, C. T. Biodegradable polymers as biomaterials. *Progress in Polymer Science (Oxford)* **32**, 762–798 (2007).
9. Utracki, L. A. *Polymer blends handbook*. Kluwer Academic Publishers (2002). doi:10.1007/0-306-48244-4
10. Wan, X. *et al.* Upregulation of stromal cell-derived factor 1 (SDF-1) is associated with macrophage infiltration in renal ischemia-reperfusion injury. *PLoS One* **9**, e114564 (2014).
11. Ceradini, D. J. *et al.* Progenitor cell trafficking is regulated by hypoxic gradients through HIF-1 induction of SDF-1. *Nat Med* **10**, 858–864 (2004).
12. Chandrashekar, G. & Udupa, N. Biodegradable injectable implant systems for long term drug delivery using poly (lactic-co-glycolic) acid copolymers. *J. Pharm. Pharmacol.* **48**, 669–674 (1996).
13. Vaishya, R., Khurana, V., Patel, S. & Mitra, A. K. Long-term delivery of protein therapeutics. *Expert Opin. Drug Deliv.* **12**, 415–440 (2015).
14. Jiskoot, W. *et al.* Protein instability and immunogenicity: Roadblocks to clinical application of injectable protein delivery systems for sustained release. *J. Pharm. Sci.* **101**, 946–954 (2012).
15. Bandekar, J. Amide modes and protein conformation. *Biochimica et Biophysica Acta - Protein Structure and Molecular Enzymology* **1120**, 123–143 (1992).
16. Vella, F. Introduction to Protein Structure. *Biochemical Education* **20**, 122 (1992).
17. Kobsa, S. & Saltzman, W. M. Bioengineering approaches to controlled protein delivery. *Pediatr. Res.* **63**, 513–519 (2008).
18. Lee, V. H. Enzymatic barriers to peptide and protein absorption. *Crit. Rev. Ther. Drug Carrier Syst.* **5**, 69–97 (1988).
19. Chen, R. R. & Mooney, D. J. Polymeric growth factor delivery strategies for tissue engineering. *Pharmaceutical Research* **20**, 1103–1112 (2003).
20. Kontermann, R. *Therapeutic Proteins: Strategies to Modulate Their Plasma Half-lives*. (John Wiley & Sons, 2012).
21. Baraniak, P. R. & McDevitt, T. C. Stem cell paracrine actions and tissue regeneration. *Regen. Med.* **5**, 121–43 (2010).

22. Pawar, R., Ben-Ari, A. & Domb, A. J. Protein and peptide parenteral controlled delivery. *Expert Opin. Biol. Ther.* **4**, 1203–1212 (2004).
23. Lapidot, T., Dar, A. & Kollet, O. How do stem cells find their way home? *Cell* **106**, 1901–1910 (2005).
24. Tuncer Degim, I. & Celebi, N. Controlled Delivery of Peptides and Proteins. *Curr. Pharm. Des.* **13**, 99–117 (2007).
25. Lee, K. Y. & Yuk, S. H. Polymeric protein delivery systems. *Progress in Polymer Science* **32**, 669–697 (2007).
26. Alberts, B. *et al.* Molecular Biology of the Cell. (2002).
27. Lu, Y., Yang, J. & Segal, E. Issues related to targeted delivery of proteins and peptides. *AAPS J.* **8**, E466–78 (2006).
28. Pawar, R., Ben-Ari, A. & Domb, A. J. Protein and peptide parenteral controlled delivery. *Expert Opin. Biol. Ther.* **4**, 1203–1212 (2004).
29. Cleland, J. L., Daugherty, A. & Mersny, R. Emerging protein delivery methods. *Current Opinion in Biotechnology* **12**, 212–219 (2001).
30. Torchilin, V. P. & Lukyanov, A. N. Peptide and protein drug delivery to and into tumors: Challenges and solutions. *Drug Discovery Today* **8**, 259–266 (2003).
31. Shaji, J. & Patole, V. Protein and Peptide drug delivery: oral approaches. *Indian J. Pharm. Sci.* **70**, 269–77
32. Takahata, H., Lavelle, E. C., Coombes, A. G. A. & Davis, S. S. The distribution of protein associated with poly(DL-lactide co-glycolide) microparticles and its degradation in simulated body fluids. *J. Control. Release* **50**, 237–246 (1998).
33. Vincent HL Lee, Satish DK, George MG, W. R. *Peptide and Protein Drug Delivery*. **19**, (CRC Press, 1990).
34. Varde, N. K. & Pack, D. W. Microspheres for controlled release drug delivery. *Expert Opin. Biol. Ther.* **4**, 35–51 (2004).
35. Mao, S., Guo, C., Shi, Y. & Li, L. C. Recent advances in polymeric microspheres for parenteral drug delivery--part 1. *Expert Opin. Drug Deliv.* **9**, 1161–76 (2012).
36. Pitt, C. G. The controlled parenteral delivery of polypeptides and proteins. *International Journal of Pharmaceutics* **59**, 173–196 (1990).
37. Siepmann, J., Siegel, R. A. & Rathbone, M. J. *Fundamentals and Applications of Controlled Release Drug Delivery*. (Springer Science & Business Media, 2011).
38. Hiroaki, O. *et al.* Drug delivery using biodegradable microspheres. *J. Control. Release* **28**, 121–129 (1994).
39. Gu, F., Neufeld, R. & Amsden, B. Sustained release of bioactive therapeutic proteins from a biodegradable elastomeric device. *J. Control. Release* **117**, 80–9 (2007).
40. Al-Tahami, K. & Singh, J. Smart polymer based delivery systems for peptides and proteins. *Recent Pat. Drug Deliv. Formul.* **1**, 65–71 (2007).
41. Schwendeman, S. P., Shah, R. B., Bailey, B. A. & Schwendeman, A. S. Injectable controlled release depots for large molecules. *J. Control. Release* **190**, 240–253 (2014).
42. Sinha, V. R. & Trehan, A. Biodegradable microspheres for protein delivery. *J. Control. Release* **90**, 261–280 (2003).

43. Hermeling, S., Crommelin, D. J. A., Schellekens, H. & Jiskoot, W. Structure-Immunogenicity Relationships of Therapeutic Proteins. *Pharm. Res.* **21**, 897–903 (2004).
44. Cleland, J. L., Powell, M. F. & Shire, S. J. The development of stable protein formulations: a close look at protein aggregation, deamidation, and oxidation. *Crit. Rev. Ther. Drug Carrier Syst.* **10**, 307–377 (1993).
45. Manning, M. C., Chou, D. K., Murphy, B. M., Payne, R. W. & Katayama, D. S. Stability of protein pharmaceuticals: An update. *Pharm. Res.* **27**, 544–575 (2010).
46. Giteau, A. *et al.* Reversible protein precipitation to ensure stability during encapsulation within PLGA microspheres. *Eur. J. Pharm. Biopharm.* **70**, 127–136 (2008).
47. Agarwal, P. & Rupenthal, I. D. Injectable implants for the sustained release of protein and peptide drugs. *Drug Discovery Today* **18**, 337–349 (2013).
48. Munarin, F., Petrini, P., Bozzini, S. & Tanzi, M. C. New perspectives in cell delivery systems for tissue regeneration: natural-derived injectable hydrogels. *J. Appl. Biomater. Funct. Mater.* **10**, 67–81 (2012).
49. Bastioli, C. *Handbook of Biodegradable Polymers. Plastic and reconstructive surgery* **128**, (2011).
50. Zhao, Z., Wang, J., Mao, H.-Q. & Leong, K. W. Polyphosphoesters in drug and gene delivery. *Advanced Drug Delivery Reviews* **55**, 483–499 (2003).
51. Park, J. H., Ye, M. & Park, K. Biodegradable polymers for microencapsulation of drugs. *Molecules* **10**, 146–161 (2005).
52. Amsden, B. G. Delivery approaches for angiogenic growth factors in the treatment of ischemic conditions. *Expert Opin. Drug Deliv.* **8**, 873–90 (2011).
53. Leong, K. W., D'Amore, P. D., Marletta, M. & Langer, R. Bioerodible polyanhydrides as drug-carrier matrices. II. Biocompatibility and chemical reactivity. *J. Biomed. Mater. Res.* **20**, 51–64 (1986).
54. Gombotz, W. R. & Pettit, D. K. Biodegradable polymers for protein and peptide drug delivery. *Bioconj. Chem.* **6**, 332–351 (1995).
55. Manoharan, C. & Singh, J. Evaluation of polyanhydride microspheres for basal insulin delivery: Effect of copolymer composition and zinc salt on encapsulation, in vitro release, stability, in vivo absorption and bioactivity in diabetic rats. *J. Pharm. Sci.* **98**, 4237–50 (2009).
56. Manoharan, C. & Singh, J. Evaluation of poly (1, 6-bis-(p-carboxyphenoxy) hexane-co-sebacic acid microspheres for controlled basal insulin delivery. *Pharm. Res.* **30**, 627–640 (2013).
57. Jiang, H. L. & Zhu, K. J. Pulsatile protein release from a laminated device comprising polyanhydrides and pH-sensitive complexes. *Int. J. Pharm.* **194**, 51–60 (2000).
58. Qiu, L. Y. & Zhu, K. J. Design of a core-shelled polymer cylinder for potential programmable drug delivery. *Int. J. Pharm.* **219**, 151–60 (2001).
59. Torres, M. P., Determan, A. S., Anderson, G. L., Mallapragada, S. K. & Narasimhan, B. Amphiphilic polyanhydrides for protein stabilization and release. *Biomaterials* **28**, 108–16 (2007).
60. Determan, A. S., Trewyn, B. G., Lin, V. S.-Y., Nilsen-Hamilton, M. & Narasimhan, B. Encapsulation, stabilization, and release of BSA-FITC from polyanhydride microspheres. *J. Control. Release* **100**, 97–109 (2004).
61. Carrillo-Conde, B., Garza, A., Anderegg, J. & Narasimhan, B. Protein adsorption on biodegradable polyanhydride microparticles. *J. Biomed. Mater. Res. A* **95**, 40–8 (2010).
62. Heller, J. *et al.* Use of poly(ortho esters) for the controlled release of 5-fluorouracyl and a LHRH analogue. *J. Control. Release* **6**, 217–224 (1987).



63. Van de Weert, M. *et al.* Semisolid, self-catalyzed poly(ortho ester)s as controlled-release systems: protein release and protein stability issues. *J. Pharm. Sci.* **91**, 1065–74 (2002).
64. Li, X., Deng, X. & Huang, Z. In vitro protein release and degradation of poly-dl-lactide-poly(ethylene glycol) microspheres with entrapped human serum albumin: quantitative evaluation of the factors involved in protein release phases. *Pharm. Res.* **18**, 117–24 (2001).
65. Hashide, R. *et al.* Poly(lactic acid) microparticles coated with insulin-containing layer-by-layer films and their pH-dependent insulin release. *J. Nanosci. Nanotechnol.* **14**, 3100–5 (2014).
66. Slager, J. & Domb, A. J. Hetero-stereocomplexes of D-poly(lactic acid) and the LHRH analogue leuprolide. Application in controlled release. *Eur. J. Pharm. Biopharm.* **58**, 461–9 (2004).
67. Jiang, W. & Schwendeman, S. P. Stabilization and controlled release of bovine serum albumin encapsulated in poly(D, L-lactide) and poly(ethylene glycol) microsphere blends. *Pharm. Res.* **18**, 878–885 (2001).
68. Schliephake, H., Weich, H. A., Schulz, J. & Gruber, R. In vitro characterization of a slow release system of polylactic acid and rhBMP2. *J. Biomed. Mater. Res. A* **83**, 455–62 (2007).
69. Chen, L., Apte, R. N. & Cohen, S. Characterization of PLGA microspheres for the controlled delivery of IL-1?? for tumor immunotherapy. *J. Control. Release* **43**, 261–272 (1997).
70. Hamishehkar, H. *et al.* The effect of formulation variables on the characteristics of insulin-loaded poly(lactic-co-glycolic acid) microspheres prepared by a single phase oil in oil solvent evaporation method. *Colloids Surf. B. Biointerfaces* **74**, 340–9 (2009).
71. Liu, J. *et al.* Controlled release of insulin from PLGA nanoparticles embedded within PVA hydrogels. *J. Mater. Sci. Mater. Med.* **18**, 2205–10 (2007).
72. Yamaguchi, Y. *et al.* Insulin-loaded biodegradable PLGA microcapsules: initial burst release controlled by hydrophilic additives. *J. Control. Release* **81**, 235–249 (2002).
73. Yang, Y. *et al.* Controllable dual-release of dexamethasone and bovine serum albumin from PLGA/ $\beta$ -tricalcium phosphate composite scaffolds. *J. Biomed. Mater. Res. B. Appl. Biomater.* **96**, 139–51 (2011).
74. Xu, W., Atala, A., Yoo, J. J. & Lee, S. J. Controllable dual protein delivery through electrospun fibrous scaffolds with different hydrophilicities. *Biomed. Mater.* **8**, 014104 (2013).
75. Jain, R. A., Rhodes, C. T., Railkar, A. M., Malick, A. W. & Shah, N. H. Controlled release of drugs from injectable in situ formed biodegradable PLGA microspheres: Effect of various formulation variables. *Eur. J. Pharm. Biopharm.* **50**, 257–262 (2000).
76. Kirby, G. T. S. *et al.* PLGA-based microparticles for the sustained release of BMP-2. *Eur. Cells Mater.* **22**, 24 (2011).
77. Golub, J. S. *et al.* Sustained VEGF delivery via PLGA nanoparticles promotes vascular growth. *Am. J. Physiol. Heart Circ. Physiol.* **298**, H1959–65 (2010).
78. Jameela, S. R., Suma, N. & Jayakrishnan, A. Protein release from poly(epsilon-caprolactone) microspheres prepared by melt encapsulation and solvent evaporation techniques: a comparative study. *J. Biomater. Sci. Polym. Ed.* **8**, 457–66 (1997).
79. Payne, L. & Andrianov, A. Protein release from polyphosphazene matrices. *Adv. Drug Deliv. Rev.* **31**, 185–196 (1998).
80. Li, Z. *et al.* Development of interferon alpha-2b microspheres with constant release. *Int. J. Pharm.* **410**, 48–53 (2011).
81. Azimi, B., Nourpanah, P., Rabiee, M. & Arbab, S. Producing gelatin nanoparticles as delivery system for bovine serum albumin. *Iran. Biomed. J.* **18**, 34–40 (2014).

82. Tabata, Y. Protein release from gelatin matrices. *Adv. Drug Deliv. Rev.* **31**, 287–301 (1998).
83. Layman, H. *et al.* The effect of the controlled release of basic fibroblast growth factor from ionic gelatin-based hydrogels on angiogenesis in a murine critical limb ischemic model. *Biomaterials* **28**, 2646–2654 (2007).
84. Pandit, A., Ashar, R. & Feldman, D. The effect of TGF-beta delivered through a collagen scaffold on wound healing. *J. Invest. Surg.* **12**, 89–100
85. Letic-Gavrilovic, A., Piattelli, A. & Abe, K. Nerve growth factor beta(NGF beta) delivery via a collagen/hydroxyapatite (Col/HAp) composite and its effects on new bone ingrowth. *J. Mater. Sci. Mater. Med.* **14**, 95–102 (2003).
86. McEwan, K. *et al.* Collagen-chitosan-laminin hydrogels for the delivery of insulin-producing tissue. *J. Tissue Eng. Regen. Med.* (2013). doi:10.1002/term.1829
87. Weiner, A. L., Carpenter-Green, S. S., Soehngen, E. C., Lenk, R. P. & Popescu, M. C. Liposome-collagen gel matrix: a novel sustained drug delivery system. *J. Pharm. Sci.* **74**, 922–5 (1985).
88. Artursson, P., Edman, P., Laakso, T. & Sjöholm, I. Characterization of polyacryl starch microparticles as carriers for proteins and drugs. *J. Pharm. Sci.* **73**, 1507–1513 (1984).
89. Hatefi, a & Amsden, B. Biodegradable injectable in situ forming drug delivery systems. *J. Control. Release* **80**, 9–28 (2002).
90. Hu, L., Zhang, H. & Song, W. An overview of preparation and evaluation sustained-release injectable microspheres. *J. Microencapsul.* **30**, 369–82 (2013).
91. Saralidze, K., Koole, L. H. & Knetsch, M. L. W. Polymeric Microspheres for Medical Applications. *Materials (Basel)*. **3**, 3537–3564 (2010).
92. Costantino, H. R. *et al.* Protein spray freeze drying. 2. Effect of formulation variables on particle size and stability. *J. Pharm. Sci.* **91**, 388–395 (2002).
93. Wang, Y. *et al.* Combination of hyaluronic acid hydrogel scaffold and PLGA microspheres for supporting survival of neural stem cells. *Pharm. Res.* **28**, 1406–1414 (2011).
94. Sukarto, A. & Amsden, B. G. Low melting point amphiphilic microspheres for delivery of bone morphogenetic protein-6 and transforming growth factor- $\beta$ 3 in a hydrogel matrix. *J. Control. Release* **158**, 53–62 (2012).
95. Meeus, J. *et al.* The Influence of Spray-Drying Parameters on Phase Behavior, Drug Distribution, and In Vitro Release of Injectable Microspheres for Sustained Release. *J. Pharm. Sci.* n/a–n/a (2015). doi:10.1002/jps.24361
96. Mao, S. *et al.* Effect of WOW process parameters on morphology and burst release of FITC-dextran loaded PLGA microspheres. *Int. J. Pharm.* **334**, 137–48 (2007).
97. Ando, S., Putnam, D., Pack, D. W. & Langer, R. PLGA microspheres containing plasmid DNA: preservation of supercoiled DNA via cryopreparation and carbohydrate stabilization. *J. Pharm. Sci.* **88**, 126–30 (1999).
98. King, T. W. & Patrick, C. W. Development and in vitro characterization of vascular endothelial growth factor (VEGF)-loaded poly(DL-lactic-co-glycolic acid)/poly(ethylene glycol) microspheres using a solid encapsulation/single emulsion/solvent extraction technique. *J. Biomed. Mater. Res.* **51**, 383–390 (2000).
99. Berkland, C., Pollauf, E., Varde, N., Pack, D. W. & Kim, K. Monodisperse liquid-filled biodegradable microcapsules. *Pharm. Res.* **24**, 1007–1013 (2007).

100. Kim, K. K. & Pack, D. W. Microspheres for Drug Delivery. *Biol. Biomed. Nanotechnol.* 19–50 (2006). doi:10.1007/978-0-387-25842-3\_2
101. Rosenkranz, K., Kasper, M. M., Werther, J. & Brunner, G. Encapsulation of irregularly shaped solid forms of proteins in a high-pressure fluidized bed. *J. Supercrit. Fluids* **46**, 351–357 (2008).
102. Sareen, S., Joseph, L. & Mathew, G. Improvement in solubility of poor water-soluble drugs by solid dispersion. *Int. J. Pharm. Investig.* **2**, 12 (2012).
103. Anderson, J. M. & Shive, M. S. Biodegradation and biocompatibility of PLA and PLGA microspheres. *Adv. Drug Deliv. Rev.* **28**, 5–24 (1997).
104. Ding, A. G. & Schwendeman, S. P. Acidic microclimate pH Distribution in PLGA microspheres monitored by confocal laser scanning microscopy. *Pharm. Res.* **25**, 2041–2052 (2008).
105. Van de Weert, M., Hennink, W. E. & Jiskoot, W. Protein instability in poly(lactic-co-glycolic acid) microparticles. *Pharm. Res.* **17**, 1159–1167 (2000).
106. Auras, R., Lim, L.-T., Selke, E. M., S. & Tsuji, H. *Poly(lactic acid): Synthesis, Structures, Properties, Processing, and Applications*. (John Wiley & Sons, 2011).
107. Ren, J. *Biodegradable Poly (Lactic Acid): Synthesis, Modification, Processing and Applications*. (Springer Science & Business Media, 2011).
108. Babasola, I. O., Zhang, W. & Amsden, B. G. Osmotic pressure driven protein release from viscous liquid, hydrophobic polymers based on 5-ethylene ketal  $\epsilon$ -caprolactone: Potential and mechanism. *Eur. J. Pharm. Biopharm.* **85**, 765–72 (2013).
109. Mi, F.-L. *et al.* Chitin/PLGA blend microspheres as a biodegradable drug delivery system: a new delivery system for protein. *Biomaterials* **24**, 5023–5036 (2003).
110. Jiang, G., Woo, B. H., Kang, F., Singh, J. & DeLuca, P. P. Assessment of protein release kinetics, stability and protein polymer interaction of lysozyme encapsulated poly(D,L-lactide-co-glycolide) microspheres. *J. Control. Release* **79**, 137–145 (2002).
111. Amsden, B. G. Biodegradable elastomers in drug delivery. *Expert Opin. Drug Deliv.* **5**, 175–87 (2008).
112. Nuyken, O. & Pask, S. D. Ring-opening polymerization-An introductory review. *Polymers (Basel)*. **5**, 361–403 (2013).
113. Duda, A. & Kowalski, A. *Thermodynamics and Kinetics of Ring - Opening Polymerization. Handbook of Ring-Opening Polymerization* (2009).
114. Dubois, P., Coulembier, O. & Raquez, J. M. *Handbook of Ring-Opening Polymerization. Handbook of Ring-Opening Polymerization* (2009). doi:10.1002/9783527628407
115. Bero, M., Czapla, B., Dobrzyński, P., Janeczek, H. & Kasperczyk, J. Copolymerization of glycolide and  $\epsilon$ -caprolactone, 2. Random copolymerization in the presence of tin octoate. *Macromol. Chem. Phys.* **200**, 911–916 (1999).
116. Dobrzynski, P. *et al.* Structure - Property Relationships of Copolymers Obtained by Ring-Opening Polymerization of Glycolide and  $\epsilon$ -Caprolactone . Part 1 . Synthesis and Characterization. *Biomacromolecules* **6**, 483–488 (2005).
117. Pack, J. W., Kim, S. H., Cho, I. W., Park, S. Y. & Kim, Y. H. Microstructure analysis and thermal property of copolymers made of glycolide and epsilon-caprolactone by stannous octoate. *J. Polym. Sci. Part a-Polymer Chem.* **40**, 544–554 (2002).
118. Kasperczyk, J. Copolymerization of glycolide and  $\epsilon$ -caprolactone , 1 Analysis of the copolymer microstructure by means of  $^1\text{H}$  and  $^{13}\text{C}$  NMR spectroscopy. **910**, 903–910 (1999).

119. Dickers, K. J., Huatan, H. & Cameron, R. E. Polyglycolide-Based Blends for Drug Delivery : A Differential Scanning Calorimetry Study of the Melting Behavior. (2002).
120. Ho, T. K., Shiwen, X., Abraham, D., Tsui, J. & Baker, D. Stromal-Cell-Derived Factor-1 (SDF-1)/CXCL12 as Potential Target of Therapeutic Angiogenesis in Critical Leg Ischaemia. *Cardiol. Res. Pract.* **2012**, 1–7 (2012).
121. Ghadge, S. K., Muhlstedt, S., Ozcelik, C. & Bader, M. SDF-1 alpha as a therapeutic stem cell homing factor in myocardial infarction. *Pharmacol. Ther.* **129**, 97–108 (2011).
122. Misra, P. *et al.* Quantitation of CXCR4 expression in myocardial infarction using 99mTc-labeled SDF-1alpha. *J. Nucl. Med.* **49**, 963–9 (2008).
123. Prokoph, S. *et al.* Sustained delivery of SDF-1?? from heparin-based hydrogels to attract circulating pro-angiogenic cells. *Biomaterials* **33**, 4792–4800 (2012).
124. Silvestre, J.-S., Smadja, D. M. & Lévy, B. I. Postischemic revascularization: from cellular and molecular mechanisms to clinical applications. *Physiol. Rev.* **93**, 1743–802 (2013).
125. Lataillade, J. J. *et al.* Chemokine SDF-1 enhances circulating CD34(+) cell proliferation in synergy with cytokines: possible role in progenitor survival. *Blood* **95**, 756–768 (2000).
126. Zerneck, A. *et al.* SDF-1 $\alpha$ /CXCR4 axis is instrumental in neointimal hyperplasia and recruitment of smooth muscle progenitor cells. *Circ. Res.* **96**, 784–791 (2005).
127. Ma, J. *et al.* Time course of myocardial stromal cell?derived factor 1 expression and beneficial effects of intravenously administered bone marrow stem cells in rats with experimental myocardial infarction. *Basic Res. Cardiol.* **100**, 217–223 (2005).
128. Tögel, F., Isaac, J., Hu, Z., Weiss, K. & Westenfelder, C. Renal SDF-1 signals mobilization and homing of CXCR4-positive cells to the kidney after ischemic injury. *Kidney Int.* **67**, 1772–1784 (2005).
129. Hill, W. D. *et al.* SDF-1 (CXCL12) Is Upregulated in the Ischemic Penumbra Following Stroke. *J. Neuropathol. Exp. Neurol.* **63**, (2004).
130. Yamani, M. H. *et al.* Peritransplant ischemic injury is associated with up-regulation of stromal cell-derived factor-1. *J. Am. Coll. Cardiol.* **46**, 1029–1035 (2005).
131. Miller, J. T. *et al.* The neuroblast and angioblast chemotactic factor SDF-1 (CXCL12) expression is briefly up regulated by reactive astrocytes in brain following neonatal hypoxic-ischemic injury. *BMC Neurosci.* **6**, 63 (2005).
132. Ponte, A. L. *et al.* The in vitro migration capacity of human bone marrow mesenchymal stem cells: comparison of chemokine and growth factor chemotactic activities. *Stem Cells* **25**, 1737–45 (2007).
133. Wynn, R. F. *et al.* A small proportion of mesenchymal stem cells strongly expresses functionally active CXCR4 receptor capable of promoting migration to bone marrow. *Blood* **104**, 2643–2645 (2004).
134. Vanden Berg-Foels, W. S. In situ tissue regeneration: chemoattractants for endogenous stem cell recruitment. *Tissue Eng. Part B. Rev.* **20**, 28–39 (2014).
135. Broxmeyer, H. E. *et al.* Transgenic Expression of Stromal Cell-Derived Factor-1/CXC Chemokine Ligand 12 Enhances Myeloid Progenitor Cell Survival/Antiapoptosis In Vitro in Response to Growth Factor Withdrawal and Enhances Myelopoiesis In Vivo. *J. Immunol.* **170**, 421–429 (2003).
136. Lapidot, T. & Kollet, O. The essential roles of the chemokine SDF-1 and its receptor CXCR4 in human stem cell homing and repopulation of transplanted immune-deficient NOD/SCID and NOD/SCID/B2m(null) mice. *Leukemia* **16**, 1992–2003 (2002).
137. Lataillade, J. J. *et al.* Chemokine SDF-1 enhances circulating CD34(+) cell proliferation in synergy with cytokines: possible role in progenitor survival. *Blood* **95**, 756–68 (2000).

138. Cheng, Z. *et al.* Targeted Migration of Mesenchymal Stem Cells Modified With CXCR4 Gene to Infarcted Myocardium Improves Cardiac Performance. *Mol. Ther.* **16**, 571–579 (2008).
139. Ruvinov, E., Cohen, S. & Sapir, Y. *Cardiac Tissue Engineering*. (Morgan & Claypool Publishers, 2012).
140. Amsden, B. G. Liquid, injectable, hydrophobic and biodegradable polymers as drug delivery vehicles. *Macromol. Biosci.* **10**, 825–35 (2010).
141. Hatefi, A. & Amsden, B. Biodegradable injectable in situ forming drug delivery systems. *Journal of Controlled Release* **80**, 9–28 (2002).
142. Sun, J. & Tan, H. Alginate-Based Biomaterials for Regenerative Medicine Applications. *Materials (Basel)*. **6**, 1285–1309 (2013).
143. Kroeze, R. J., Helder, M. N., Govaert, L. E. & Smit, T. H. Biodegradable Polymers in Bone Tissue Engineering. *Materials* **2**, 833–856 (2009).
144. Sabir, M. I., Xu, X. X. & Li, L. A review on biodegradable polymeric materials for bone tissue engineering applications. *J. Mater. Sci.* **44**, 5713–5724 (2009).
145. Alconcel, S. N. S., Baas, A. S. & Maynard, H. D. FDA-approved poly(ethylene glycol)–protein conjugate drugs. *Polymer Chemistry* **2**, 1442 (2011).
146. Zhu, J. Bioactive modification of poly(ethylene glycol) hydrogels for tissue engineering. *Biomaterials* **31**, 4639–4656 (2010).
147. Klibanov, A. L., Maruyama, K., Torchilin, V. P. & Huang, L. Amphipathic polyethyleneglycols effectively prolong the circulation time of liposomes. *FEBS Lett.* **268**, 235–237 (1990).
148. Müller, M. *et al.* Surface modification of PLGA microspheres. *J. Biomed. Mater. Res. A* **66**, 55–61 (2003).
149. Knop, K., Hoogenboom, R., Fischer, D. & Schubert, U. S. Poly(ethylene glycol) in Drug Delivery: Pros and Cons as Well as Potential Alternatives. *Angew. Chemie Int. Ed.* **49**, 6288–6308 (2010).
150. Knop, K., Hoogenboom, R., Fischer, D. & Schubert, U. S. Poly(ethylene glycol) in drug delivery: pros and cons as well as potential alternatives. *Angew. Chem. Int. Ed. Engl.* **49**, 6288–6308 (2010).
151. Woodruff, M. A. & Hutmacher, D. W. The return of a forgotten polymer—Polycaprolactone in the 21st century. *Prog. Polym. Sci.* **35**, 1217–1256 (2010).
152. Choong, C. S. N., Hutmacher, D. W. & Triffitt, J. T. Co-culture of bone marrow fibroblasts and endothelial cells on modified polycaprolactone substrates for enhanced potentials in bone tissue engineering. *Tissue Eng.* **12**, 2521–2531 (2006).
153. Fonseca, C. P., Jr, F. C., Amaral, F. A., Souza, C. A. Z. & Neves, S. Thermal and Conduction Properties of a PCL-biodegradable. **2**, 52–63 (2007).
154. Dobrzynski, P. *et al.* Structure-property relationships of copolymers obtained by ring-opening polymerization of glycolide and epsilon-caprolactone. Part 1. Synthesis and characterization. *Biomacromolecules* **6**, 483–8 (2005).
155. Sharma K., S. & Mudhoo, A. *A Handbook of Applied Biopolymer Technology: Synthesis, Degradation and Applications*. (Royal Society of Chemistry, 2011).
156. Ebewele, R. O. *Polymer Science and Technology*. (CRC Press, 2000).
157. Sridhar, R. & Ramakrishna, S. Electrosprayed nanoparticles for drug delivery and pharmaceutical applications. *Biomatter* **3**,
158. Zamani, M., Prabhakaran, M. P. & Ramakrishna, S. Advances in drug delivery via electrospun and electrosprayed nanomaterials. *Int. J. Nanomedicine* **8**, 2997–3017 (2013).

159. He, W., Baird, M. H. I. & Chang, J. S. The effect of electric field on droplet formation and motion in a viscous liquid. *Can. J. Chem. Eng.* **69**, 1174–1183 (1991).
160. Jadhav, A., Wang, L. J., Lawrence, C. & Padhye, R. Study of Electro spraying Characteristics of Polymer Solution Coating on Textile Substrate. *Adv. Mater. Res.* **332-334**, 710–715 (2011).
161. Zhang, L., Long, C., Pan, J. & Qian, Y. A Dissolution-Diffusion Model and Quantitative Analysis of Drug Controlled Release from Biodegradable Polymer Microspheres. *Can. J. Chem. Eng.* **84**, 558–566 (2008).
162. Wise, D. L. *Handbook of Pharmaceutical Controlled Release Technology*. (CRC Press, 2000).
163. Qian, H., Wohl, A. R., Crow, J. T., Macosko, C. W. & Hoyer, T. R. A Strategy for Control of ‘Random’ Copolymerization of Lactide and Glycolide: Application to Synthesis of PEG-b-PLGA Block Polymers Having Narrow Dispersity. *Macromolecules* **44**, 7132–7140 (2011).
164. Thomas, C. & Bibal, B. Hydrogen-bonding organocatalysts for ring-opening polymerization. *Green Chem.* **16**, 1687–1699 (2014).
165. *Polymers: A Property Database, Second Edition*. (CRC Press, 2008).
166. D’Avila Carvalho Erbetta, C. Synthesis and Characterization of Poly(D,L-Lactide-co-Glycolide) Copolymer. *J. Biomater. Nanobiotechnol.* **03**, 208–225 (2012).
167. Shiny, J., Ramchander, T., Goverdhan, P., Habibuddin, M. & Aukunuru, J. V. Development and evaluation of a novel biodegradable sustained release microsphere formulation of paclitaxel intended to treat breast cancer. *Int. J. Pharm. Investig.* **3**, 119–25 (2013).
168. Yagfarov, M. S. & Mitrofanova, E. P. Recrystallization and secondary crystallization in polymers. *Polym. Sci. U.S.S.R.* **28**, 1011–1017 (1986).
169. Piorkowska, E. & Rutledge, G. *Handbook of Polymer Crystallization*. (John Wiley & Sons, 2013).
170. Jain, N. K. & Roy, I. Effect of trehalose on protein structure. *Protein Sci.* **18**, 24–36 (2009).
171. Kijima, T. *et al.* Regulation of Cellular Proliferation , Cytoskeletal Function , and Signal Transduction through CXCR4 and c-Kit in Small Cell Lung Cancer Cells Regulation of Cellular Proliferation , Cytoskeletal Function , and Signal Transduction through CXCR4 and c-Kit i. 6304–6311 (2002).
172. Gu, F., Neufeld, R. & Amsden, B. Osmotic-driven release kinetics of bioactive therapeutic proteins from a biodegradable elastomer are linear, constant, similar, and adjustable. *Pharm. Res.* **23**, 782–789 (2006).
173. Ford Versypt, A. N., Pack, D. W. & Braatz, R. D. Mathematical modeling of drug delivery from autocatalytically degradable PLGA microspheres--a review. *J. Control. Release* **165**, 29–37 (2013).
174. Fu, Y. & Kao, W. J. Drug release kinetics and transport mechanisms of non-degradable and degradable polymeric delivery systems. *Expert Opin. Drug Deliv.* **7**, 429–444 (2010).
175. Sandor, M., Ensore, D., Weston, P. & Mathiowitz, E. Effect of protein molecular weight on release from micron-sized PLGA microspheres. *J. Control. Release* **76**, 297–311 (2001).
176. Klose, D., Siepmann, F., Elkharrar, K., Krenzlin, S. & Siepmann, J. How porosity and size affect the drug release mechanisms from PLGA-based microparticles. *Int. J. Pharm.* **314**, 198–206 (2006).
177. Blanco, M. . & Alonso, M. . Development and characterization of protein-loaded poly(lactide-co-glycolide) nanospheres. *Eur. J. Pharm. Biopharm.* **43**, 287–294 (1997).
178. Thiel, P., Kaiser, M. & Ottmann, C. Small-molecule stabilization of protein-protein interactions: An underestimated concept in drug discovery? *Angewandte Chemie - International Edition* **51**, 2012–2018 (2012).

179. Sophocleous, A. M. *et al.* The nature of peptide interactions with acid end-group PLGAs and facile aqueous-based microencapsulation of therapeutic peptides. *J. Control. Release* **172**, 662–70 (2013).
180. Liu, W. H., Song, J. L., Liu, K., Chu, D. F. & Li, Y. X. Preparation and in vitro and in vivo release studies of Huperzine A loaded microspheres for the treatment of Alzheimer's disease. *J. Control. Release* **107**, 417–27 (2005).
181. Gao, P. *et al.* In Vitro and in Vivo Characterization of Huperzine A Loaded Microspheres Made from End-Group Uncapped Poly(d,l-lactide acid) and Poly(d,l-lactide-co-glycolide acid). *Chem. Pharm. Bull. (Tokyo)*. **54**, 89–93 (2006).
182. Fredenberg, S., Reslow, M. & Axelsson, A. Measurement of protein diffusion through poly(D,L-lactide-Co-glycolide). *Pharm. Dev. Technol.* **10**, 299–307 (2005).
183. Chapanian, R., Tse, M. A. N. Y., Pang, S. C. & Amsden, B. G. Osmotic Release of Bioactive VEGF from Biodegradable Elastomer Monoliths Is the Same In Vivo As In Vitro. **101**, 588–597 (2012).
184. Righetti, P. G. & Tudor, G. Isoelectric points and molecular weights of proteins. *J. Chromatogr.* **220**, 115–194 (1981).
185. Murphy, J. W., Yuan, H., Kong, Y., Xiong, Y. & Lolis, E. J. Heterologous quaternary structure of CXCL12 and its relationship to the CC chemokine family. *Proteins* **78**, 1331–7 (2010).
186. Sanna, V. *et al.* Development of novel cationic chitosan-and anionic alginate-coated poly(D,L-lactide-co-glycolide) nanoparticles for controlled release and light protection of resveratrol. *Int. J. Nanomedicine* **7**, 5501–16 (2012).
187. Zhang, Y., Sophocleous, A. M. & Schwendeman, S. P. Inhibition of peptide acylation in PLGA microspheres with water-soluble divalent cationic salts. *Pharm. Res.* **26**, 1986–94 (2009).
188. Fu, W., Zhang, R., Li, B. & Chen, L. Hydrogen bond interaction and dynamics in PMMA/PVPh polymer blends as revealed by advanced solid-state NMR. *Polym. (United Kingdom)* **54**, 472–479 (2013).
189. Ghassemi, A. H. *et al.* Controlled release of octreotide and assessment of peptide acylation from poly(D,L-lactide-co-hydroxymethyl glycolide) compared to PLGA microspheres. *Pharm. Res.* **29**, 110–20 (2012).
190. Boussif, O. *et al.* A versatile vector for gene and oligonucleotide transfer into cells in culture and in vivo: polyethylenimine. *Proc. Natl. Acad. Sci. U. S. A.* **92**, 7297–301 (1995).
191. GIL, E. & HUDSON, S. Stimuli-responsive polymers and their bioconjugates. *Prog. Polym. Sci.* **29**, 1173–1222 (2004).
192. Fredenberg, S. *et al.* Development of mass transport resistance in poly(lactide-co-glycolide) films and particles - A mechanistic study. *Int. J. Pharm.* **409**, 194–202 (2011).
193. Zhuang, Y., Chen, X., Xu, M., Zhang, L. Y. & Xiang, F. Chemokine stromal cell-derived factor 1/CXCL12 increases homing of mesenchymal stem cells to injured myocardium and neovascularization following myocardial infarction. *Chin. Med. J. (Engl)*. **122**, 183–187 (2009).
194. Fehmann, H. C. & Habener, J. F. Homologous desensitization of the insulinotropic glucagon-like peptide-I (7-37) receptor on insulinoma (HIT-T15) cells. *Endocrinology* **128**, 2880–8 (1991).